Hydrophilic Drug Delivery based on Gelatin Nanoparticles

Dissertation

zur Erlangung des Grades

des Doktors der Naturwissenschaften

der Naturwissenschaftlich-Technischen Fakultät

der Universität des Saarlandes

von

Agnes-Valencia Weiß

Saarbrücken

2018

Tag des Kolloquiums: 22.06.2018

Dekan: Prof. Dr. Guido Kickelbick

Berichterstatter: Prof. Dr. Marc Schneider

                                    Prof. Dr. Claus-Michael Lehr

Vorsitz: Prof. Dr. Andriy Luzhetskyy

Akad. Mitarbeiter: Dr. Stefan Boettcher

"Look wide, and even when you think you are looking wide — look wider still."

Robert Stephenson Smyth Baden-Powell 1857 − 1941

Table of Content

1 Abstract

For the ascending class of hydrophilic, macromolecular drugs, gelatin based nanocarriers are a very promising approach for the application as drug delivery systems. Due to the chemical characteristics and instability of drugs in biological fluids, their embedment into carriers is crucial for most biologicals. For the successful application of nanoparticles (NPs) physicochemical parameters, such as size, shape, surface chemistry and mechanical properties, are vitally important. In the present thesis the elasticity of crosslinked gelatin NPs is determined in Young´s moduli by the nanoindentation method in scanning probe microscopy. The influence of storage and different crosslinking time are investigated in regard to the particles' stiffness. Here the biological relevance of the mechanical characteristics is tested *in vitro*. In order to avoid an inactivation, caused by the covalent coupling of the drug to the gelatin by a crosslinker, an innovative stabilization approach was taken by coating or embedment of freshly prepared, uncrosslinked gelatin NPs. Therefore, a formulation for a new platform delivery system, based on biodegradable and biocompatible materials, was developed. This was evaluated as a non-viral vector for gene delivery by the entrapment of locked nucleic acid and in transfection studies using a plasmid coding for green fluorescent protein. The exact polymer distribution was investigated in cryo transmission electron microscopy and energy filtered transmission electron microscopy.

2 Kurzzusammenfassung

Für den Transport von hydrophilen makromolekularen Wirkstoffen stellen Gelatinenanopartikel (GNP), aufgrund der Eigenschaften von Gelatine und deren Biokompatibilität, eine vielversprechende Möglichkeit dar. Eigenschaften wie Partikelgröße und -form, Oberflächenbeschaffenheit und mechanische Aspekte spielen eine Rolle in Bezug auf die zelluläre Aufnahme sowie Verteilung und Verweildauer der Partikel im Körper. In der vorliegenden Arbeit wurde die Elastizität von quervernetzten GNP als Young´s Moduli durch Nanoindentation im Rasterkraftmikroskop ermittelt. Darüber hinaus wurde der Einfluss der Quervernetzungszeit und der Lagerung auf die Partikelhärte getestet. Die biologische Bedeutung der Elastizität wurde durch die zelluläre Aufnahme in A549 Zellen untersucht. In einem weiteren Schritt wurde an einer innovativen Stabilisierung für GNP gearbeitet, bei der auf das bisher unausweichliche

Quervernetzen verzichtet wurde. Dadurch soll eine mögliche Wirkstoffinaktivierung durch eine kovalente Bindung an Gelatine mittels Quervernetzer umgangen werden. Für die Formulierung wurden ausschließlich biokompatible und bioabbaubare Polymere verwendet. Die Eignung hinsichtlich der Nutzung als non-viraler Vektor wurde mittels Beladung von *locked nucleic acid* und der Transfektion von, mit grün fluoreszierendem Protein codierendem Plasmid, beladenen Partikeln evaluiert. Außerdem wurde eine Strukturanalyse mittels kryo-Transmissionselektronenmikroskopie (TEM) und energiegefiltertem-TEM durchgeführt.

3   Introduction

The progress in research and technology opened up the discovery of biochemical processes, gene defects, and receptor specifications associated with diseases. The possibility to solve protein structures by crystallography helped identifying new potential drug binding sites and enabled a structure based drug discovery.[1] This development, coupled with rapid progress in biotechnological methods, promoted the investigation in hydrophilic macromolecular drugs as a new class of therapeutics. Biologicals are characterized by very specific binding properties and a high potency, which opens the possibility to treat and cure new diseases with reduced undesired pharmacological effects. From the approval of the first recombinant insulin in 1982, drugs developed further from pure proteins to monoclonal antibodies, interferons and nucleic acid therapeutics.[2] Despite all these progresses and advantages in therapy, biotherapeutics are often very unstable in biological fluids and due to their hydrophilic characteristics and the high molecular weight they lack the ability to be easily absorbed after administration.[3] This results in a low bioavailability which has previosly caused the termination of clinical and preclinical studies of once promising treatment candidates.[4] Overcoming these drawbacks presents a challenging task in research.

Nanostructured delivery systems, composed of biocompatible and biodegradable materials, are a very promising approach, which already led to market releases such as a depot formulation for the luteinizing hormone-releasing hormone leuprolide (Lupron Depot®).[5] Favorable materials for the delivery of biotherapeutics are hydrophilic polymers, such as gelatin, which show superior loading rates compared with more lipophilic materials, like poly lactic-*co*-glycolic acid or polycaprolactone.[6] Due to the excellent characteristics including the classification as safe material from the U.S. food and drug administration (FDA)[7], the biodegradability to nontoxic metabolites, the biocompatibility or the easy availability of the raw material, gelatin is an ideal material for the encapsulation of hydrophilic drugs and use as a drug delivery system.[8] Therefore, in the present thesis gelatin nanoparticles (GNPs) for the delivery of hydrophilic macromolecules are investigated. In order to alter the interaction with cells, the distribution in organs and the half-life time nanoparticles´ shape, size and surface characteristics are well known parameters, which can be addressed. In more recent years, the mechanical properties of nanoparticles (NPs) and their influence on *in vitro* and *in*

vivo application gained in interest.[9] The development of a measurement protocol for first investigations of elastic moduli of GNPs is part of this thesis. In the wake of this, the effects of crosslinker incubation times and storage have been addressed. The resulting influence in elastic moduli was studied in regard to the influence on particle-cell interactions. Therefore, the cellular uptake of crosslinked GNPs (cGNPs) into the adenocarcinomic human alveolar basal epithelial cell line A549 was investigated. All current formulation methods for GNPs have in common an inevitable chemical crosslinking step directly after production.[8] This unspecific reaction can covalently bind the biotherapeutic and thus, hinder the interaction with the target. To evade the inactivation through the crosslinkage, an innovative formulation strategy by the embedment of freshly produced GNPs in a core forming polymer could already be achieved with Eudragit® E 100.[10] The material conversion to an exclusive use of biodegradable and biocompatible polymers is addressed in the second part of the thesis. The formulation development is amongst others, accomplished with investigations of the system as a non-viral transfection vector and a structure analysis was performed using innovative imaging methods, such as cryo- transmission electron microscopy and energy filtered transmission electron microscopy, a method for element specific imaging in the nanometer range.

3.1 Nanoscale Carrier Systems for Drug Delivery

3.1.1 Need of Drug Delivery Systems

Hydrophilic macromolecules as active pharmaceutical ingredients (APIs), such as peptides, recombinant therapeutic proteins, enzymes, monoclonal antibodies and antibody-drug conjugates gained immense in importance.[5] The market share for biologicals was already more than one third of the top 100 medicines available only on prescription in 2015 and is projected to increase to around the half of the marked share by 2022.[11] Their specificity and potency is, in the most cases, superior compared to small chemical molecules.[5] However, most biologics suffer from low bioavailability.[12] In principle their application can be carried out through numerous routes to enter the body for systemic or local therapy. The most popular one is still the oral drug administration by tablets, suspensions, capsules, or granules. Other application examples would be pulmonary, parenteral, transdermal or rectal. Figure 3-1 summarizes the most commonly

used application routes in therapy. No matter which route is chosen, the barriers, exhibited by the human body, to protect itself from harmful environmental influences, needs to be overcome by the drug, so it can be delivered to the desired place of action. Up to now biologicals are mostly applied parenteral. This requires the usage of syringes and needles which is often associated with a low patient's compliance. In addition, many biologicals require repeated administrations as they show very low half-life values of minutes or hours due to a fast clearance.[3] This results in the need of alternative application routes and formulations with a sustained release to improve the patient's compliance and the therapeutic efficacy.
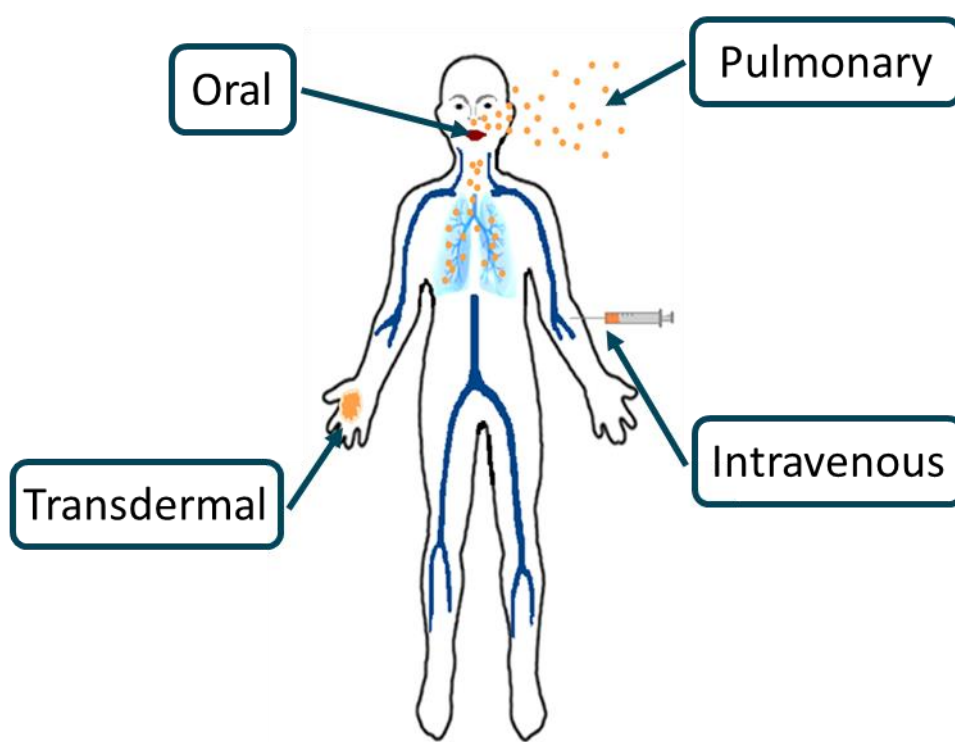
Figure 3-1: Prominent application routes in drug delivery. Adopted from: "Toxicology and clinical potential of nanoparticles"[13], Copyright © 2011 Elsevier Ltd.

This paragraph highlights the properties of three alternative applications and different hurdles, which need to be overcome for a successful und efficient therapy. Starting with the most common route, the oral delivery, the gastrointestinal tract (GIT) needs to be overcome. Even though, for orally administered drugs the patient compliance is still by far the best, it is accompanied with a number of challenges especially for the growing field of hydrophilic macromolecules.[14] The large epithelial surface in the gut is covered by a mucosal layer and in addition, the epithelial cells are connected by tight junctions. This exhibits an effective barrier, limiting the resorption of large and hydrophilic molecules,

and building a physical barrier, not only for drug application. Different drug absorption possibilities are illustrated in Figure 3-2. Due to the hydrophilic properties and size, passive diffusion is very limited. Intestinal protein carriers provide an active transport mechanism for the transcellular pathway. However, those drugs are often substrates for the efflux pump p-glycoprotein.[15, 16] The paracellular pathway, which is possible to pass by less lipophilic molecules, is only surmountable for molecules smaller then 100 to 200 Da.[17] In addition to the physical barrier, the conditions in the GIT form a chemical barrier. In the stomach, a relatively acidic pH leads to denaturation and degradation of biological molecules. Furthermore, enzymatic digestion by pepsin and other degradative enzymes strengthen the chemical barrier.[18] Different strategies are used to deliver peptides and proteins if they are able to be absorbed in the gut. Enteric coating, for example, can prevent biomolecule degradation in the stomach. With a careful selection of coating materials, colon targeting can be achieved where proteolytic activity is very low.
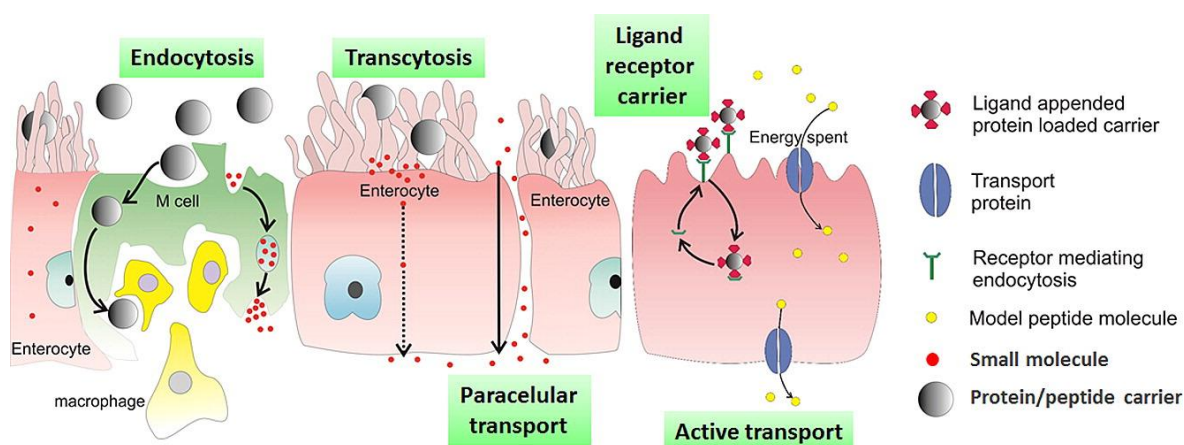
Figure 3-2: Drug absorption processes in the gut for small molecules and macromolecular drugs. Reprinted with permission from: "Targeting of gastrointestinal tract for amended delivery of protein/peptide therapeutics: Strategies and industrial perspectives",[17] Copyright © 2014 Elsevier B.V.

Another approach to bypass the physical barrier properties, would be to co-administer protease inhibitors and adsorption enhancers. A promising approach, not only for oral delivery, is the protection in particle systems such as nanoparticles, microparticles, liposomes and exosomes. With the appropriate choice of excipients, mucoadhesive formulations can be achieved. A non-formulation-based concept is chemical modifying drugs with the aim to enhance membrane permeability and chemical stability. These strategies can be used either alone or in combination but up to now, no matter which approach is chosen, the bioavailability of hydrophilic macromolecules after oral administration remains very poor.[18, 19]

Looking at the skin, with around 15 % of the total body weight[20] and a surface area of approximately 2 m² in adults,[21] it is one of the largest organs in our body. Its purpose is the protection of the human body and therefore, the skin is endowed with a complex structure and a number of functionalities. This enables the skin to preserve the body from chemicals, UV radiation, microorganisms and water and electrolyte loss. Additionally, it plays a role in immunology, regulates the body temperature, has sensory abilities and exhibits excretory activity.[22] Beyond the barrier properties the skin, as a regulating organ, shows a certain permeability, which can be exploited for local and systemic delivery of drugs.[23] Three layers can be distinguished including epidermis, dermis and subepidermal tissue. The outermost layer, the epidermis, constitutes the main barrier and consists of several layers by itself. These layers are predominantly composed of keratinocytes. In approximately two weeks keratocytes move through the layers and alter to annucleated, cornified and flat cells, the corneocytes.[21] The stratum corneum is described by the so-called "brick and mortar" model.[24] The hydrophilic corneocytes (brick) are surrounded by a lamellar lipid matrix (mortar) and connected by corneodesmosoms, which confer excellent stability to the stratum corneum.[25] Penetrations routes through the skin are summarized in Figure 3-3.
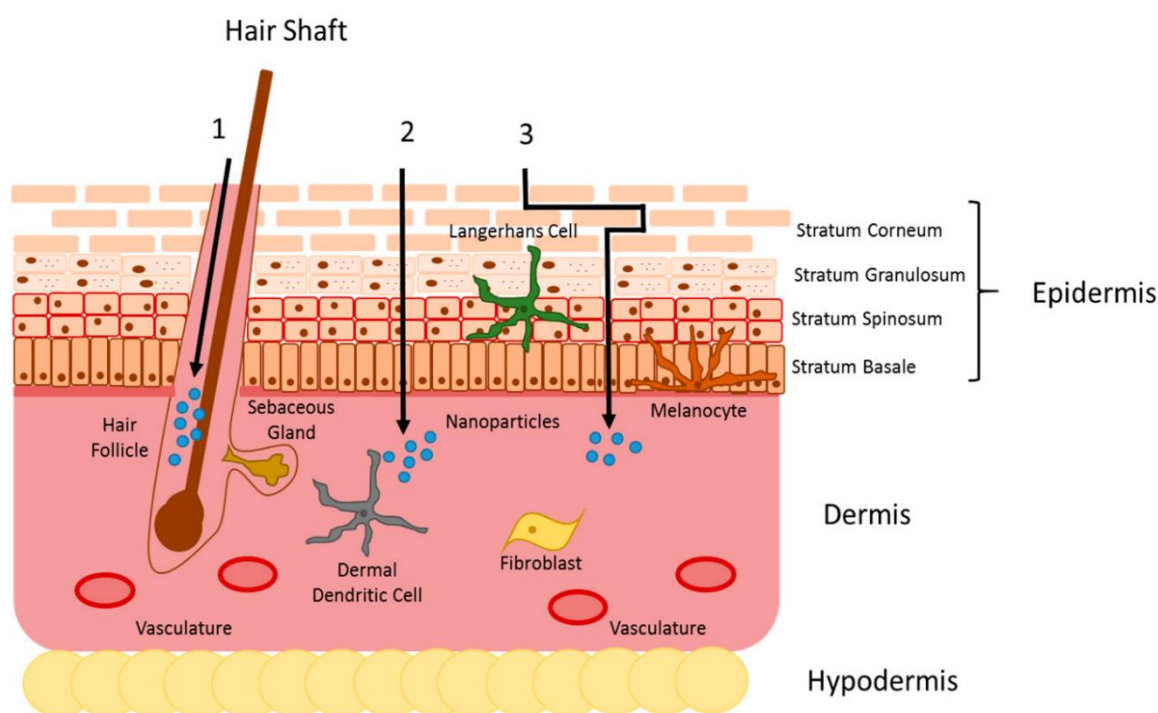

Figure 3-3: Structure of the skin with their three layers (Epidermis, dermis and subdermal tissue). Three possible drug penetration routes are drawn in the figure (1: appendageal, 2: transcellular, 3: intercellular). Reprinted from: "Nanoparticle-Enabled Transdermal Drug Delivery Systems for Enhanced Dose Control and Tissue Targeting"[26] (CC BY 4.0)

Drugs for transdermal delivery have to fulfill certain physicochemical requirements which are particularly limited by the molecule size, limited to approximately 500 Da and a high lipophilicity, with a partition coefficient logP between -1.0 and 4.0. Furthermore, solubility, polarity, melting point (below 150°C) and the daily dose, which should not exceed a few milligrams, have to be considered.[27] Due to this, hydrophilic macromolecules are rather unattractive molecules for transdermal delivery. However, because of the circumvention of the first-pass effect, the painless application and the possibility of a continuous administration over several hours or days with the result of a constant blood level, this route remains of interest and approaches to conquer the skin barrier have been established. Besides the chemical modification of molecules, a co-administration of penetration enhancers can raise the therapeutic efficiency. Here usually solvents, which extract the stratum corneum lipids, and surfactants, breaking the lipid bilayer, are employed. However, with this method the transport is only optimized for relative small and lipophilic molecules in a satisfying manner.[23] Different physical approaches, with the aim of an enhanced permeation have been developed. They include electroporation, which could be utilized for insulin,[28] ultrasound, already used to apply heparin[29] or tetanus toxoid,[30] and iontophoresis, with which the delivery of leuprolide could be achieved *in vitro*.[31] All physical methods in common is the need of a special device, which limits the application to specialized centers and therefore, are not suitable for daily use. Another physical strategy is the creation of micropores, which are considered to not damage the skin in a clinically relevant level and can be used for the delivery of APIs. These pores can be achieved by a laser, used in the delivery of human growth hormone,[32] or by microneedles. Microneedle patches can be designed in different manners and are based on a range of materials. They can be loaded with the therapeutic compounds, or just be used to produce pores for drug transport of NP-formulations.[33] Polymeric NPs are known to accumulate in hair follicles.[34] Several studies showed enhanced blood levels compared to the application of the pure drug.[35] An example would be a transdermal delivery by the use of starch-NPs.[36] The design of very soft and deformable carriers with sizes of approximately 150 nm is discussed to enable the penetration through the stratum corneum. Transferosomes® are one of the very few carrier systems, which succeeded to the market as a commercially available delivery

system through the stratum corneum.[37] Nevertheless, an efficient transdermal delivery still remains challenging.

Inhalative drug application is an attractive route, as it presents a needle free administration, evading the first-pass effect. This results in a large number of preclinical and clinical trials for local and systemic acting medicines.[23] The lung function, which is primarily the gas exchange and as a result the oxygen supply, is ensured by a large surface area of 75 to 140 m².[38] The gas exchange takes place in the respiratory zone, including respiratory bronchioles, alveolar ducts and alveolar sacs. For systemic treatment, the drug has to enter this area too. Therefore, it has to pass the conductive zone branching out from the pharynx and larynx over the trachea, primary bronchi, and bronchioles to the terminal bronchioles.[38] Characteristic for the alveolar region is the thin epithelium of 0.5 to 1.0 µm.[35] To the alveolar side around 90 % of the surface is covered by AT1 cells. A very flat cell type, which is responsible for the gas exchange. Around 7 % are covered by AT2 cells producing the surfactant, which reduces the surface tension. Inhaled albumin, with a relative large molecular weight of 68 kDa, can penetrate through the thin epithelium and was shown to have a maximum plasma concentration (T_{max}) after 20 h.[39] This makes the pulmonary application a very attractive route, not only for local therapy.
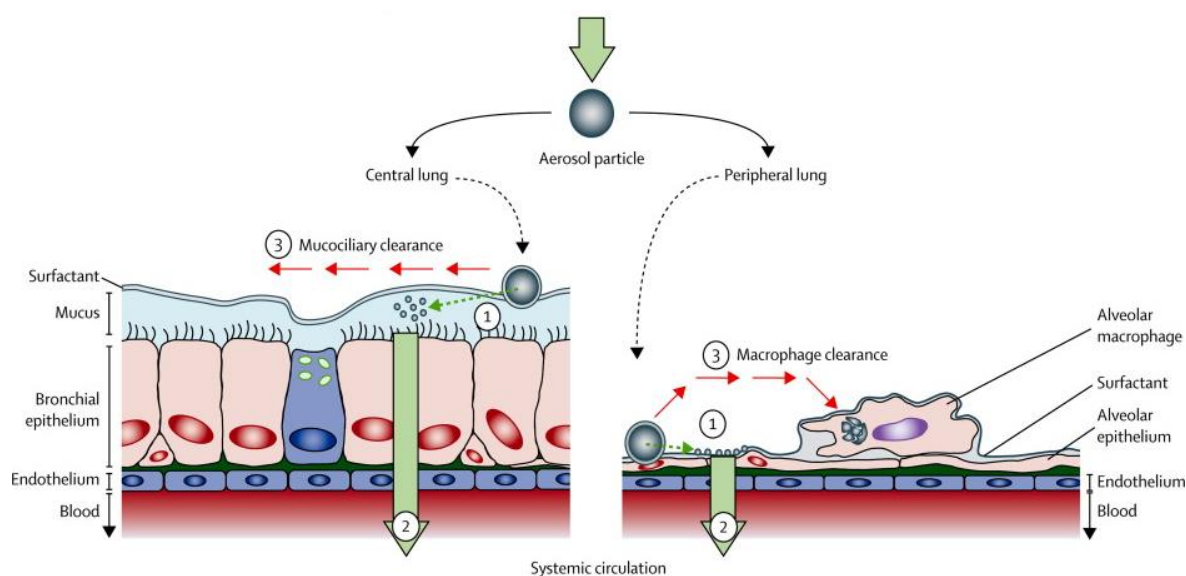
Figure 3-4: Fate of aerosols after pulmonary application. 1) Contact with lung fluid and drug release. 2) API absorption through the epithelium. 3) Undissolved particles can be cleared by macrophages or mucociliary clearance. Modified with permission of: "Pulmonary drug delivery: from generating aerosols to overcoming biological barriers—therapeutic possibilities and technological challenges"[40] Copyright © 2013 Elsevier Ltd.

A critical parameter, highly influencing the deposition site, is the aerodynamic diameter. With deposition maxima for mass median aerodynamic diameter of around 10 nm and

5 μm.[41] The fate of an aerosol after pulmonary deposition, and the different penetration possibilities through the epithelium are shown in Figure 3-4. For dry powder formulations, only the maximum in the micrometer range is used for drug delivery. In order to protect the macromolecule after absorption to the blood stream a popular formulation strategy is the construction of nano-structured microparticles.[42] After disintegration in the lung, NPs can penetrate and protect the loaded drug from degradation. An approach to deliver a greater mass of drug is the application of rod shaped particles, composed of biodegradable and biocompatible materials using the asbestos frays as a model.[43] Even though in the last years plenty of formulations for systemic acting macromolecules made it to the pipeline, there are still challenges to overcome. In particular the mucociliary clearance, the mucus barrier, the limits in dosing and the reduced permeability in diseased and smoking patients have to be named here.[23] After conquering the application barrier, the stability of biologicals is in general relatively low. Enzymatic degradation by peptidases, proteases or nucleases, especially in blood, liver, and kidney is a factor with respect to fast degradation and deactivation of hydrophilic macromolecules.[44] Efflux pumps, like the multi drug resistant protein p-glycoprotein,[45] and fast elimination through the kidney[44] play, together with the enzymatic degradation, an important role to fight against exogenous invasion. Here as well nanoencapsulation is a strategy to protect vulnerable macromolecular drugs. Chemical modification, like the methylene bridge in locked nucleic acid (LNA), can be a possibility to evade degradation, but LNA still lacks from overcoming the lipophilic cell membrane in order to be delivered to the side of action.[46] Nanoparticles can be utilized to overcome this barrier.[47] The interaction of nanoparticles with cell membranes and thus factors how NPs can improve intracellular delivery, will be discussed in detail in chapter 3.2.

An important barrier, protecting the central nervous system, is the blood brain barrier. This barrier is, like the previously discussed ones, an epithelial barrier, which hinders the delivery of APIs to the central nervous system. Nanoparticulate approaches have been developed to surmount this obstacle.[48] Summarizing the challenges in delivery of biologicals, nanoparticulate delivery systems display a promising tool in order to obtain effective treatments: overcoming the main barriers while using the high potency and selectivity of biological drugs.[6]

3.1.2 Delivery Systems for hydrophilic Drugs

As discussed above nanoscale delivery systems can enhance the therapeutic efficacy. Different strategies can be exploited for the design of carrier systems in this size range. To the common colloidal carrier systems belong liposomes,[49] solid lipid nanocapsules,[50] polymer particles, or nanocapsules. Materials for the formation of drug delivery systems (DDSs) should be preferably biodegradable and bioerodible. In addition, a good biocompatibility and low antigenicity is required. It has to be considered that degradation products can exhibit a different toxic potential than the polymer itself. It is important that all arising molecules are nontoxic.[51] The drug encapsulation is highly dependent on the interaction between API and carrier material. The often used poly(lactic-co-glycolic acid) (PLGA), a hydrophobic polymer, which meets the requirements for a good polymer in drug delivery, has the drawback of low loading rates for hydrophilic drugs.[52] Nanostructured hydrogel composites seem to exhibit superior properties for the encapsulation of biologicals. Characteristic for hydrogel NPs is the chemically or physically crosslinked polymer network, hydrated with up to 90 % water, the relative soft mechanical properties and a low interfacial tension to water or biological fluids.[53] Hydrogel NPs can be produced from natural or artificial polymers, both having advantages and drawbacks. Examples for artificial polymers are different methacrylate derivatives, vinyl acetate, different PEG-polymers or betaines.[51] To the frequently used natural derived polymers belong alginate,[54] chitosan,[55] starch derivatives[36] or proteins.[56] Whereas the exact chemical composition and molecular weight can be well-defined and tuned relatively easy for artificial polymers, their monomers do often exhibit a toxic potential. For naturally derived polymers, this is the other way around. They often have relative wide ranges of molecular weights and can show batch-to-batch variations. This can result in less defined particle characteristics, which can be seen for some GNP preparation methods, as there is a relative broad size distribution.[57] The advantage of natural materials is the low toxic potential of degradation products[53] and the renewable resources.[56]

To the large group of protein-based NPs belong animal proteins, like gelatin, collagen, albumin, milk proteins, silk proteins or elastin and plant proteins such as zein, gliadin, soy proteins and lectins.[56] Due to their chemical nature, a hydrophilic backbone with numerous functional groups at the amino acid side chains, they offer a great number of

different loading mechanisms, such as electrostatic attraction, hydrophobic interaction, or covalent binding. In addition, this offers the possibility of various surface modifications, which can be used for a targeted drug delivery. Protein NPs are postulated to show a prolonged half-life time and sustained release. Furthermore, an enhanced stability after application and an increased solubility could be found due to the chemical nature. This can be used for an optimized bioavailability of sensitive and poorly soluble APIs.[56] As the present thesis is primarily interested in investigations on relevant subjects for optimized gelatin-based nanocarriers, the material properties, strategies in the formulation of GNPs and the current application possibilities will be discussed in detail in the following chapters.

3.1.3 Gelatin as Matrix Polymer

Gelatin, a naturally derived polymer, is a hydrophilic macromolecular polypeptide with a relatively wide molecular weight range of 15,000 to 250,000 Da. It belongs to the family of protein polymers and is derived from collagen by alkaline or acidic hydrolysis. The collagen can be extracted from bones, skin, tendons or pork rind. A schematic description of the partial hydrolysis is displayed in Figure 3-5. The sorted triple helices are disbanded during heating and, while cooling, become partially ordered again.
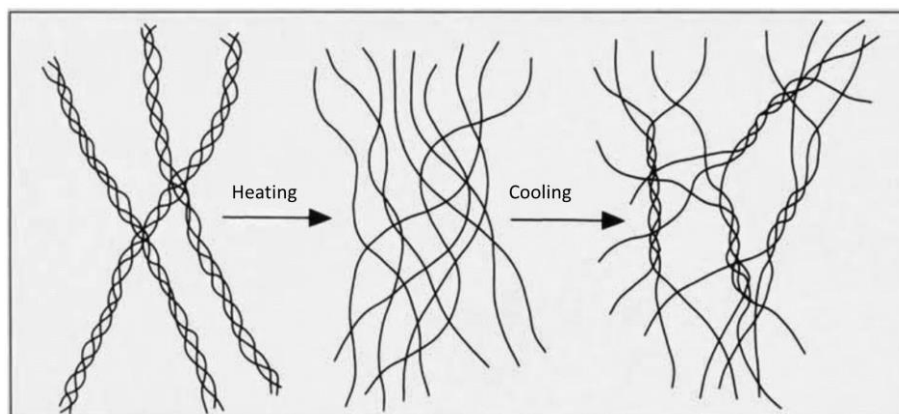
Figure 3-5: Partial hydrolysis of collagen, here by heat; the macromolecular changes are in good consistency to the chemical hydrolysis by acids and bases. Reprinted from: "Gelatin - A versatile biopolymer"[58] Copyright © 1999 - 2018 John Wiley & Sons, Inc.

The numerous possible collagen sources already indicate the broad variety in the collagen structure. All collagen types have the triple helical structure in common but length and position of non-helical areas are dependent on the type. The primary gelatin structure is given by the amino acid sequence, which is slightly different depending on the type of hydrolysis. An overview of the percentage composition is given in Figure 3-6. The

essential amino acid tryptophan is missing. Therefore, two unusual amino acids, 4-hydroxyproline and ε-hydroxylysine can be found in the primary structure. Both are built by posttranslational modifications.[58]
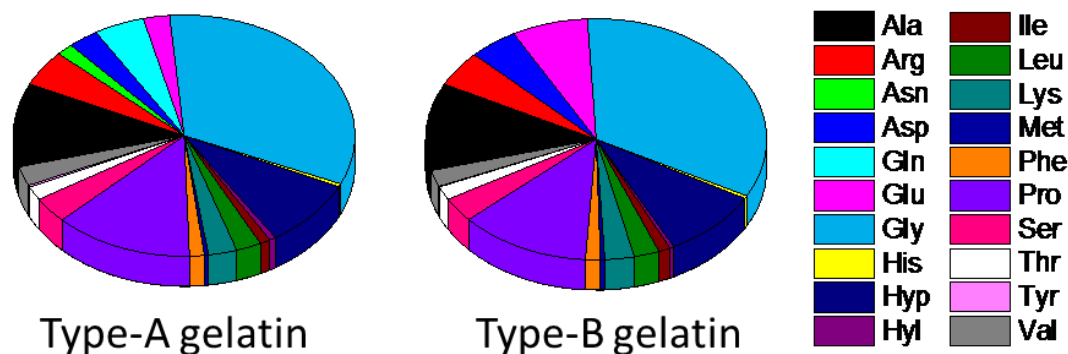
Figure 3-6: Percentage amino acid composition of gelatin One third is made up by glycine, the second third is made up by proline and 4-hydroxyproline. The other amino acids account the remaining ~33 %.[58]

Due to the characteristics of the amino acids, gelatin has cationic and anionic groups alongside with hydrophobic areas in approximately equal ratios. Positively charged areas (~13 %) are built from lysine and arginine, the negative charged sector (~12 %) is composed by glutamic and aspartic acid and the hydrophobic part (~11 %) by leucine, isoleucine, methionine and valine. Glycine, contributing to the structure with one third, forms, in equal amounts with proline and 4-hydroxyproline the rest of the primary structure.[8] An outstanding property is the ability of the thermoreversible gel-sol transition. By cooling a 0.5 % gelatin solution below 35 to 40°C the viscosity is greatly increasing and with further cooling the gel formation can be observed. In the beginning, a helix arrangement takes place driven by an accumulation of individual dissolved α-chains. This is stabilized by hydrophobic amino acids. In a following step, crystal formation can be noted by the accumulation of two and more α-helices. These crystalline areas are in a final step stabilized by the formation of hydrogen bonds inside and in between single helices. Water molecules build additional hydrogen bonds between hydrophilic side chains containing hydroxyl-groups. The temperature of the gel-sol transition is known as the melting or solidification point, which usually is between 30 and 40°C.[58] The gelation strength is a material property, which is indicated with the bloom strength. The European pharmacopoeia knows gelatin type A (partial acid hydrolysis, isoelectric point between pH 6.0 to 9.5) and type B (partial basic hydrolysis, isoelectric point between pH 4.7 and 5.6) and includes, except of the well-known bovine and porcine resources, gelatin obtained

from fishes and poultry. When bones are used for the production, the European Pharmacopeia stipulates that skull and spinal cord have to be removed ahead of the manufacturing process for safety issues. The origin of the raw material should be from a country stated as class I and II in regard to minimize the risk of bovine spongiform encephalopathy. After the extraction, gelatin has to be sterilized before the use as pharmaceutical excipient is allowed.[59] The biocompatibility is underlined by the classification as GRAS material by the FDA.[7] The peptide bonds can be enzymatically cleaved into the amino acids, which are then metabolized into carbon dioxide, water and urea.[60] Gelatin is used in pharmaceutical formulations for oral application as wall forming excipient in capsules, agglutinant in granules or for the encapsulation of oleic products. The application goes beyond the oral administration route. Gelatin can be also found in emergency surgery as plasma expander[61], in a hydrolyzed non gelling form as additive in vaccines[62], as gel foam in surgery for wound absorbable dressings (Gelfoam®)[63] and in micro capsulate formulations with sustained release for example in Lupron Depot®.[64] Due to its hydrophilic properties, the biocompatible and biodegradable characteristic, and the easy and cheap availability gelatin is a well-researched polymer for micro- and nanoparticle formation.

3.1.4   *Gelatin Nanoparticles as Carrier System for Hydrophilic Macromolecules*

This versatile polymer brings ideal characteristics for the preparation of NPs for the use as drug delivery system. First attempts have been reported in 1978 for gelatin nanoparticles[57] and 1985 for nanocapsules formed by gelatin.[65] Up to now numerous works were performed to obtain improved particle characteristics and to develop various methods for the formation of gelatin nanoparticles. Desolvation by the addition of agents like acetone or isopropanol, which dehydrates the gelatin and forces the formation of coils, was the first approach. Due to the relative broad distribution of molecular weights in gelatin this method results in inhomogeneous particle sizes.[57] An improvement of this technology is the two-step desolvation by Coester *et al.* where gelatin strains with a high molecular weight are precipitated in a first step in order to remove low molecular weight gelatin. After separation the gelatin is redissolved and in a second desolvation step NPs with a narrow size distribution were achieved.[66] This relative complex and time consuming procedure was further improved by Ofokansi *et al*. By adjusting the pH and the temperature the initial desolvation step could be skipped.[67] Other important

preparation techniques are the emulsification-solvent evaporation,[68] the coacervation-phase separation,[69] reverse phase microelmulsion,[70] self-assembly after chemical modification with molecules like polyethylenglycole (PEG)[71] or hexanoyl anhydrides.[72] Another method, which was used in the present thesis too , is the nanoprecipitation, or solvent displacement method.[73] This straight forward and fast method was originally developed for hydrophobic polymers,[74] but got adopted for the production of hydrophilic nanoparticles made by polyvinylalcohol (PVA)[75] or gelatin.[73] A closer look to the principle of nanoprecipitation follows, as this was the technique of choice for the production of cGNPs in the present thesis. The method is based on two miscible solvents. In one the polymer is dissolved and in a second solvent, in which the polymer has to be insoluble, called the nonsolvent, a stabilizer is dissolved. The nonsolvent has to be present in excess. In this way, the polymer remains insoluble in the mixture too. The polymer solution is now added to the nonsolvent. Due to the miscibility of the solvents small polymer containing droplets arise. This spontaneous reaction is also named the "Ouzo-effect" a liquid-liquid droplet nucleation caused by a supersaturation, which is describing the turbidity of the Greek beverage "Ouzo".[76] Driven by diffusion the solvents start to mix and the polymer in the droplet becomes insoluble as the saturation concentration is reached. The values of supersaturation, the interfacial tension, the diffusion coefficients during nucleation, growth and the Ostwald ripening influence the final particle size, the concentration and the polydispersity of the particle formulation.[77] An additional influence has the polymer concentration in the solvent and the solvent to nonsolvent ratio.[78] Furthermore, the type of solvent plays an important role on the mean particle size. Here the viscosity and diffusion coefficient of the solvent in the nonsolvent seem to be important parameters. The mixing time, easily tunable in microfluidic systems, has an impact on the particle size too. Shorter mixing times result in smaller NPs diameters.[79] The use of stabilizers in the nonsolvent solution prevent the freshly formed particles from coalescense.[77] All different production approaches for GNPs in common is the need of crosslinking to obtain stable nanoparticles.[8] A crosslinked gelatin matrix, as well as a closer look on a crosslinker bond by glutaraldehyde, is outlined in Figure 3-7. Different chemical compounds are customarily used for this purpose. Carbodiimides in combination with N-hydroxysuccinimide were successfully used for the stabilization of GNPs.[80] Another possible substance is genipin.[81] This compound, derived by extraction from the gardenia

fruit covalently connects two primary amino functions provided from the amino acid lysine.[82]
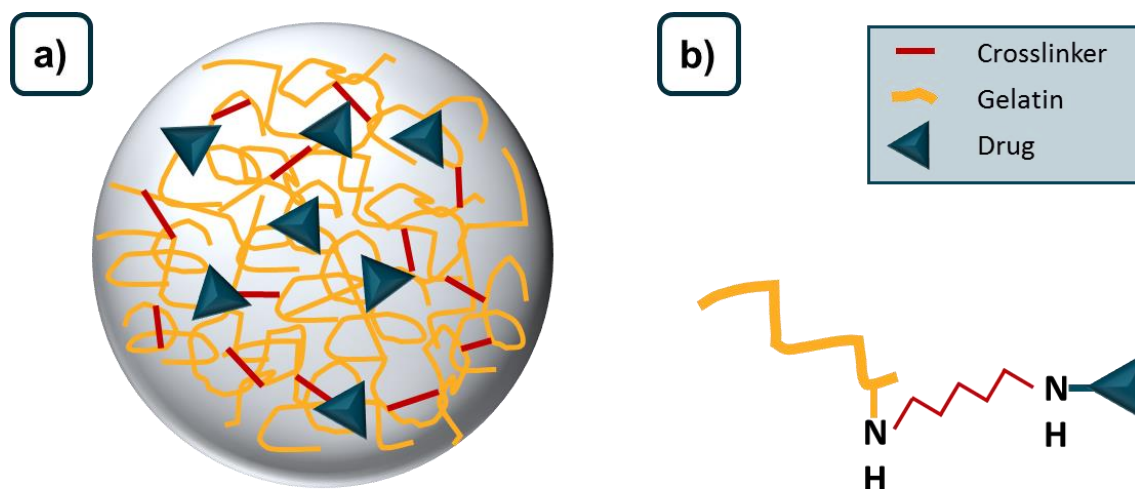

Figure 3-7: Sketch of a gelatin matrix particle after crosslinking in A and in B a zoom to a glutaraldehyde crosslinking

Enzymatic crosslinking was achieved with microbial transglutaminases connecting a primary amine with an amide of glutamine.[83] The most popular group of crosslinkers are aldehydes. Dialdehydes connect two primary amino groups of lysine and hydroxylysine. Glutaraldehyde, which is used in the present thesis too, is a non-zero length crosslinker. For acid reaction conditions, a crosslinking mechanism involving the hydroxyl groups of proline and hydroxyproline is discussed. However, in the present study a neutral pH was used for this reaction, which should involve two primary amino functions and therefore, form a Schiff base during the crosslinking process.[84] The chemical reaction is shown in Figure 3-8.
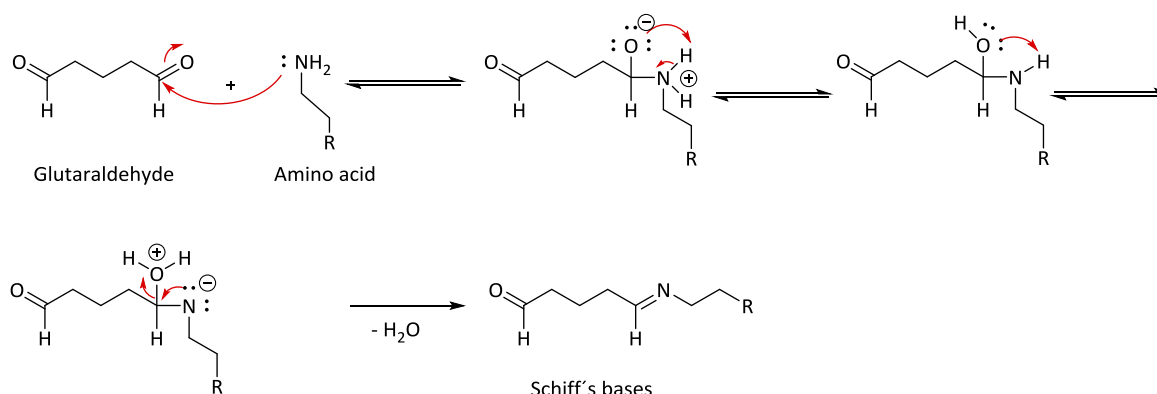

Figure 3-8: Crosslinking mechanism of glutaraldehyde und the formation of a Schiff base, which causes autofluorescence of GNPs.

The creation of the Schiff base causes an autofluorescence of cGNPs, which can be used to monitor the fate of GNPs in cells.[85] A less toxic representative of the aldehyde group is

glycerylaldehyde. Crosslinkers commonly have unspecific chemical reaction. In this way intra- and interchain connections are built to stabilize the freshly prepared nanoparticles. In case of the encapsulation of drugs, providing the same functional groups, they can be bound covalently to the matrix and subsequently are trapped in there. To prevent the inactivation of the loaded API more recently an alternative stabilization method for GNPs was investigated. Kahn *et al.* embedded freshly prepared GNPs in a Eudragit® E matrix.[10] Eudragit® E, a methacrylic-acid derivate, limits the application, of the nanoparticle formulation, as the polymer is soluble at pH <5.0 and it is not biodegradable.[86] Adjusting the materials to exclusively use biodegradable and biocompatible materials is part of the present thesis.

Gelatin expresses sequences like Arg-Gly-Asp (RGD),[87] which binds specifically to $\alpha_v\beta_3$ integrin, a transmembrane receptor of the integrin family. The receptor is overexpressed in tumor tissue and is, amongst others, responsible for cell adhesion. GNPs can be used for a targeted drug delivery to tumor tissues using RGD.[88] Gelatin nanoparticles are utilized for the delivery of a broad range of APIs such as anticancer drugs,[89] anti-viral APIs like stavudine, a drug used in HIV therapy,[90] antibiotics,[91] proteins such as insulin for oral delivery[92] or tetanus toxoid in vaccines.[93] The versatility of application possibilities demonstrate the high potential of gelatin nanocarriers in disease treatment.

3.2 Nanoparticle Properties Influencing the Fate after Administration in Drug Delivery

A multitude of particle properties is influencing the interaction of NPs with cells *in vitro* and, for a drug delivery system far more important, the fate after *in vivo* application.
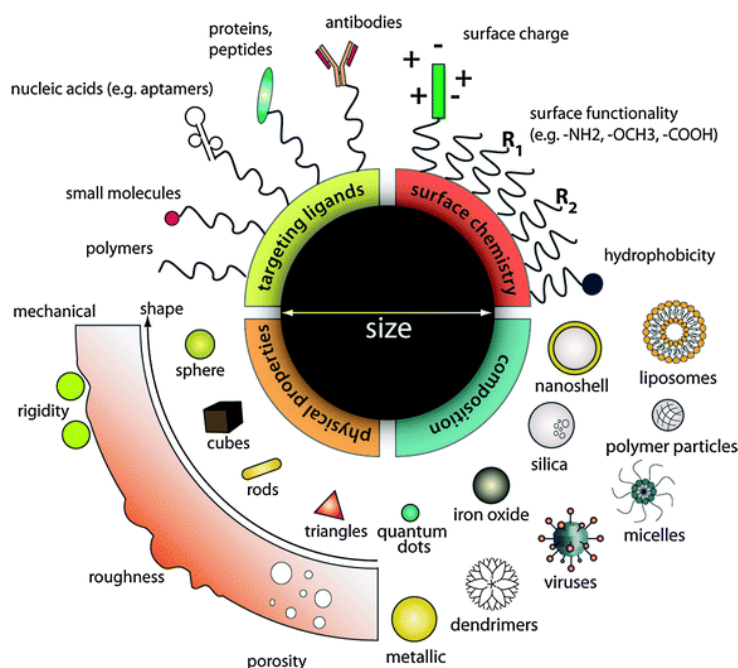

Figure 3-9: Possible strategies in carrier design for a targeted delivery in therapy and diagnostics. Reprinted from: "Strategies for the intracellular delivery of nanoparticles",[94] Copyright © 2010 Royal Society of Chemistry

Hence, the biodistribution and bioavailability is highly influenced by particle attributes, different strategies have been developed in order to create successful drug delivery systems. Figure 3-9 represents an illustration of influencing factors for the interaction of carriers and cells. In the following section, several of these parameters will be highlighted.

3.2.1 Size of Nanoparticles

The size of nanoparticulate formulations ranges from few nanometers to several hundreds of nanometers. Looking at *in vitro* processes the internalization into cells is, besides others, a size dependent process. In Figure 3-10 different routes of cellular uptake are summarized. Particles in the micrometer scale are taken up by phagocytosis or micropinocytosis. Clathrin-mediated endocytosis is the most reported internalization route for receptor mediated uptake of positively charged NPs with a diameter of around ~100 nm.[95] Its primary function is the nutrient uptake in eukaryotic cells and in addition, it is used for internalization by several viruses.[96]
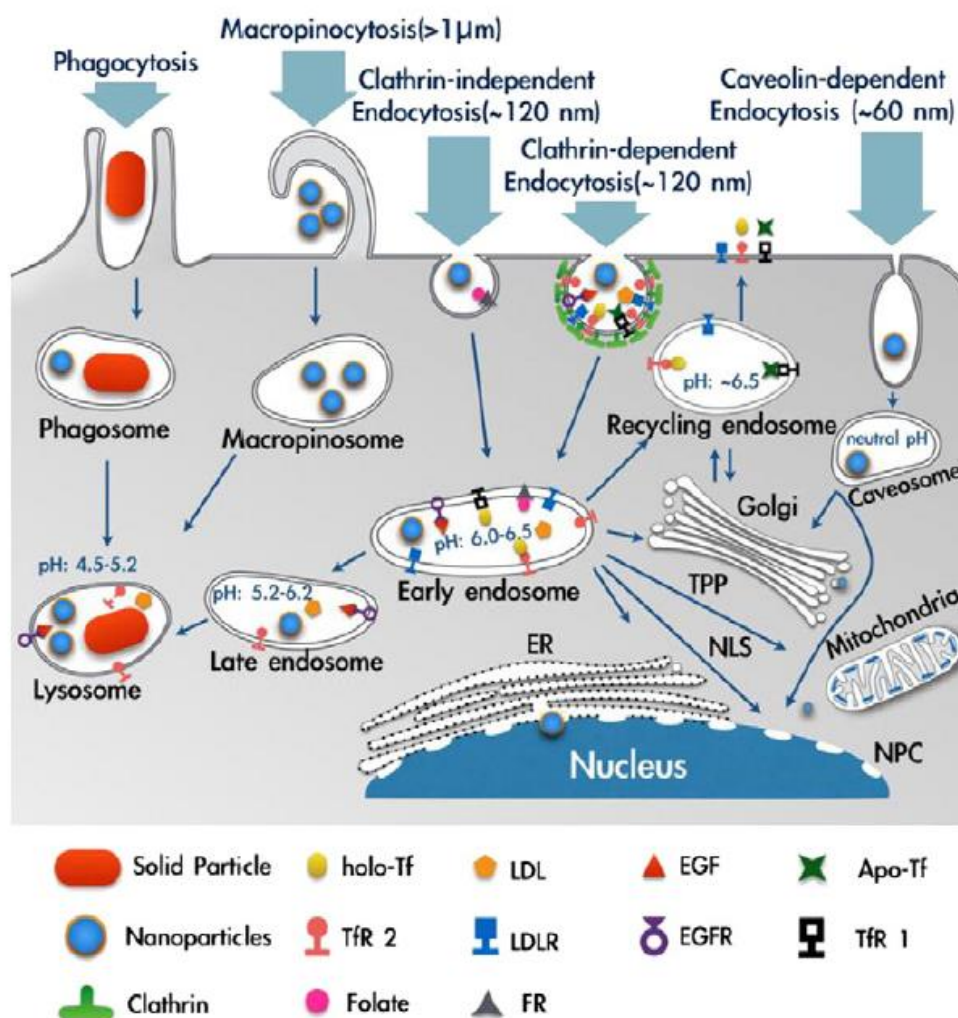
Figure 3-10: Possible cellular uptake mechanisms depending on the particle size. Reprinted from: "Targeting receptor-mediated endocytic pathways with nanoparticles: Rationale and advances", Copyright © 2012 Elsevier B.V.

Caveolin dependent endocytosis is the pathway for particles ranging in the size of around 60 to 80 nm. In this signal regulated mechanism the particle becomes coated by caveolins, a hairpin-like structure. Caveolae are small flask-like shaped invaginations in the cell membrane. They can be found in endothelial cells, adipocytes, fibroblasts and smooth muscles.[97] Furthermore, caveolae are associated with transendothelial transport and release of NPs in the subendothelial tissue.[98] Larger particles are taken up either by micropinocytosis or phagocytosis. Micropinocytosis, a process driven by actin, includes the uptake of external fluid. The vesicles are formed by an extension of the membrane and have a size of 0.2 to 5 μm.[99] It is mediated by growth factor receptors as well as particles like viruses, bacteria, apoptotic and necrotic cells.[100] Through the pathway of phagocytosis, usually responsible for the cellular uptake of pathogens and dead cells, material up to 10 μm can be internalized. The emerged phagosome adopts the shape of

the enclosed substrate.[96] Phagocytosis is mediated by receptors and can take place at several cell types such as epithelial cells,[101, 102] fibroblasts[103] and various immune cells.[104] NPs with sizes between 10 and 60 nm seem to be taken up to a greater amount.[105]

Besides the effects on the cellular level a number of factors, influencing the NPs fate after administration, are size dependent. Particles smaller than 6 nm undergo renal clearance from the blood by glomerular filtration and tubular excretion.[106] Particles with larger diameters are accumulated in spleen and liver to a greater amount. J.M. Caster *et al.* demonstrated a size dependent accumulation for particles between 50 and 150 nm.[107] In general particles with a diameter lager than 200 nm are known to be trapped in liver and spleen and subsequently processed by cells of the mononuclear phagocyte system (MPS).[108] Due to fenestrations in the endothelial blood vessel cells, nanoparticles of a size between 30 and 200 nm can penetrate to tumor tissue and accumulate there. This passive drug targeting is known as enhanced permeation and retention (EPR) effect and is used for contrast agents and anticancer treatment. After extravasation, small particles of around 20 nm diffuse deep in the tumor tissue, but are cleared from the tumor after 24 h, whereas bigger particles cannot pass through the extracellular matrix and remain close to the blood vessel.[109] As blood vessels in healthy tissue form openings in the size of 10 nm this size should be exceeded if NPs size is used for passive drug targeting.[110] Highlighting the delivery to the brain it seems that NPs of a size <50 nm can pass the blood-brain barrier.[105] Regarding the sizes and *in vivo* distribution the formation of a protein corona, which can change the particle size after administration, should always be considered.[108] A closer look to this phenomenon can be found in chapter 3.2.3 All these size depended events lead, together with other factors, to a broad variance in blood retention half times.[111]

3.2.2 Carrier Shape

The vast majority of nano- and microscale carriers are formed in a spherical shape. Under the first investigations of *in vitro* macrophage interaction with differently shaped carriers is a study from Champion and Mitragotri.[112] As can be seen in Figure 3-11 is the successful phagocytosis and the internalization speed dependent on the radius of the particle´s curvature at the first contact between macrophage and carrier.[112] In follow-up studies the efficacy of cell adherence could be ranked according to the shape in the order

elongate > oblate > sphere. However the internalization showed a divergent pattern following oblate >> sphere > elongate.[113]
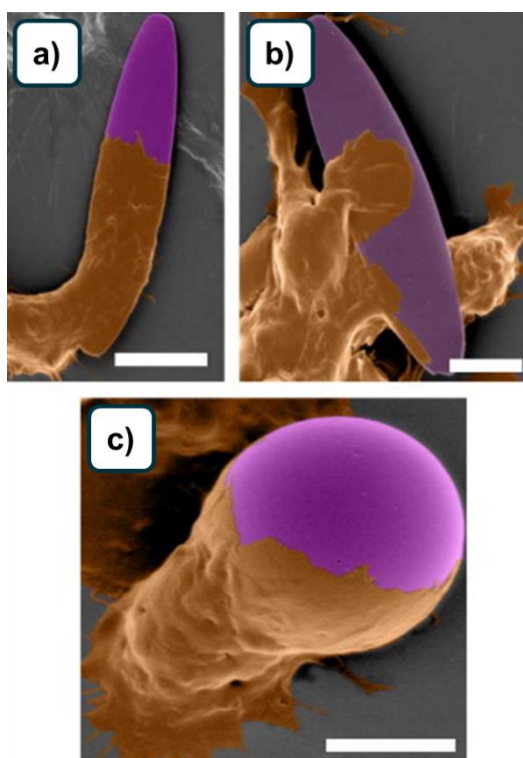

Figure 3-11: Colored SEM images of macrophages in brown and microparticles in purple. a) Elliptical disks which got in contact with the high curvature side. (Scale bar = 10 µm.) b) A macrophage attached to the flat side and is not able to phagocyte the disk. (Scale bar = 5 µm) and c) is showing a spherical microparticle after half phagocytosis. (Scale bar = 5 µm) Reprinted from: "Particle shape: A new design parameter for micro- and nanoscale drug delivery carriers"[112] Copyright © 2007 Elsevier B.V.

For extreme aspect ratios, resulting in worm-like or needle-like structure, a failure in phagocytosis was demonstrated. This can be used to circumvent macrophage clearance.[114] Smaller particles seem to exhibit a less consistent behavior. Kinnear *et al.* explained this with the variety of materials, sizes, surface chemistry and the differences in cell types. However, for particles of a size range from 100 to 800 nm the trend shows a preferable uptake for disks in comparison to spheres.[114] Following the interaction route, objects in the size range of around 20 nm, were found to have a stronger association with HeLa cells in disc shape. Despite this, spherical particles have been internalized to an greater amount.[115] Particles obtained by the PRINT®-technique have been used to study different aspect ratios and cubes. The particles with the highest aspect ratio showed the fastest uptake. This is explained by the higher surface area leading to more interaction with the target cell.[116] Decuzzi *et al.* studied the *in vivo* distribution of cylindrical, discoidal, hemispherical and spherical SiO_2 nano-objects and found a reduced amount of discoidal carriers in the liver. The high amount of this shape in organs like the lung or

heart is explained by the evasion of clearance by Kupffer cells after retention in the liver.[117] So-called filomicelles with a cross-section between 26 - 60 nm and a length from 2 to 18 μm have been proven to persist significantly longer in blood circulation of mice and confirm previous findings about an altered biodistribution profile.[118] Beyond this, shape and size of gold NPs have been found to be related with the antibody formation when used as adjuvant in vaccines. The efficacy could be inversely related to the specific surface after comparing spheres and rods with diameters of 20 and 40 nm respectively.[119] In our lab the shape effect of microrods is used for pulmonary delivery. Kohler *et al.* developed a template assisted method to produce nanostructured microrods of a well-defined size and aspect ratio,[120] which have subsequently been developed and recently showed to be able to target pulmonary macrophages in order to manipulate them in the context of immunodesease.[121] These studies show the ability of improving the efficacy of carrier systems by a careful selection of the shape, alongside with the other physicochemical parameters, in the accordance to the target side.

3.2.3   Surface Chemistry

The *in vitro* uptake rate of nanoparticles was shown to be faster for positively charged NPs in comparison to particles with a neutral or even negative surface charge.[122] Electrostatic interactions between the negatively charged cell membrane and the carrier system are postulated to be responsible for this diversity. In addition, positively charged chitosan NPs have been proofed to be able to be released from the lysosome, after phagocytosis, whereas particles with a neutral and negative surface charge remained in there.[123] In a recent study it could be shown that a change of surface decorating molecules alters the deposition and the cellular internalization after convection-enhanced delivery to rat brains. This can be used for a targeted delivery to tumors.[124] Surface decoration by coupling of various molecules such as antibodies, carbohydrates or tumor markers is a popular method to biofunctionalize NPs. In Figure 3-12 the most common strategies are summarized. Peptides can be used to enhance the delivery into the cytoplasm and cell nucleus, but as well for an aimed accumulation in specific tissues. Magnetic NPs, presenting antibodies or antibody fragments on their surface, can be used as *in vivo* diagnostic tools.[125]
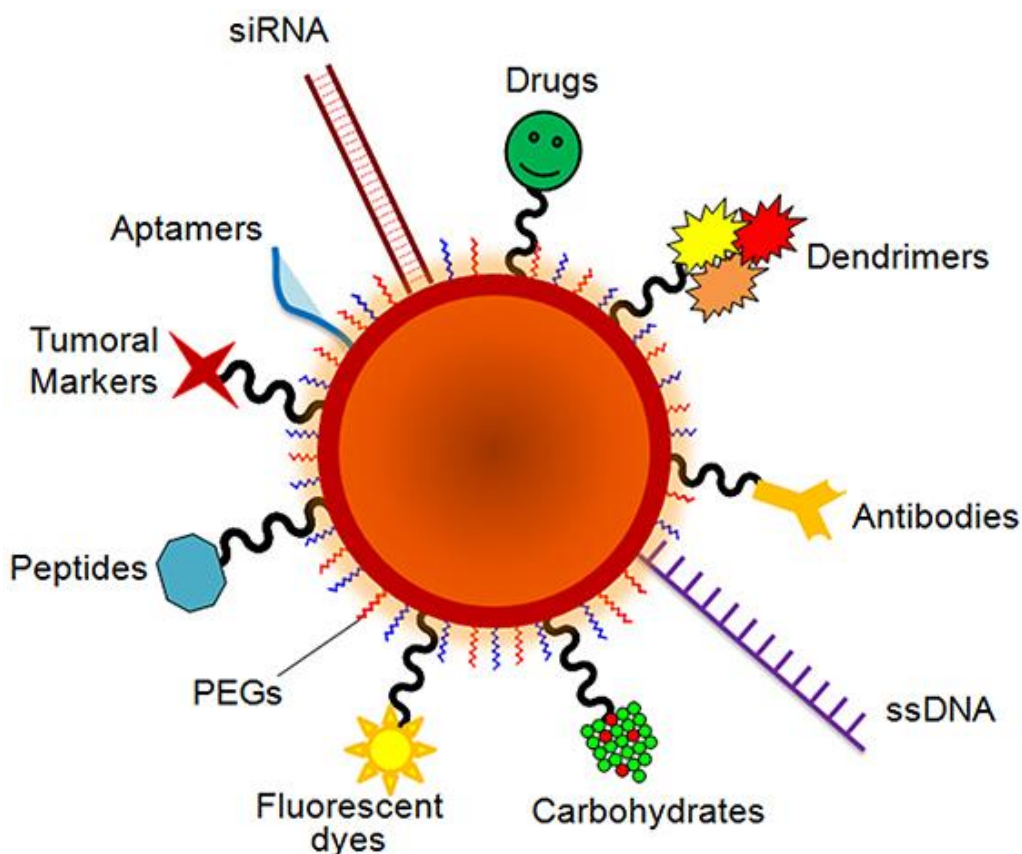
Figure 3-12: Common surface functionalization methods to enhance the efficacy of nanoparticles in drug delivery and diagnostics by a targeted NP delivery and prolonged blood circulation. Reprinted from: "Revisiting 30 years of biofunctionalization and surface chemistry of inorganic nanoparticles for nanomedicine"[125] Copyright © 2014 Conde, Dias, Grazú, Moros, Baptista and de la Fuente;

After invading in an *in vivo* system NPs come in contact with liquids of complex composition no matter which administration route was chosen. Proteins and apolipoproteins are known to interact with nanomaterials and form a protein corona, which affects the particle size but also the surface composition and the recognition by the immune system.[126, 127] Different approaches are used to avoid, or at least minimize, the interaction with proteins and clearance strategies after administration. The most popular strategy for sure is the formation of so-called stealth-particles. Composites with a PEG decorated surface showed a prolonged circulation time when a dense PEG-chain pattern could be achieved.[128] Yang *et al.* showed a reduced macrophage phagocytosis and unspecific interaction with red blood cells (RBCs). The *in vivo* distribution was highly dependent on the molecular weight of the PEG chains and needs to be relatively high for a successful circulation prolongation.[129] Other studies, examining the difference in the protein corona composition, showed a higher content of complement and coagulation proteins for PEGylated poly(glycidyl methacrylate) NPs, whereas the apolipoprotein

content was significantly decreased.[130] An innovative strategy to produce long circulating NPs is the formation of zwitterionic surfaces. This could be shown to protect NPs from cell uptake and reduce the plasma protein interaction with the formulation.[131] In order to obtain increased delivery efficiency, the surface properties have been further improved, to achieve a trigger-related change in the surface charge. During their blood circulation, the zwitterionic properties are of high advantage. The lower pH in tumor tissues, caused the formation of cationic particle interface, results in an improved cell uptake.[132] All these studies show the importance of a carefully designed particle surface, according to the targeting side, to obtain an effective delivery system.

3.2.4 Mechanical Properties

The impact of the mechanical carrier properties just gained attention in the last decade. Although it is a particle characteristic, about which the knowledge is up to now relatively low, its influence is as important as other particle properties. Looking in detail to the *in vitro* interactions, an enhanced and faster uptake for particles with a higher elastic modulus, possibly calculated as Young´s modulus, can be seen.[133] In more detail, Banquy *et al*. studied the effect of mechanical properties in macrophage cell uptake with NPs made by N,N-diethyl acrylamide and 2-hydroxyethyl methacrylate with hydrodynamic diameters of 150 to 170 nm and Young´s moduli from 18.08 to 221.39 kPa. By the use of specific inhibitors for different uptake mechanisms, a correlation between the mechanical properties and the uptake route could be achieved. While hard particles have been predominantly taken up by a clathrin-mediated process, soft particles have been preferentially absorbed by micropinocytosis and particles of intermediate Young´s moduli showed multiple uptake routes resulting in an overall higher uptake.[134] Other studies, investigating in the role of NP uptake by macrophages, demonstrated a higher uptake of stiffer particles.[9, 135] The same tendency can be found in endothelial cells where a higher uptake into human lung microvascular endothelial cells (HMVEC)[136] and human umbilical vein endothelial cells (HUVEC)[137] was reported. Even though other studies showed more diverse results the majority of investigations confirm the higher and more rapid uptake of harder NPs into endothelial cells.[133] A pronounced heterogeneity in the results can be found for cancer cells, typical target cells for nanoparticulate drug delivery.
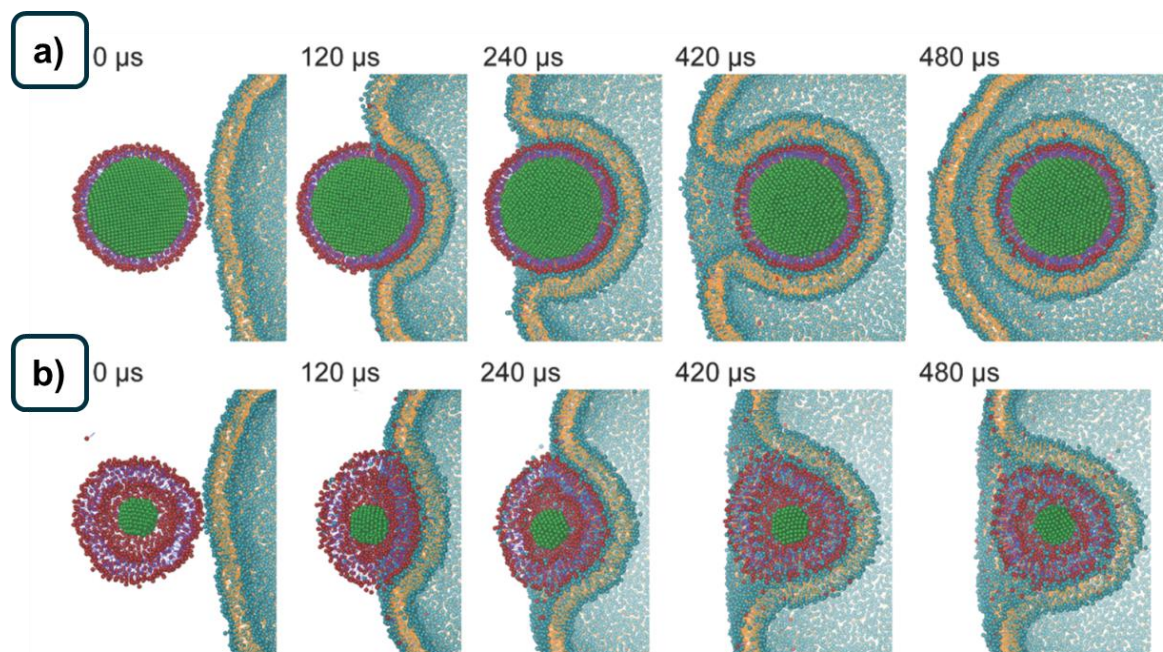
Figure 3-13: Model of the uptake of rigid NPs in a) and soft NPs in b) showing the particle deformation during cell wrapping for soft particles. Rigid particles are completely internalized whereas soft counterparts are trapped at the cell surface. From "Tunable Rigidity of (Polymeric Core)–(Lipid Shell) Nanoparticles for Regulated Cellular Uptake"[137] Copyright © 1999 - 2017 John Wiley & Sons, Inc.

Here the variation in cancer cell types and in the absolute Young´s moduli of the investigated NPs can explain the broad distribution in findings.[133] Taking into account shape and mechanical properties Alexander *et al.* compared the uptake of hard and soft, cubic and spherical nanosized carriers with the result of an enhanced uptake for cubic particles in comparison to spheres. In both cases the uptake was higher for the more rigid formulation.[136] Simulations of NPs uptake, investigating in the wrapping process, postulate a full and faster cell membrane wrapping for stiff particles, whereas softer particles might even only be wrapped partially due to particle deformation during the uptake process. This is explained by a lower adhesion energy needed for the uptake of stiffer particles.[138] The postulated carrier deformation during membrane wrapping is illustrated in Figure 3-13.[137] Anselmo *et al.* showed a prolonged *in vivo* circulation time for softer hydrogel NPs composed of poly(ethylene glycol) diacrylate (PEGDA) with different polymer volume fractions. They produced NPs with a size of around 200 nm and bulk moduli ranging from 10 kPa to 3 MPa. The distribution half-life (α^{-1}) was 1.48 h for soft and 0.11 h for hard particles in mice. Same tendency was seen in the elimination half-life (β^{-1}) with 61.4 h and 9.7 h respectively. This is resulting in a longer circulation time in the blood for softer particles. After 12 h the differences in the organ distribution were nearly adjusted.[9] In another study Merkel *et al.* studied the effect of elastic properties of 6 µm-

sized microparticles mimicking the shape of red blood cells produced by the PRINT® technology. Particles with a Young´s modulus of 7.8 kPa showed a 30 times longer blood circulation time in mice then their stiff counterparts with a Young´s modulus of 63.6 kPa. The biodistribution into tissue, here measured after 2 h was found to be highly dependent on the elastic modulus too. Softer particles penetrated less into the lung and in addition, harder particles triggered pulmonary embolism, which couldn´t be found in animals treated with the softer particles.[139] A third study, which has to be mentioned here, is about a soft NP formulation, which shows a low accumulation in the spleen. Zhang *et al.* designed soft zwitterionic NPs composed of poly(carboxybetaine) and poly(sulfobetaine) with a particle size of around 250 nm. The bulk moduli are ranging from 0.18 to 1.35 MPa. The circulation half time, calculated by a one-compartment model, was between 9.1 and 19.5 h with a longer circulation for the softer NPs. A lower splenic filtration is postulated underlined by an *in vitro* model mimicking the filtration process. The biodistribution after 48 h showed the lowest accumulation in the spleen for the softest particles, whereas these NPs have been found in the highest concentration in the blood. All other organs seemed to uptake equivalent particle amounts.[140] The trend of an prolonged blood circulation time, which is seen by other studies too,[133] can be used in drug delivery for a longer drug release in blood vessels and an enhanced delivery to the target side and therefore, a more effective drug delivery. Beyond the prolonged circulation time could a reduced accumulation in different tissues minimize side effects and could, through a lower accumulation in the liver, avoid the elimination by MPS associated cells can.[141]

4 Aim and Scope of the Thesis

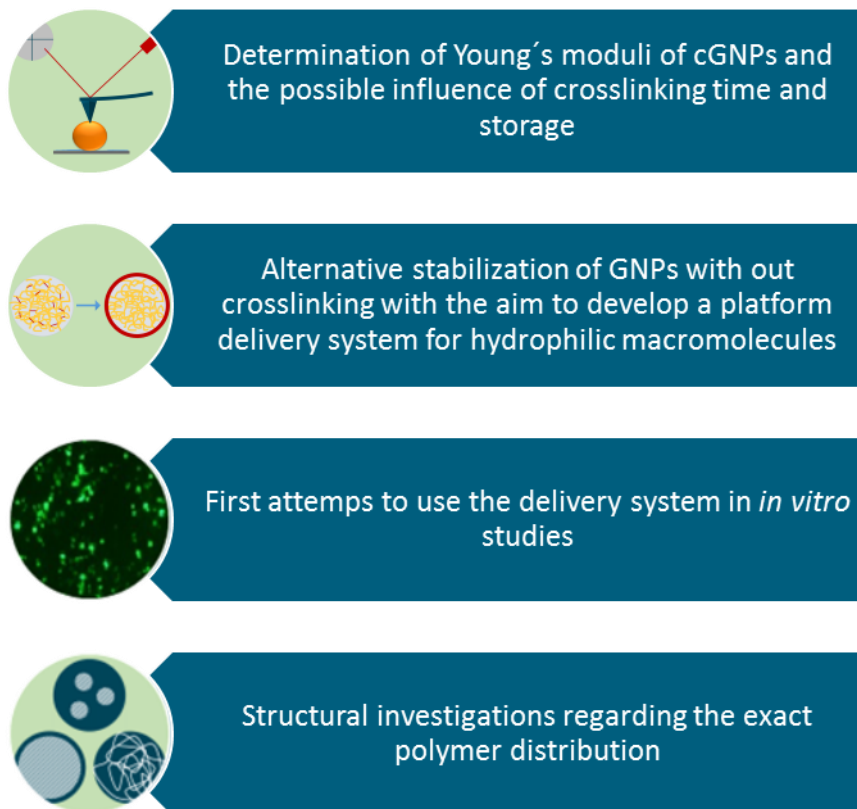The aim of the present thesis is divided in four work packages. In Figure 4-1 the milestones are summarized briefly.

Figure 4-1: Overview over the four milestones addressed in the present thesis.

The first work package, dealing with the investigation in Young´s moduli of cGNPs, is presented in its own chapter (Chapter 5 Elasticity Determination of Gelatin Nanoparticles). The need of these investigations is based on the influences of elasticity in regard to cell internalization *in vitro* and biodistribution *in vivo*.[9] Although cGNPs are of high interest in pharmaceutical research and have, due to their characteristics, a high potential to be used in therapy as a drug delivery system, nothing is known about their mechanical properties and how they can be influenced. Here studies are performed to obtain first insights into the subject.

Gelatin as drug delivery system has several outstanding advantages, beside the very good loading rates, which can be up to 80%, it shows excellent characteristics as a particle forming polymer. Nevertheless, commonly used systems are stabilized by a crucial crosslinking, thus the cargo can be coupled with the particle, which can destroy their efficacy. This substantiates the need of a new formulation stabilizing GNPs in an innovative way. Therefore, a formulation process with a coating or embedment of the

freshly produced GNPs in Eudragit ® E100 has been developed. In the selection of the used materials, an exclusive use of biodegradable and biocompatible materials was intended for a possible application in drug delivery. Thus PLGA was chosen as a coating polymer well-suited with respect to its degradation profile.

The third work package demonstrates the *in vitro* testing to evaluate the GNP based system in terms of toxicity, drug load and the use as non-viral transfection vector in gene delivery. Here the drug delivery system was tested in regard of LNA encapsulation as well as transfection with plasmid DNA.

The final work package investigates the determination of the exact inner structure of the final formulation. To know about the inner structure and the polymer distribution within a particle is an important part of the development of new formulations and helps to understand and eventually even foresee the particle characteristics. The results give feedback to the development. Thus, the evaluation of new analytical methods, such as energy filtered transmission electron microscopy, for the determination of the particles´ structure, could be used for an eventual further improvement of the platform technology.

5 Elasticity Determination of Gelatin Nanoparticles

5.1 Introduction

The importance of mechanical properties on the *in vitro* and *in vivo* fate of carrier systems is discussed in chapter 3.2.4.[133] Although, as discussed in chapter 3.1.4, GNPs exhibit excellent characteristics as carrier systems for the already popular and still aspiring group of hydrophilic macromolecular APIs,[8] nothing is known about the mechanical characteristics and the possibility to influence them. This is even more surprising as varying the crosslinking density is a common approach for the production of NPs with different elastic characteristics.[133] This was already proven to be a possible parameter to adjust the elastic properties of crosslinked gelatin gels.[142] In order to promote the development of targeted drug delivery based on cGNPs, the aim of the following study was to obtain first insight into the characteristics of GNPs and moreover to test the influence of different crosslinker incubation times on the elasticity measured as Young's modulus. To complete the study the influence of storage at 4°C was evaluated. The determined change in the Young´s modulus was used in a follow up investigation to evaluate the relevance in biological systems.

5.2 Experimental

5.2.1 Materials

A detailed list of the used chemicals and devices is attached at the end of this thesis in chapter 9. Gelatin, as protein based, hydrophilic particle forming biopolymer, is already described in 3.1.3.

5.2.2 Fabrication of Crosslinked Gelatin Nanoparticles

Crosslinked gelatin nanoparticles (cGNPs) were produced with the nanoprecipitation method which, whose principle was described in chapter 3.1.4. Gelatin was dissolved in deionized water at 50°C under continuous stirring. To form NPs 1 ml solution, containing 20 mg gelatin, was dropped slowly and under continuous stirring at 750 rpm into the antisolvent, which consists of 15 ml acetone containing 1 ml deionized water and 2.81 % (w/V) poloxamer 188 as stabilizer. To obtain stable NPs the freshly formed particles were crosslinked with 500 µl of a 1.85 % (w/V) glutaraldehyde in acetone solution containing 5.55 % water. The cross linker needs to be added very slowly to prevent the irreversible

formation of gelatin aggregates. Glutaraldehyde was incubated for 3, 6, 15 or 18 h and the so gained cGNPs were purified three times by centrifugation at 10,000 g for 10 min at 15°C.

5.2.3 Size and Zeta Potential of Gelatin Nanoparticles

Determining hydrodynamic diameters, size distribution and surface potentials are relatively fast measurements for initial particle characterization and therefore an efficient method to control and monitor production processes. Furthermore, as described in chapter 3.2, particles´ size and ζ-potential have a high impact on the drug delivery characteristics of NP-formulations. The hydrodynamic diameters and size distribution are determined by dynamic light scattering (DLS) which can also be referred to photon correlation spectroscopy too. The method makes use of the Brownian motion of particles below 5 μm suspended in a liquid. This suspension is illuminated by a monochromatic laser beam. The light is scattered by the particle motion which is related to the particle size. When the light hits a moving particles a slight shift in the wavelength occurs which causes a small Doppler shift,[143] a slight change in the frequency of the scattered light. Smaller particles move faster, thus cause a quicker light fluctuation. By an autocorrelation, of the measured intensity and the time, the translational diffusion coefficient (D) can be calculated and converted to the hydrodynamic diameter (D_H) by the Stokes-Einstein equation:

$$D_H = \frac{k_B T}{3\pi\eta D} \tag{1}$$

The further variables are the temperature (T), the Boltzmann constant (k_B) and the viscosity of the dispersant (η).[144] Based on a cumulants analysis defined in ISO 22412:2017, the Z-average diameter (ZD), the intensity correlated mean diameter, and the polydispersity Index (PdI), a dimensionless number characterizing the particle size distribution width, are derived. A PdI of 0.08 is defined as relatively monodisperse, if the PdI becomes larger than 0.7 a very broad particle size distribution can be assumed.[145] The surface charge of particles in liquid is approximated by the measurement of the zeta potential. Particles are surrounded by ions dissolved in the dispersant. This ions form two layers. An inner "Stern layer" with strongly bound ions and an outer region where the ions are less strong attached. When a particle moves a shear plane occurs, within the

plane the interaction between particles and ions is strong enough, so they follow the particle movement.
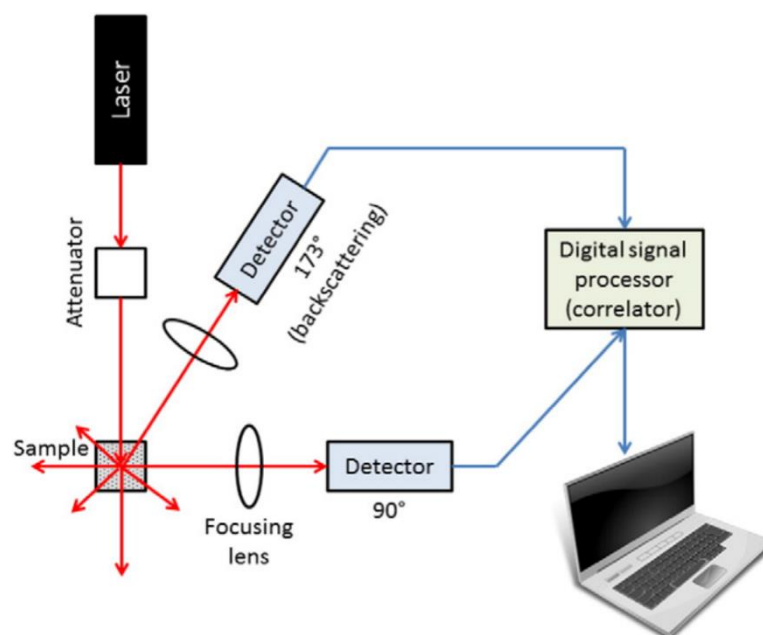

Figure 5-1: Construction of a DLS measurement device with its characteristic components. Reprinted from: "DLS and zeta potential – What they are and what they are not?"[146] Copyright: © 2016 Elsevier B.V

The potential existing at the slipping plane is the ζ-potential. Particles and emulsion droplets with a zeta potential greater than (+) 30 mV or lower than (-) 30 mV are considered to form a stable formulation as they repel each other when they come too close.[147] Zeta potentials are strongly influenced by the pH of the dispersant. For proteins the potential is positive at pH values below the isoelectric point (IEP) and negative if the pH is higher. For the measurement an external electric field is applied. This results in an electrophoretic mobility which can be used for the determination of the zeta potential. Viscous effects of the medium work in the opposite direction. In the state of equilibrium the particle moves with a constant velocity which is influenced by the electric field strength, the dielectric constant of the medium, the viscosity and the zeta potential. The zeta potential can be measured by the laser Doppler velocimetry (LDV) which measures the fluctuation of scattered light in an electrophoresis experiment in the angle of 17 degree and compare this with a reference beam. The fluctuation is proportional to the particle speed. Another method is the M3-PALS. A combination of phase analysis light scattering (PALS) with mixed mode measurement (M3). This is the combination of a slow field reversal and fast field reversal of the electric field to compensate a possible shift of the determined zeta potential through electro osmosis, a movement of the surrounding

phase in the applied electric field. The use of PALS improves the results especially for samples with low particle mobility as the phase shift is more sensitive than the frequency shift used in LDV.

To determine the hydrodynamic diameter, the particle size distribution and the zeta potential a NanoZS zetasizer was used. The device operates in the non-invasive back-scatter technology (NIBS) for the size measurements and M3-PALS to determine zeta potentials.[148] Samples have been prepared by dilution with purified water in a ratio of 1:20 to obtain a suitable particle concentration. A disposable folded capillary cell (type DTS 1070) was used for the measurement. All samples have been evaluated immediately after purification and after four weeks of storage at 4°C.

5.2.4   Electron Microscopy

5.2.4.1   Visualization of the NP Morphology by Scanning Electron Microscopy

With the development of the scanning electron microscope a resolution down to the nanometer scale got accessible. The investigated area is scanned by a small electron beam produced by a cathode and accelerated with an anode at a defined voltage. Cathodes are either made of lanthanum hexaboride (LaB_6) or tungsten. The electron beam is focused by electric or magnetic condenser lenses. A scan coil, located above the objective lens, controls the position of the beam and thus allows the beam to scan the sample in X and Y directions. The set-up is displayed in Figure 5-2. To avoid interactions with atoms, before reaching the sample surface, the whole set up is placed in a vacuum chamber. When the electron beam reaches the specimen, different interactions between the electron beam and the sample are occurring.
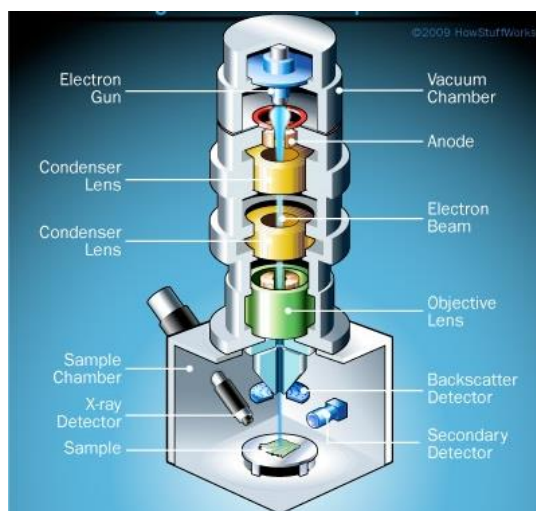

Figure 5-2: Typical construction of a scanning electron microscopy machine, Copyright © 2009 How stuff works

For imaging typically either secondary electrons, which are scattered inelastically from the interaction with electrons close to the surface (<2 nm) or back scattered electrons (BE), which arise from elastic interaction with the nuclei, are used. As BE electrons have a higher energy, they can be detected from deeper levels of the sample. Using secondary electrons the scanning electron microscopy (SEM) represents a very good method for surface morphology examinations.[149] More electron beam-specimen interaction will be described later in chapter 6.2.5.3. Samples have been prepared on a silica wafer which is attached to a pin stub with a carbon disk. Approximately 50 µl of NP suspension was dropped on the wafer.

The drop was incubated for one minute, in order to let the NPs adsorb to the surface, before the supernatant was removed with a lint-free tissue. To gain an electro conductive surface, which is required for imaging, a 10 nm gold layer was sputtered in a Quorum Q150R ES sputter coater to prepare GNP samples for imaging in an EVO HD15 SEM using an acceleration voltage of 5.0 kV and the secondary electron image (SEI) detector.

5.2.4.2   Transmission Electron Microscopy

The principle of transmission electron microscopy (TEM) will be explained in chapter 6.2.5.2. For sample preparation 50 µl of a particle suspension was dropped on a holey-carbon film (Plano S147-4). The dispersant was evaporated completely before imaging in a JOEL JEM 2100 TEM. For electron generation a LaB6-cathode was used and for imaging a Gatan Orius SC100 camera.

5.2.5   Scanning Probe Microscopy

5.2.5.1   Principle of Scanning Probe Microscopy

The scanning probe microscope (SPM), also called atomic force microscope (AFM), is a microscope which scans the surface of a specimen with a probe, mounted on a cantilever. The technique was invented in 1986 by Binnig and colleagues[150]. The resolution in x, y and z direction is outstanding with the possibility to resolve from micrometers down to the angstrom scale. To detect the cantilevers deflection a laser beam is used. The back side of the cantilever reflects the beam which is then brought over a mirror to a position-sensitive photodiode (PSPD). This principle is called the optical lever arm, as a small cantilever displacement is magnified in a relative large beam motion on the detector.[151]

An illustration of a SPM machine is shown in Figure 5-3. Every cantilever displacement will cause a change in the position where the laser beam hits the PSPD.
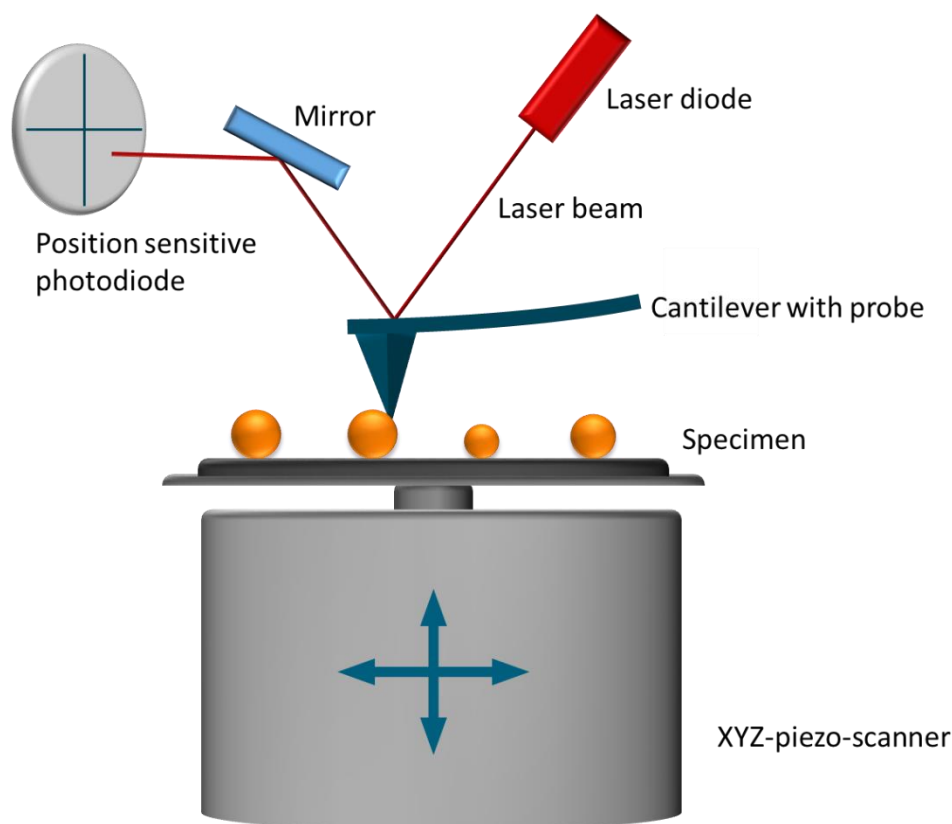

Figure 5-3: Schematic of a scanning probe microscope.

Two imaging methods are commonly used. In the contact mode the probe is always in touch with the sample. While scanning the specimen line by line, either the cantilever deflection can be measured or, in order to keep the force on the sample gentler, the feedback signal needed to keep the deflection constant, is measured. For measurements in ambient air, the capillary forces, produced by a thin water film on the sample, are very strong. This can be eliminated by measurements in liquid. The second mode, the tapping or intermittent contact mode, makes use of a cantilever oscillating with a frequency, close to its resonance frequency. At the minimum of the oscillation amplitude, the tip is in very brief contact with the specimen surface. If the cantilever is very close to the surface, different forces (van der Waals forces, dipole-dipole interactions, electrostatic forces) are impinging on the cantilever and therefore influence the amplitude. In order to keep the cantilever amplitude constant these forces go into the feedback loop, controlling the cantilever height. As the surface is only touched very shortly, the damage to the specimen is reduced in comparison to contact mode measurements. The repulsive and adhesive forces have an influence on the frequency and result in a phase shift, which is influenced

by the surface characteristics. In this way differences in surface composition, which cannot be seen in the height profile, are accessible.[152] Even gentler, as the tip does not come in contact with the specimen, is the third possibility, the noncontact mode. This mode makes use especially of van der Waals forces. Oscillation amplitudes of less than 10 nm are used. Van der Waals forces are usually the strongest from 1 nm to 10 nm distance to the surfaces. In this mode the distance between tip and cantilever are kept constant. The options to run SPM measurements under various conditions (ambient air, vacuum, different gases and liquid) and from low to high temperatures open a broad range of possibilities. In liquid even the imaging of living cells is possible.[153] In addition, the water capillary forces which are present in ambient air condition at the tip-sample interface are removed.[154] For the purpose of characterization of hydrogel particles with the application in drug delivery, a more realistic investigation can be performed in liquid conditions too. The analytical capabilities of a SPM go far behind simple imaging of surfaces. The usage of SPM for the quantitative measurement of elastic material characteristics is described in chapter 5.2.5.2. Through the combination with other techniques such as SEM or fluorescence microscopy, the spectrum of possibilities is even broader. In this way the interaction between single viruses and cells could be studied.[155]

5.2.5.2 Sample Preparation for SPM in Water and Air

To perform AFM experiments under liquid conditions, the NPs needed to be fixed to the substrate. This could be achieved with electrostatic interactions between a positively coated silicon wafer and the negatively charged GNPs. Therefore silica wafers have been cleaned with absolute ethanol in an ultrasound bath (Elmasonic P) for 5 min at a frequency of 37 kHz. Afterwards, the surface was activated in UV/ozone for 15 min (UV/Ozone ProCleaner™). Subsequently, the wafer was incubated with a 1 % (w/V) polyethylenimine (PEI; average Mw of 25 kDa) solution in deionized water. Coated wafers have been rinsed with filtered deionized water in which they have been kept wet and stored at 4°C until final sample preparation. The substrate was coated for a maximum of 24 h before usage. Immediately before the experiment, samples have been diluted 1:3 with deionized water and 50 µl of the dilution was transferred to the coated substrate. After one minute of incubation the excess was rinsed from the wafer with filtered deionized water in which they have been kept wet afterwards until the end of the measurement. For SPM topography images, taken under ambient conditions, 10 to 20 µl

of the sample have been applied to freshly cleaved mica. After an incubation time of approximately one minute the rest of the sample was removed with a lint free tissue and measured in intermittent contact mode after complete drying.

5.2.5.3 Elasticity Measurements

Scanning probe microscopes cannot only be used for topography measurements. Due to the possibility to measure small forces (even in the pN range) the interaction between materials can be investigated. Furthermore, mechanical properties of various materials can be determined. First nanoindentation experiments have been performed in the 1970s. [156] Since then the technique was developed and in the 1990s adopted to the use by SPM. This raised the possibility to determine the elastic moduli on nanoparticles.[157] A sketch of the simplified principle of an indentation experiment is depicted in Figure 5-4. A SPM probe is used to indent the NP by a piezo displacement. The displacement can be plotted against the force, exposing the cantilever during the indentation, resulting in a force-distance curve. Since the cantilever acts like a spring, the indentation depth can be calculated if the spring constant is determined prior to the experiment.
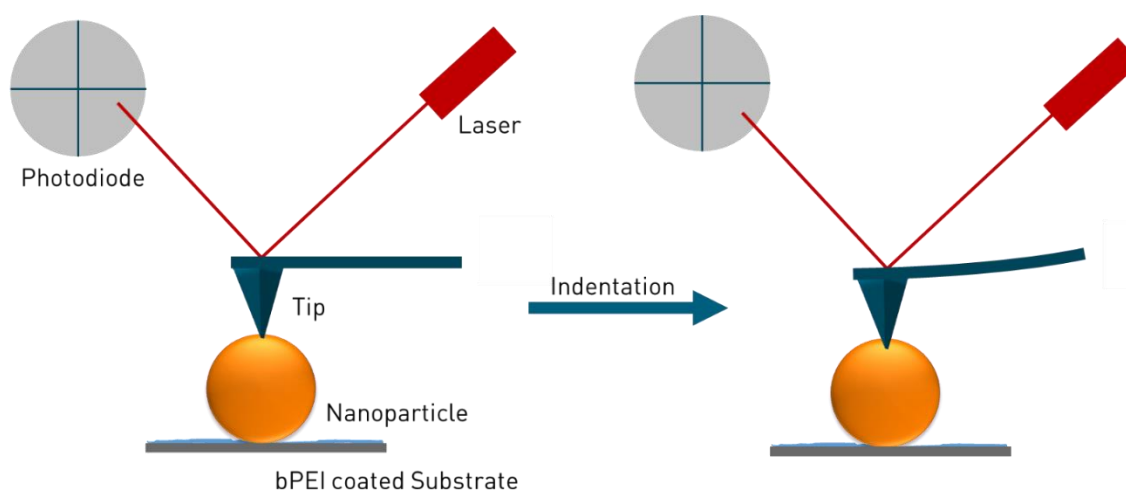

Figure 5-4: Simplified principle of the nanoindentation performed by a SPM measurement.

A typical example of such a curve is illustrated in Figure 5-5. Four characteristic segments are highlighted in this graph. The experiment starts with an approach of the SPM probe to the NP surface, which runs free of force. When the tip approaches close enough to the surface, attractive forces between probe and surface can cause a jump into contact. This results in a negative force. While further lowering the piezo the zero-force baseline is crossed again, this is the so-called contact point, which is set to the origin of the coordinate system. From this point on the probe indents the nanoparticle until a defined

setpoint force is reached. This is displayed in the third measurement segment. The calculation of the Young´s modulus is based on the fit of the resulting slope in this sector. The retract part, displayed in green, represents the lifting of the cantilever. Due to adhesion forces between tip and sample surface a negative force can be obtained. The adhesion force is a combination of the electrostatic force, van der Waals force, the capillary force and forces brought to the system through chemical bonds or acid-base interactions.[157] It can be calculated by the area between the retract curve and the baseline. A cantilever movement without force, until the original cantilever position is reached, finishes the indentation loop.
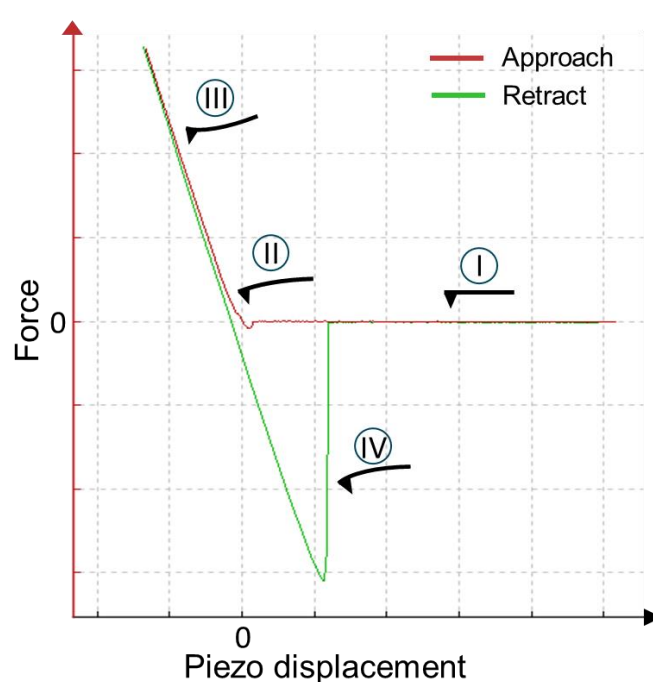

Figure 5-5: Typical force-distance curve of a nanoindentation experiment on cGNPs with characteristic segments. I) Force free approach, II) jump into contact, III) indentation of the tip into the sample, IV) retract with segment with the possibility to determine adhesion forces.

All nanoindentation experiments were performed with a JPK NanoWizard I SPM. To get a more realistic insight in the elastic characteristics of cGNPs all experiments were operated under liquid conditions. A quadratic pyramidal tip of the MLCT type was used as an indenter. The probe is made by non–conductive silicon nitride with a gold coated back side. The C cantilever with a nominal spring constant of 0.03 N/m was used throughout the entire force-distance measurements. Directly before the measurement of a new sample, the thermal noise method according to Hutter *et al.*[158] was used to determine the cantilever's actual spring constant on a cleaned silica wafer. To roughly localize the distribution of cGNPs on the substrate an overview scan was done initially. Subsequently

one particle was chosen randomly and depicted closely do determine the exact position and be able to perform 10 force-distance measurements in the middle of the NP. After the fifth and tenth indentation the particle is relocalized to ensure all data are actually acquired in the middle of the particle. Measurement settings have been defined to an approach and retract rate of 3.33µm/s and an applied force of 2 nN. Ten force distance curves per particle on ten particles per sample, resulted in 100 data points obtained per sample. The obtained curves are fitted and processed by the Hertzian model. Therefore, a linear relation of stress to strain is obligatory. This was checked prior to the determination of the Young's moduli. Therefore, forces between 0.5 and 2.5 nN have been applied. To extract the necessary parameters for the calculation of stress and strain the original jpk-data files have been converted into text files and then read out with the AFMToolkit in R Studio.[159] Subsequently, the stress, defined as $\sigma = F/A$ with F being the applied force and A the contact area between indenter and nanoparticle, is calculated according to the following equations. For a quadratic pyramidal tip A is composed by the parameters

$$A = 4h_c{}^2 \frac{tan\,\alpha}{cos\,\alpha} \tag{2}$$

The tip half angle a was taken from the official product description whereas the contact depth h_c has to be calculated by:

$$h_c = \frac{2}{\pi * \Delta l} \tag{3}$$

Here Δl is the indentation depth which was calculated by the following equation

$$\Delta l = z - \delta_c \tag{4}$$

Where z is the piezo displacement and δ_c the cantilever deformation.[160] As the cantilever can be compared with a spring, the deformation can be obtained by Hook's law $F = k*\delta_c$. F is the applied force and k the spring constant, which is determined in advance of each experiment. The strain is expressed by $\varepsilon = \Delta l/l_0$. Being Δl the indentation depth defined in equation (4) and l_0 the initial NP height. The calculated values are then plotted against each other and fitted with a regression line. The chosen application force of 2 nN is in the tested linear range and allows measurements with an indentation of less than 10 % of the absolute particle height. This is fundamental as infinite sample thickness is one of the assumptions made by the Hertz model.[161]

5.2.5.4 Evaluation of Force-Distance Curves

To obtain the Young's moduli from the measurement data, the curves are handled in the JPK-SPM Data Progressing Program (DP). Young´s moduli can be extracted by fitting the recorded curves, after editing[1], with the Hertz model. As this is based on a parabolic tip an adjustment for the quadratic pyramidal tips is required. The modified Hertz model

$$F = 0.7453 * \frac{E}{1-v^2} * \delta^2 * \tan(\alpha) \tag{5}$$

is used by the DP. Where F is the applied force, E is the Young´s modulus, v is the Poisson´s ratio, which is assumed to be 0.5, δ is the indentation depth and a stands for the half angle of the tip used. To start the data processing the cantilever deflection needs to be calibrated by the cantilever´s spring constant and sensitivity which was determined prior to the measurement. The next step is the baseline subtraction to correct the vertical offset and subsequently the contact point can be detected. The now depicted curve still represents the piezo displacement, which is greater than the actual indentation into the particle. The difference is caused by a deflection coming from the force the cantilever is exposed to. This needs to be corrected by the tip-sample separation. The obtained force-distance curve is steeper and can be fitted by the modified Hertz model to finally obtain the Young´s modulus.

5.2.6 Cellular Interaction in Dependency of Particle Stiffness

As a consequence of the data the following experiments were realized during a diploma thesis at the institute by Thorben Fischer.

The biological relevance of the change in the particle stiffness of GNPs was investigated with the alveolar cancer cell line A549 with 18 h crosslinked FITC-Dextran$_{70}$ loaded GNPs. The aim of these experiments was, to investigate in the importance of the mechanical properties with respect to the interaction between cells and NPs. Therefore, 20 mg of gelatin were dissolved in 800 µl deionized water and mixed with 1 mg FITC-Dextran$_{70}$ dissolved in in 200 µl deionized water and coprecipitated in acetone containing 2.81 % (w/V) poloxamer 188 as stabilizer with an agitation speed of 750 rpm. Crosslinking was done with 500 µl of a 7.4 % (w/V) glutaraldehyde solution. After 18 h particles have been purified three times by centrifugation with 10,000 g for 10 min at 15°C. A549 cells have

---

[1] Editing includes the baseline-correction to bring the baseline to zero-force, the correction of the contact point to zero-length and a tip-sample-separation.

been grown in RPMI-1640 medium with the addition of 2 mM glutamine and 10 % (V/V) fetal calf serum (FCS) in µ-Slide 8 well ibiTreat® microscopy chambers for three days. GNPs have been investigated one day after production and after four weeks storage at 4°C in water. After an incubation time of 4 h and 8 h respectively with 1.05 mg particles per well, cells have been washed twice with Hanks Balanced Salt Solution (HBSS) buffer. For the visualization in the confocal scanning microscope (CLSM) cell cores have been stained with 200 µl of a 10 µg/ml 4',6-Diamidine-2'-phenylindole dihydrochloride solution (DAPI). N-Hydroxysuccinimid Alexa Flour® 633 was used in a concentration of 5 µg/ml to stain the cell membranes. Both dyes have been incubated for 15 min. To remove excess material, A549 cells have been washed three times with HBSS buffer after each step. The labeled NPs have been excited with an argon laser at 488 nm, Alexa Fluor 633 was detected with an argon laser too but at a wavelength of $\lambda = 633$ nm and for DAPI a laser diode 405-30 with a wavelength of $\lambda = 405$ nm was used. Images have been taken with M 27 objective with a numeric aperture of 1.2 and a 40 x magnification. As CLSM is also used later in chapter 6.2.5.1 to colocalize different polymers a brief introduction to the technique is given here.

CLSM is a light microscopy technique based on fluorescence emission, caused by excitation with a laser of an appropriate wavelength which scans the specimen. The emitted light is sectioned by a pinhole. Only light from the in-focus plane can pass through this partial filter unit to the photodetector. By this limitation to the focus plane the sample can be dissected into thin optical slices. This allows a 3D reconstruction of the sample from the slices acquired from different positions. Therefore, compared to normal light microscopy, sharper images are obtained. This method has a lateral resolution of around 0.23 µm and approximately 1.1 µm in the vertical direction (Calculated for Alexa Fluor 633 and the used settings). To image cells or tissue the specimen has to be labelled fluorescently with dyes or with antibodies bound to a relevant dye. By scanning the sample with different lasers and the corresponding appropriate dyes, diverse information about the region of interest can be assembled in one image.[162] As the focus can be varied through the specimen, pictures from different planes can be obtained. Moving the focus plane stepwise through the sample allows assembling a so-called z-stack. From this, a 3D image can be digitally reconstructed.

5.3 Results and Discussion

5.3.1 Sizes and Zeta Potential of Gelatin Nanoparticles

For all crosslinking times the hydrodynamic diameters, particle size distributions and ζ-potentials have been determined with a zetasizer Nano-ZS. The results are combined in Figure 5-6. The sizes and PdIs stayed constant over the range of glutaraldehyde incubation times and the storage period. All formulations show a mean for the hydrodynamic diameter between approximately 300 to 350 nm. For the PdIs of around 0.2 the particle size distribution can be assumed to be narrow but not monodisperse.[145] The constancy in regard of size and PdI supports a stable nanoparticulate formulation.
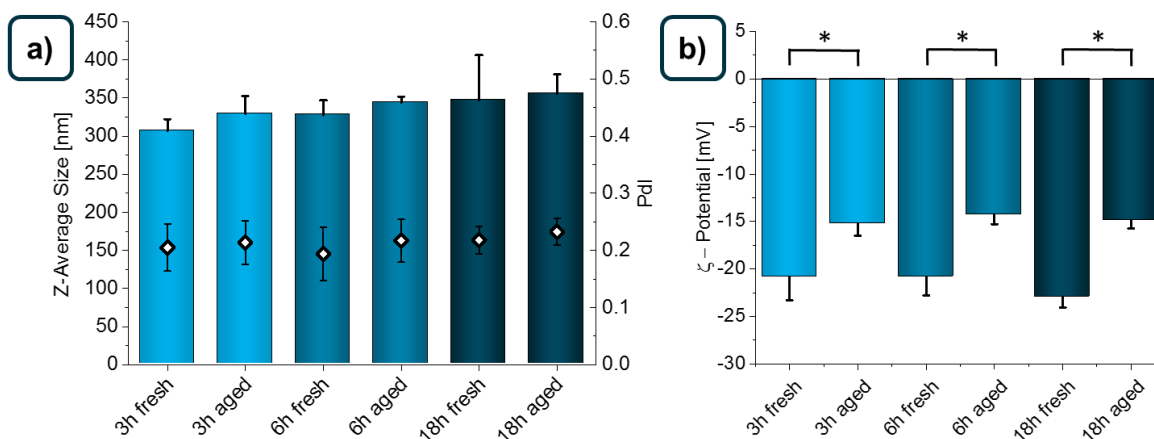
Figure 5-6: Sizes and PdIs of cGNPs after 3, 6, and 18 h of crosslinking. One day after production (fresh) and after four weeks of storage at 4°C (aged) in a). In b) the ζ-potential for the same formulations is displayed.

In Figure 5-6 b) the zeta-potentials are shown. Here a decrease of around 5 mV from approximately -20 mV to -15 mV can be measured. With $p < 0.05$ this change was stated to be significant. A possible explanation for this can be the triple helix formation over time. These helices are stabilized by hydrogen bonds either formed between a carboxylic and an amide group or, with a water molecule as linker, between two carboxyl groups. As negatively charged CO-functions are involved in the helix stabilization, they cannot contribute to a negative surface charge anymore.[163, 164, 165]

5.3.2 Visualization of Crosslinked Gelatin Nanoparticles

To check the morphology and shape, cGNPs have been visualized in SEM, SPM and TEM. For all images in Figure 5-7, cGNPs have been captured in dried conditions. SEM in a) and TEM in b) under high vacuum. The SPM image in c) is taken in tapping mode at atmospheric conditions. The round particle shape is clearly visibly. In the TEM image the

homogeneous material distribution throughout the entire particle is apparent. The height, determined after SPM measurements of 28 nm, shows the hydrogel particles collapse while drying. Comparing the SPM cross-sections in Figure 5-8 of cGNPs imaged in air and in deionized water demonstrates the superiority of SPM images taken under liquid conditions which is the only method to get realistic values about the 3D occurrence of hydrogel nanoparticulate formulations.
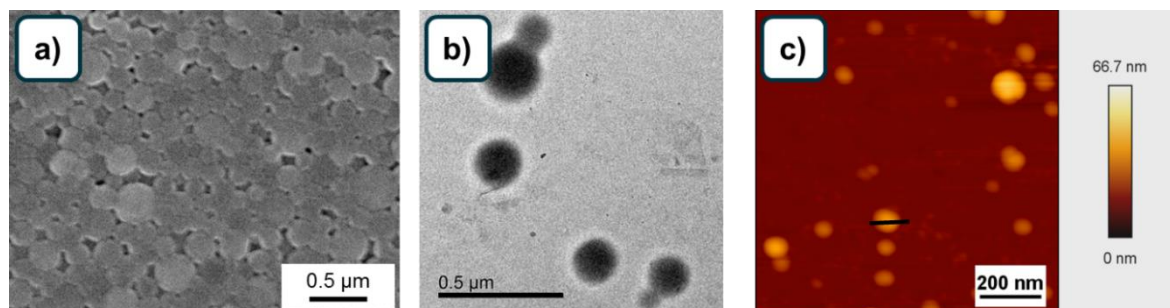

Figure 5-7: Visualization of cGNPs a) in SEM, b) in TEM, c) in SPM. SEM and TEM under high vacuum and SPM in air at atmospheric pressure. Particles are roundly shaped and have a smooth surface.

In SPM-cross-sections the 3D shape is easily accessible. Two of them are displayed in Figure 5-8. In a) from a NP captured in air and in b) from a SPM measurement performed in liquid conditions. Comparing the y-axes the advantages of the liquid surrounding is well visible. In air a height of approximately 28 nm remains whereas the height in liquid meets with 140 nm nearly the same value than the diameter (175 nm). A possible indication of the slightly smaller height in comparison to the diameter is a compression caused by the SPM probe during the measurement.
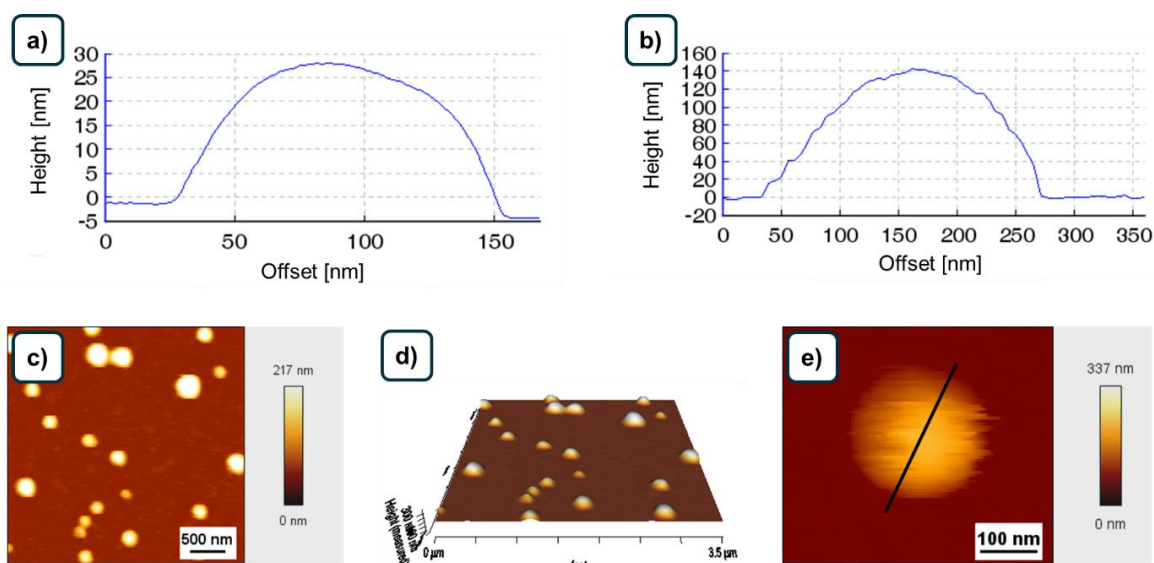
Figure 5-8: SPM visualization and analytics of cGNPs captured in liquid (b) to e)). a) shows a representative cross-section through a crosslinked gelatin NP imaged in the dry state in air. The attention has to be at the y-axes showing the particle collapse during drying in a) whereas the particle in b) keeps the spherical form.

The SPM images in Figure 5-8 are showing 2D and 3D views of particles imaged in deionized water in c) and d) respectively. The height of particles measured in liquid meet the expectations gained from particle size determinations. Figure 5-8 e) shows a close zoom to a single cGNP captured in water. The black bar indicates the line of the cross-section in b).

5.3.3 Elasticity Determination – Force-Distance Measurements

To get first insights in the mechanical properties of cGNPs nanoindentation experiments have been performed. The first step in the elasticity determination of a new system is to check for linearity. As described above forces of 0.5 to 2.5 nN have been tested and evaluated for their stress to strain correlation. The results are summarized in Figure 5-9 for 3 h incubated cGNPs in a) and 18 h in b). Both formulations show a linear dependency what is supported by correlation coefficients of 0.928 and 0.964 respectively. This proofs that the calculation of Young's moduli can be done with the help of a Hertzian fitting. A force of 2 nN was chosen for the further investigations because it is in the examined linear range and allows a stable measurement without being susceptible to external influences and meets the requirement of an indentation of less than 10 % of the original height.[161]
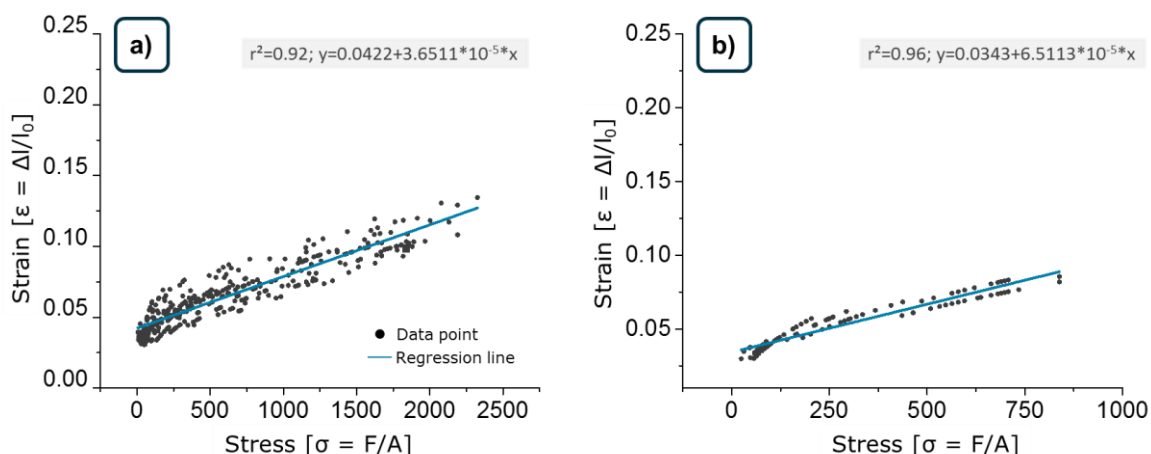

Figure 5-9: Linear dependency of stress and strain of particles crosslinked for 3 h in a) and 18 h in b). The correlation coefficients are 0.928 for A and 0.964 for B and therefore proofing the linear dependency of stress and strain.

Subsequently to the proof of linearity cGNPs have been investigated in regard of their Young's moduli. As can be seen in Figure 5-10 cGNPs crosslinked for 3, 6 and 18 h are examined one day after production and after four weeks of storage at 4°C in water. For all fresh formulations a Young's modulus of 30 to 35 MPa could be calculated. Whereas there was no detectable difference in stiffness between the fresh particles a clear

influence of storage could be verified. This alteration is more pronounced the longer the crosslinking time was; ranging from 36 % for 3 h crosslinked particles and over 62 % to 129 % for 6 h and 18 h-crosslinked particles respectively. Overall, the change in the mean mechanical properties was found to be significant by two-sided student's t-tests with p < 0.0055 (Bonferroni adjustment).
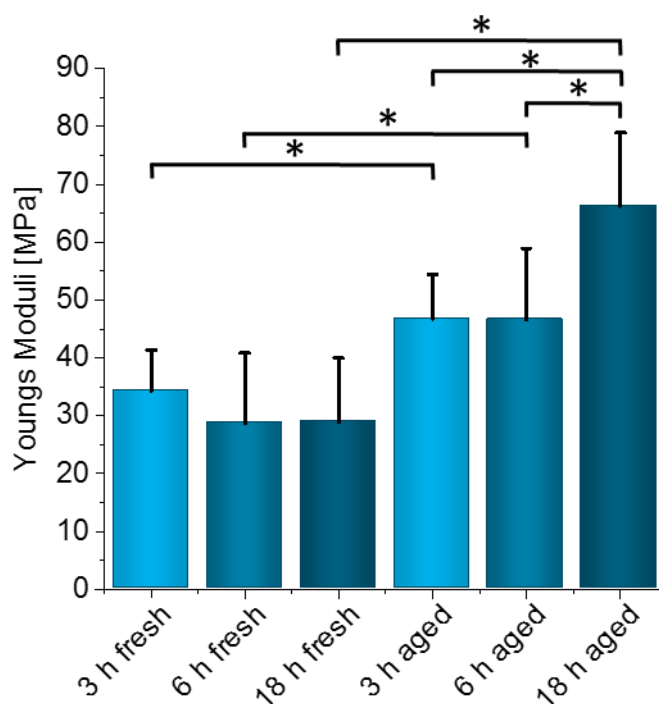

Figure 5-10: Young's moduli of cGNPs crosslinked for 3, 6 and 18 hours one day after production and after 4 weeks of storage.

It was expected to see a difference in the mechanical properties of fresh cGNPs as a correlation between crosslinking extend and the elastic behavior of gelatin gels could already be demonstrated.[142, 166] Possible explanations why no change could be observed are, that either the particles are fully crosslinked after three hours, or the slight increase is too small to be detected. Shorter crosslinking times have to be addressed to check for the possibility of the formation of softer cGNPs. However, particles crosslinked for less than three hours could not be purified by centrifugation and because of that haven´t been considered in this study in order to keep the conditions constant. Methods like dialysis, size exclusion or cross-flow filtration would need to be established for cGNPs to study the influence of shorter crosslinking times or lower cross linker concentrations. As the production procedures should be kept as constant as possible, in order to exclude possible changes in the resulting particles, this was not done in the present study.

Looking in detail to the hardening over the storage time, it can be said that this was already studied for solid gelatin films[167] but up to now never was taken in account for gelatin nanoparticles. A possible effect leading to the enhanced stiffness is the formation of triple helices. Triple helices are thermodynamically preferred. Therefore, gelatin has the tendency to form these crystalline areas until the equilibrium between the breakage and the formation of new stabilizing hydrogen bonds is reached.[163, 164, 165]

5.3.4   Cellular Interaction in Dependency of Particle Stiffness

The biological relevance of the change in the elastic modulus while storing the formulation was tested in qualitative and quantitative interaction studies of 18 h crosslinked cGNPs with A549 cells. The qualitative interaction study was evaluated by CLSM. The quantitative data was obtained according to the protocol described in Shi *et al.* 2015.[168]
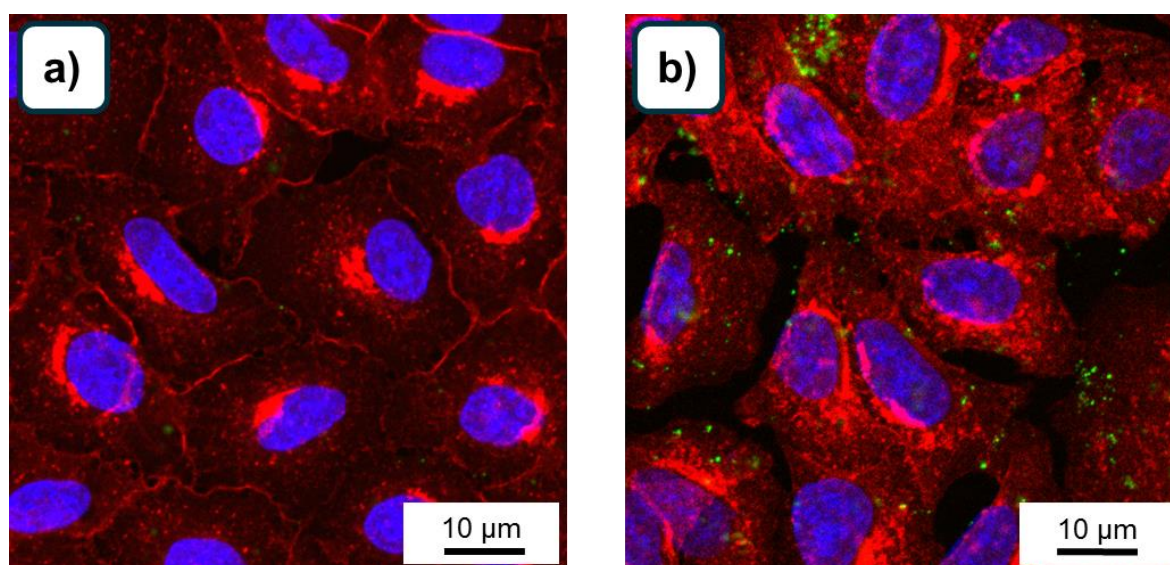
Figure 5-11: CLSM image of stained A549 cells after 8 h incubation with FITC-dextran$_{70}$ loaded cGNPs. In a) cGNPs have been used one day after production and in b) cells are incubated with four week old cGNPs. cGNPs are displayed in green, cell cores in blue and cell membranes red.

The CLSM images in Figure 5-11 display the cellular interaction with FITC-dextran loaded cGNPs is investigated after 8 h of NP incubation. In terms of cellular internalization a clear advantage of the aged particles displayed in b) was visible. Particles were counted in relation of cell numbers in at least five pictures of fresh and aged cGNPs. In comparison to the fresh formulation the amount of interacting NPs increased 4.8 fold. These results have been further investigated for quantitative cell uptake; here the measured increase after 8 h was 4.2 fold. Both methods result in a similar outcome. However, after 24 h the cellular interaction of fresh and aged particles was nearly aligned. The results show the

need of further investigations of both changes in the elastic moduli of cGNPs and the effect to biological systems. Therefore, more time points should be evaluated so uptake kinetics can be calculated. In addition, other cell lines, such as macrophages and human noncancerous cells, have to be studied to be able to strengthen the biological relevance of particle stiffness. This, paired with investigations of internalization routes, could help to gain a better understanding of the exact role of elastic moduli for hydrogel nanoparticulate systems.

5.4 Conclusion

The value of nanosized hydrogels in drug delivery was discussed in chapter 3.1.2. In the present thesis the influence and the importance of the measurement conditions for hydrogel NPs analytic could be shown. It was possible to visualize cGNPs in liquid by fixation by electrostatic interactions between substrate and NPs and map cGNPs in an environment closer to condition after application. By the switch of visualization in SPM to liquid conditions it was possible to image the spherical shape in a 3D view. This is an impressive difference to the data obtained by measurements in air. Furthermore, for the first time, an insight in the elastic characteristics of cGNPs could be achieved. The use of the nanoindentation method in SPM and fitting the obtained force-distance curves with the Hertz model is a suitable method to define Young´s moduli quantitatively. The investigated crosslinking times had no impact on the determined Young´s moduli for NPs analyzed one day after production. By comparing these results with the Young´s moduli obtained after four weeks of storage at 4°C in water a significant increase was detectable. In biological studies, performed with A549 cells, the effect of NPs elastic characteristics on the interaction with cells was demonstrated. As the other determined physical chemical parameters stayed constant, the increased interaction of cGNPs over the observed storage time correlates with the elasticity. This underlines the outstanding importance of the knowledge of elastic moduli and NPs age besides size, shape and surface properties. By a possible tuning of the particle stiffness, the *in vitro* fate, and most likely as well the destiny *in vivo*, of cGNPs could be altered in order to achieve a targeted drug delivery and prolonged blood circulation times. Further studies are necessary to determine possibilities of a modified production in order to design GNPs with editable Young´s   moduli.

6 Stabilizing Gelatin Nanoparticles without Crosslinking

6.1 Introduction

The importance, which biological therapeutics gained over the last years is indisputable. Their outstanding specificity and potency made them to an already important and still growing share on the market.[11] Due to their low stability *in vivo* and the hydrophilic properties,[3] the development of a delivery system can prolong the circulation time and smuggle the drug over the multitude of lipophilic barriers resulting in an enhanced bioavailability. A lot of work is invested in the encapsulation into PLGA NPs. However, due to the hydrophobic characteristics, the loading rates are rather low.[52] Due to the excellent characteristics of nanoparticulate carrier systems formed by gelatin, which are discussed in detail in chapter 3.1.4, GNPs seem to be a promising system for this purpose. To overcome the drawback of the still inevitable crosslinking is addressed in the following chapter. The described investigations are based on the possibility of an alternative crosslinking-free stabilization of GNPs by the embedment in Eudragit® E 100 spheres.[10] The application limitation of the non-biodegradable Eudragit® should be removed by the exclusive use of biodegradable and biocompatible materials to achieve the development of a nontoxic, biodegradable platform technology for the use as drug delivery system for hydrophilic macromolecular drugs.

6.2 Experimental

6.2.1 Materials

For the formulation of the hydrophilic delivery platform, only biocompatible and biodegradable materials are chosen. The main compounds are gelatin B for the hydrophilic part, which is already described in detail in chapter 3.1.3 and PLGA for stabilization of the freshly prepared GNPs.

6.2.1.1 Poly lactic-co-glycolic acid

PLGA is a copolymer composed of lactic and glycolic acid in various ratios. The high interest in pharmaceutical research is based on its biodegradable and biocompatible characteristics. The chemical structure of the artificial polymer is shown in Figure 6-1. With a variation of the ratio of lactic and glycolic acid or the polymers' molecular weight,

the glass transition temperature, degradation rate and hydrophobicity are adjustable. As a result, the drug release changes due to the chemical composition.[169, 170]
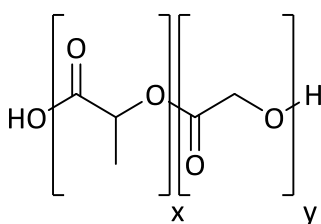

Figure 6-1: Chemical structure of poly lactic-co-glycolic acid. The ratio between glycolic acid (marked with the y) and lactic acid, (signed with the x) can vary.

PLGA is degraded in its monomers, lactic and glycolic acid, by hydrolysis. They are then eliminated through the Krebs cycle as carbodioxid or along the renal pathway. The degradation process is highly dependent on temperature, pH and, under controversial discussion, enzymes.[171, 172] First sustained drug delivery systems based on PLGA have been introduced in the 1970s for naltrexone, an opioid antagonist[173] and for microcapsules loaded with norethisterone, a contraceptive agent.[174] Nanoparticles composed of PLGA gained an increasing importance since the 1990s.[175] Several pharmaceutical products based on PLGA have been introduced to the market such as implants (Zoladex®) or micro particles (Enantone Depot®). The PLGA type used in the present thesis is the Resomer® RG 503 H. It is acid terminated, has a lactide:glycolide ratio of 50:50 and a molecular weight of 24,000 – 38,000. The degradation time is given to be three months and the glass transition temperature is stated to be between 44 and 46°C from the supplier.

6.2.2   Formulation Development of GNPs in PLGA

6.2.2.1   Size and Zeta Potential of Gelatin Nanoparticles

The hydrodynamic diameter, PdI and the zeta potential of GNPs in PLGA have been determined by a Zetasizer NanoZS. For size measurements, DLS with a backscatter detector in an angle of 173° was used. In contrast, the zeta-potential was determined with forward scattering at an angle of 12.8° by M3-PALS. After the last purification step samples were dispersed in 5 ml deionized water. Before the measurement the samples have been diluted 1:20 and have then been measured in disposable folded capillary cells of the type DTS 1070.

6.2.2.2 Visualization of the NP Morphology by Scanning Electron Microscopy

The principle of the SEM has been described in chapter 5.2.4. Here the focus is on the working conditions used for the visualization of GNPs in PLGA. Therefore, a drop of the NP-suspension was distributed on a cleaned silica wafer. After approximately one minute of incubation, the remaining liquid was removed by a lint-free cloth. The sample was dried at room temperature and subsequently sputter coated to avoid charging effects. For sputter coating and SEM two different devices have been used. Which of the both set-ups was used is indicated for each picture shown in this work. For the first set-up, the samples have been sputter coated with platinum (Edwards S150) and imaged with 5.0 kV by the lower secondary electron image (LEI) detector in a JEOL JSM-7500F scanning electron microscope. These experiments have been performed at the Structure & Technology Research Laboratory (Marburg, Germany). A second device was used for this work which is placed at the Helmholtz Institute for Pharmaceutical Research Saarland (HIPS, Saarbrücken, Germany). A 10 nm gold layer was sputtered in a Quorum Q150R ES sputter coater to prepare samples for imaging in an EVO HD15 SEM using an acceleration voltage of 5.0 kV and the secondary electron image (SEI) detector.

6.2.2.3 Atomic Force Microscopy for Visualization

For the visualization of GNPs in PLGA a JPK NanoWizard® I was used. Samples have been prepared on freshly cleaved mica surfaces. Therefore, 50 to 100 µl of the sample have been dropped on the surface to enable NPs to adhere. The remaining sample was removed with a lint-free tissue after 1 min of incubation time. Samples have been imaged in the intermittent contact mode in air using OMCL-AC160TS cantilevers (reflex side aluminum coated) with a resonance frequency of 300 kHz and a nominal spring constant of 26 N/m having tetrahedral tips with a final tip radius of 7 nm. Images have been processed with the JPK-SPM Data Processing Program.

6.2.2.4 Gelatin Load and Release from GNPs in PLGA

GNPs in PLGA have been tested for gelatin in regard of entrapment efficiency, load and release via bicinchoninic acid assay (BCA assay). The use of the QuantiPro™ BCA Assay Kit allowed protein detection in a linear fashion from 0.5 to 30 µg/ml. The working principle is the formation of Cu^{2+}-protein complexes at alkaline conditions, which leads to a reduction of Cu^{2+} to Cu^{1+} in a proportional amount to the protein concentration. BCA then

forms a purple-blue complex with Cu^{1+} in basic conditions, which can be read out by absorption at a wavelength of 562 nm.[176] The structural formula of the formed complex is illustrated in Figure 6-2
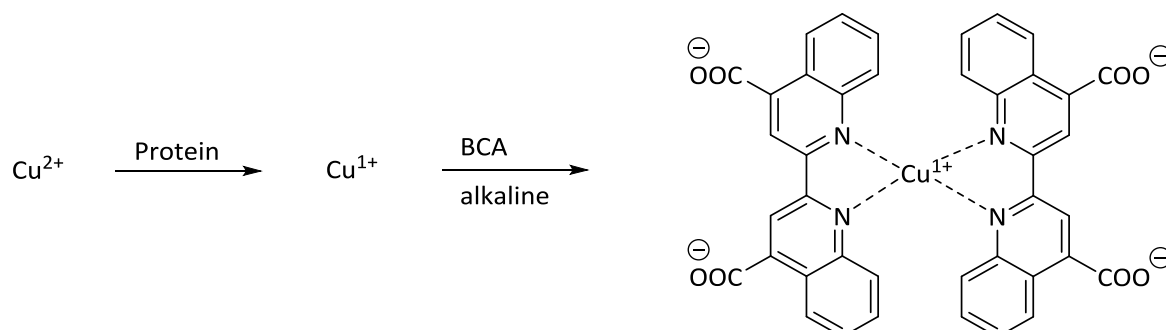

Figure 6-2: Reduction of copper II to copper I by proteins and formation of a complex with bicinchoninic acid under alkaline conditions

To determine the efficiency of the GNP embedment 10 mg freeze-dried NPs have been dispersed in 1 ml NaOH (0.5 M) to dissolve PLGA at 37°C for 90 min. After this time, a clear solution was obtained and the pH was adjusted to pH 7. The volume was filled up to 10 ml and 150 µl samples have been pipetted to a 96 well plate in triplicate and mixed with an equal amount of BCA reagent. The plates have been incubated for 2 h at 37°C and measured at 562 nm with the Infinite®M200 plate reader. Calibration curves have been prepared with different gelatin concentrations; as blank PLGA NPs have been used. Both gelatin and PLGA NPs underwent the same treatment as GNPs in PLGA samples. The entrapment efficiency was calculated by the following formula:

$$\text{Entrapment Efficiency (\%)} = \frac{\text{Mass Gelatin in NPs(g) / Mass NPs (g)}}{\text{Mass Gelatin used (g) / Mass Polymer used (g)}} * 100 \qquad (6)$$

For the calculation of the relative amount of gelatin in the formulation the equation below was used:

$$Load(\%) = \frac{\text{Mass Gelatin (g)}}{\text{Mass Nanoparticles (g)}} * 100 \qquad (7)$$

To evaluate the stabilization efficacy the gelatin release was tested. Therefore, GNPs in PLGA have been freeze dried with dissolved sorbitol to ensure complete redispersibility afterwards. 10 mg NPs have been dispersed in 10 ml PBS-Buffer (pH 7.4) and divided in 1 ml aliquots. Samples have been incubated at 37°C for different durations until examination of released gelatin mass. Afterwards, samples were centrifuged at 20,000 g for 15 min at 15°C. 900 µl supernatant was collected and investigated in triplicates of 150 µl mixed with 150 µl of BCA reagent as described above.

6.2.2.5 Influence of Solvent, Nonsolvent and Stabilizer

To obtain a suitable carrier system gelatin should be encapsulated in the highest possible amount. At the same time a sufficient stabilization of gelatin by the PLGA-coating is needed, resulting in sustained release of gelatin from the particles. Briefly, the production scheme was as described hereafter: Gelatin was dissolved and precipitated in an antisolvent. Subsequently, the so obtained GNPs were mixed with a PLGA solution. This nanodispersion was then emulsified in an aqueous PVA solution. To obtain GNPs coated and stabilized in PLGA the organic solvents were removed by solvent evaporation. Different antisolvents, solvents and stabilizers have been tested on their influence to the obtained NPs characteristics. The range of solvents tested was limited through the requirements they underlie. The demands are illustrated in Figure 6-3.
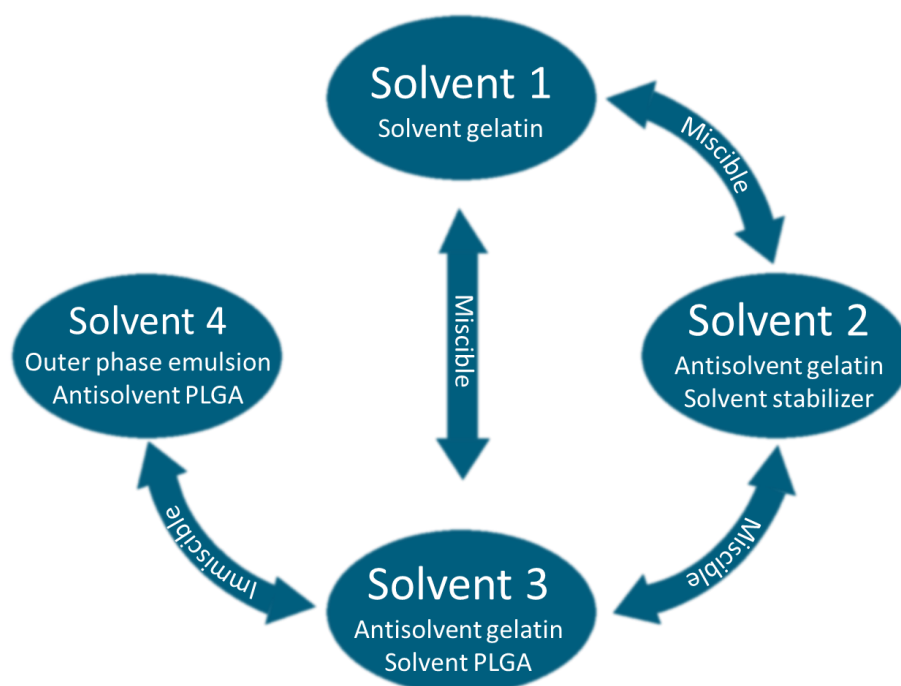
Figure 6-3: Demands on the solvents to their behavior towards gelatin, stabilizers, PLGA and to each other

The solvent of the gelatin (solvent 1) has to be miscible with the antisolvent (solvent 2). Therefore DMSO and water, inclusively their mixtures in different ratios have been chosen to dissolve gelatin at 50°C. For the nanoprecipitation, acetone and DMF have been the antisolvents of choice. The further requirements for the antisolvent are on one hand the possibility to dissolve a stabilizer for the freshly prepared GNPs and on the other hand the miscibility with the solvent of the PLGA phase (solvent 3), which has to be an antisolvent for gelatin itself, and thus was chosen to be ethyl acetate. The last step is the formation of an emulsion, which brings the last requirement for the solvent used to

dissolve PLGA as it must not be miscible with the outer phase (solvent 4) which is a 2 % (w/V) PVA solution in water. As stabilizer two substances have been tested. The first was dodecylamine (DDA) which was chosen because of the relative small size. The other tested compound was poloxamer 188. The block-co-polymer was chosen as it was shown to have, in comparison to other additives, the best results in regard to the encapsulation and release of proteins into PLGA.[177] The experiments have been evaluated in terms of hydrodynamic diameter, zeta-potential, encapsulations efficacy, load and release of gelatin by BCA assay and visualized with SEM and SPM.

6.2.2.6   Standard Formulation

After testing the influence of solvent, nonsolvent and stabilizer a standard formulation was set. 40 mg gelatin B derived from bovine animals was melted in 40 µl deionized water at 50°C and subsequently dissolved in 1 ml DMSO under continuous stirring at 50°C. 260 µl gelatin solution was precipitated dropwise in 1.5 ml of a 1:1 mixture of acetone and DMF, containing 6.67 % [w/V] poloxamer 188 as stabilizer at 750 rpm.
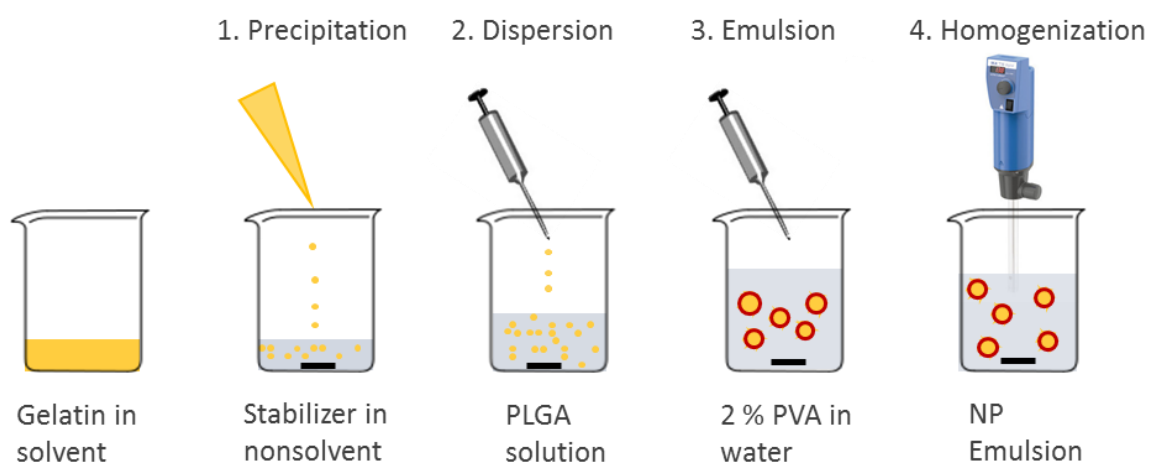
Figure 6-4: Production scheme of GNPs in PLGA. Gelatin is dissolved and subsequently precipitated in a stabilizer containing antisolvent. The obtained NPs are mixed with a PLGA solution. This mixture is then emulsified in a 2 % aqueous PVA solution. If drugs are incorporated, they have been co-precipitated

The freshly prepared NP dispersion is transferred to 5 ml of an ethyl acetate solution with 50 mg dissolved PLGA. This dispersion is slowly dropped in a 2 % aqueous solution to form an emulsion with the inner phase consisting of gelatin nanoparticles surrounded by PLGA. The emulsion was homogenized by an UltraTurrax® T25 using the S 25 N − 8 G disperser tool at 12,000 rpm for 5 min. The production is illustrated in Figure 6-4. Vials are filled up

with water and stirred over night with open lid for solvent evaporation and finally GNPs in PLGA have been purified by centrifugation three times at 10,000 g for 15 min at 15°C.

6.2.2.7   Varying the Gelatin to PLGA Ratio

To enhance the hydrophilic fraction, and thus provide a higher proportion for the encapsulation of hydrophilic drugs, it is of high interest to vary the ratio of gelatin to PLGA during the NP production. In the standard procedure 10 mg gelatin were used with 50 mg PLGA. This means a ratio of 1:5. Compositions are varied to 1:1.25 and 1:0.625. The rest of the protocol was kept constant to the standard procedure described in 6.2.2.6. To examine the particle formation, the morphology was tested by SEM and SPM. Furthermore, hydrodynamic diameter, PdI and zeta potential have been determined. To test the efficiency of GNP entrapment and stabilization the load and release of gelatin was determined by BCA assay as described in chapter 6.2.2.4.

6.2.2.8   Gelatin A Nanoparticles in PLGA

The chemical characteristics of gelatin A and B are slightly different. Here, the attention is on the different IEPs of the two types of gelatin. For gelatin type B, used for the standard formulation, it is between pH 4.7 to 5.9 and for gelatin A between 6.0 and 9.5.[58] This results in different zeta potentials at the same pH. NPs made from gelatin A show a positive zeta potential at neutral pH. This should modify the interaction between the freshly produced GNPs with the PLGA. To address this, GNPs in PLGA have been produced according to the standard procedure described in chapter 6.2.2.6 with the following differences. Gelatin B was replaced by gelatin A (Bloom 175, Mw 40,000 – 50,000Da). In addition, the used amount of gelatin was varied to 10 mg, 20 mg and 30 mg respectively. All formulations have been investigated with and without poloxamer 188 in the nonsolvent phase as triplicates. Particle morphology was examined in SEM. Zeta potential and hydrodynamic diameters have been measured by DLS and gelatin load was analyzed by BCA assay.

6.2.3   Cell Viability Assay

The toxic potential of new formulations is usually firstly examined *in vitro* with cell viability tests to gain insights in the biocompatibility. As only materials are included in the formulation whose biocompatibility is already proven and which are already in use for parenteral applications a very low toxic potential was expected. The cell work in this

section was performed in collaboration with Thorben Fischer within his Diploma thesis. Cell viability was investigated with a MTT assay on adenocarcinoma human alveolar basal epithelium cells A549. The MTT assay displays a rapid and precise method to quantify viable cells. The principle is a reductive ring opening, in mitochondria of living cells, from the yellow 3-(4,5-dimethythiazol-2-yl)-2,5-diphenyl tetrazolium bromide (MTT) to the dark blue formazan and measured at a wavelength of 550 nm.[178] The reaction is illustrated in Figure 6-5.

3-(4,5-dimethylthiazol-2-yl)-2,5-
diphenyl-2*H*-tetrazoliumbromide
(MTT)

yellow

(*Z,E*)-5-(4,5-dimethylthiazol-2-yl)-
1,3-diphenylformazan
(Formazan)

purple
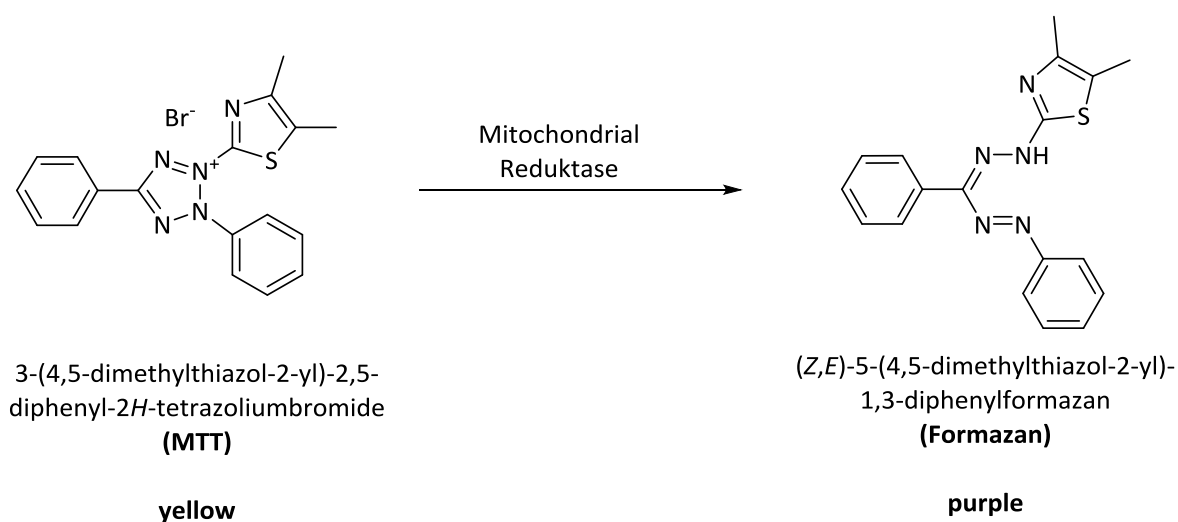
Figure 6-5: Reaction of the tetrazolium salt MTT to formazan during the cell viability test

A549 cells have been chosen in regard of a possible further use of the NPs to develop a nano-structured microparticulate drug delivery system for pulmonary application. A549 cells are widely used to mimic drug metabolism and interactions with drug delivery systems of type II pulmonary epithelial cells *in vitro.*[179] A549 have been cultivated in RPMI-1640 with 2 mM glutamine and 10 % FCS in sterile 96-well plates until a cell number of approximately 10,000 cells per well. Cells have been washed with HBSS buffer two times and incubated with different concentrations of GNPs in PLGA for 4 h. For the evaluation, a positive and a negative control have to be included in the experiment. For a positive control the cells are treated with 2 % Triton X-100 which causes cell lysis due to the surface activity. HBSS was taken as positive control, to keep the cells in not harmful condition, so no induced cell death will occur during the incubation time. Before the cells have been incubated with 200 µl of MTT reagent for 4 h at 37°C they have been washed with HBSS buffer again. After the incubation time allowing for uptake of the tetrazolium salt and reduction to formazan the supernatant was removed. The formed formazan in

the metabolic active cells was then dissolved in DMSO for a quantitative read out at a wavelength of 550 nm with an Infinite®M200 plate reader. Positive and negative controls have been used to calculate the cell viability

$$Cell\ viability\ (\%) = \frac{absorption\ sample - absorption\ positive\ control}{absorption\ negative\ control - absorption\ positive\ control} * 100 \qquad (8)$$

All samples have been tested from three separately produced batches in triplicate.

6.2.4 Loading of Drugs

This NP formulation was developed as a delivery platform for the use of different hydrophilic macromolecular drugs. Therefore, we investigated the load of compounds with different sizes and chemical characteristics. In the present thesis the loading processes and read outs for three of the examined compounds are described. The entrapment efficiency was calculated with the following equation:

$$Entrapment\ Efficiency\ (\%) = \frac{Mass\ Drug\ in\ NPs(g)\ /\ Mass\ NPs\ (g)}{Mass\ Drug\ used\ (g)\ /\ Mass\ Polymer\ used\ (g)} * 100 \qquad (9)$$

If the load in percent was examined it was calculated as follows

$$Load\ (\%) = \frac{Mass\ Drug\ (g)}{Mass\ Nanoparticles\ (g)} * 100$$

$$(10)$$

6.2.4.1 Loading of Locked Nucleic Acid

Locked nucleic acids are nucleic acid analogs with a 2′-O,4′-C-methylene bridge stabilizing the furanose in the C3′-*endo* conformation which is illustrated in Figure 6-6. LNA monomers can be coupled with other DNA or RNA monomers or phosphodiester linkers. The modification leads to an extraordinary binding affinity to the complementary strain. This holds true for fully modified strains as well as for mixmers (a combined oligomer of alternating short segments of LNA and DNA or RNA). The increased stability of LNA*DNA or LNA*RNA in comparison to the natural duplexes results in a raised thermal stability of 4.0 to 9.3°C per induced LNA monomer. The modification results in a resistance to nucleases, which is an important aspect with respect to the use of LNA as therapeutic *in vivo* or diagnostic tool *in vitro* as nucleases are ubiquitous and so challenge nucleic acid therapeutics for example in serum samples or the target cells.[180] The combination of these LNA characteristics lead to a prolonged half-life time *in vivo* which is reported to be up to 1 week in mice and 2 to 3 weeks in monkeys in comparison to free plasmid DNA which shows half-times of a few minutes.[181] *In vivo* studies demonstrated a good

tolerance with less immuno-stimulation and acute toxicity, like complement activation or prolonged bleeding time, than nucleic analogs of earlier generations. After *i.v.* administration LNA accumulates in kidney, liver, bone marrow, spleens and lymph nodes, but does not reach brain, spinal cord, testis and lenses. LNA antisense strains are developed for example for the treatment in cancer, metabolic disorders or infectious diseases with ongoing clinical trials in different phases.[182] The ability of LNA to cross cellular membranes is very low. This justifies the need of a biocompatible delivery system for LNA. Therefore, there are studies with complexes of LNA with polyethylenimine (PEI) which is a common positively charged complexing agent for transfection studies of nucleic acids.[183] PEI is showing good transfection efficiencies but is related to toxic effects too.[184] Therefore in this study the ability to load LNA into GNPs in PLGA as a potential non-viral vector is investigated.
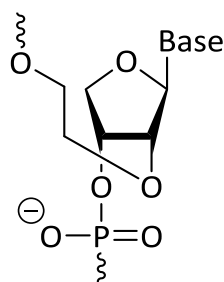
Figure 6-6: Structure of LNA in the β-D-ribo configuration

GNPs in PLGAs have been produced according to the standard procedure described in 6.2.2.6. For quantification LNA was labeled radioactive with phosphorus-32 (^{32}P) which decays into sulfur-32 by β^--decay (Figure 6-7).

$$\ce{^{32}_{15}P} \longrightarrow \ce{^{32}_{16}S} + e^- + V_e$$
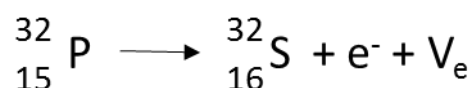
Figure 6-7: Decay of ^{32}P into ^{32}S by β−decay

LNA was kindly provided by the Gruenweller lab at the department of Pharmaceutical Chemistry at the Philipps University of Marburg. Labelling was done by Dr. Kerstin Gruenweller-Lange from the same working group. For particle preparation 10 mg of dissolved gelatin was mixed with the necessary amount of labelled LNA to obtain 20,000, 100,000 and 250,000 counts per minute (cpm) respectively. Gelatin was then precipitated together with LNA to obtain loaded GNPs in PLGA. After purification on the next day all samples have been divided and freeze dried and the gravimetric yield determined in

triplicate. Therefore, Eppendorf tubes have been weighted empty and after freeze drying with an analytical balance. In addition, the cpm of these samples were measured. This was used to calculate the entrapment efficiency of LNA with equation (9). For protection, all work was carried out behind an acrylic glass shield. NPs loaded with unlabeled LNA were used to measure hydrodynamic diameters and particle size distribution in the Zetasizer and morphology in SPM and SEM.

6.2.4.2 Loading and Transfection with eGFP PEI,

The cell work described in the following chapter was performed by Dr. Nadine Wilhelm at the Fraunhofer Institute for Biomedical Engineering (IBMT, Sulzbach/Saar, Germany and at the external side in Oxford, United Kingdom).

The read out for this particle formulation was the expression of enhanced green fluorescent protein (eGFP) after the transfection of human embryonic kidney cells (HEK293T). This is a cell line which was derived in the late 1970s by the transfection of human embryonic kidney cells with DNA fragments of the adenovirus type 5.[185] The plasmid for the expression of eGFP was isolated from Max Jacobs and Nadine Wilhem at the Fraunhofer IBMT (Sulzbach/Saar, Germany). The extraction followed the protocol of the used EndoFree Plasmid Mega Kit (no.: 12381). For the transfection studies sterile particles have been produced. Therefore, all vessels and devices, which were in contact with the formulation, have been autoclaved in a FVS/2 autoclave before use. Gelatin was autoclaved in a concentration of 40 mg/ml too. The production was performed in a laminar airflow workbench (Technoflow 2F120-II GS). Immediately before particle production 200 µl of a 1.5 mg/ml plasmid solution was mixed with 250 µl of gelatin solution. After NP assembly and purification according the normal protocol described in chapter 6.2.2.6. 2.5 ml of the NP suspension were dispersed in 10 ml of a 2 % (w/V) PEI in water solution and incubated for 15 min. PEI coated samples have been purified twice in the centrifuge at 6,000 g for 10 min. To be able to redisperse the particles after freeze drying, NPs have been collected in a freshly sterile filtered D-sorbitol solution after centrifugation and subsequently lyophilized in an Alpha 2-4 LSC freeze dryer. Preliminary transfection experiments with uncoated and positively PEI coated NPs, showed the predominance of the positively charged particles. Therefore, in the experiment with the sterile particles only this formulation was used. After freeze drying a part of the formulation was tested for sterility. For this test NPs have been incubated on agar plates

for 5 days at 37°C as well as autoclaved gelatin solution and a negative and a positive control. Afterwards the agar plates have been investigated for bacterial growth. Sterile particles have been redispersed in Dulbecco´s Modified Eagle Medium (DMEM). The transfection was started 24 h after cells are seeded and medium was refreshed to DMEM 24 h after transfection. Images for evaluation have been taken 48 h after medium change at a wavelength of 543 nm. As control, cells have been grown without treatment and have been transfected with pure plasmid.

6.2.4.3   Fluorescein-labelled Dextran

Both already described tested substances are relatively small. As the objective of this thesis was to develop a platform system, which can be loaded with various drugs of an as large as possible size range, there is a need to investigate larger substances too. Therefore, fluoresceinisothiocyanat-labelled dextrans (FITC-dextran) with different molecular weights (20 kDa, 70 kDa, 150 kDa) have been encapsulated. Loading dose was 1 mg per batch, which was added from stock solutions to the gelatin before precipitation. The following procedure was as described in 6.2.2.6. The read out was the loading and the encapsulation efficiency based on the fluorescence signals. Both were determined after particle hydrolysis in 0.5 ml NaOH (0.5 M) to dissolve PLGA at 37°C for 90 min and neutralization to pH 7 with 0.5 M HCl. Samples have been filled up with deionized water to 1 ml and measured in triplicate at a wavelength λ = 520 nm in 96-well plates with an Infinite®M200 plate reader.

6.2.5 Further Analytics for Structure Analysis

For smaller molecules good encapsulation efficiencies could be achieved, nevertheless the load was always relatively small and did not exceed 0.11 µg FITC-dextran$_{70}$/mg NPs. This, together with a general interest in the exact particle structure, was the driving force to investigate in the exact particle structure. Three possible inner structures of polymer distribution are postulated which are illustrated in Figure 6-8. The optimal distribution of gelatin and PLGA would be one gelatin NP stabilized by a surrounding PLGA layer (a)). In b) the possibility of small GNPs embedded in a PLGA matrix is shown whereas c) represents the possibility of a hybrid particle where gelatin and PLGA are meshing over the entire particle.
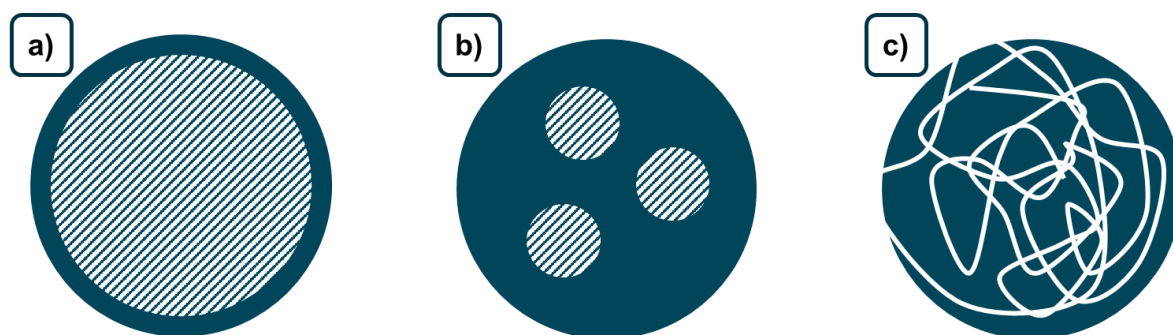
Figure 6-8: The three possible structures postulated for the standard formulation. The white part with blue lines indicates gelatin, the solid blue area represents PLGA.

6.2.5.1 Confocal Laser Scanning Microscopy for Structure Analysis

The first analysis regarding the structure was performed to investigate in the colocalization of gelatin and PLGA. Therefore, both polymers have been colored and examined in the confocal microscope. The working principle of CLSM is already explained in 5.2.6 for the interaction between cGNPs and A549 cells. In contrast to these experiments the following work was performed at a Zeiss Axiovert 100M. For the NP production the standard procedure described in 6.2.2.6 was adopted to have fluorescent dyes which can be detected separately from each other in both polymers. Therefore 250 µl of the dissolved gelatin was mixed with 20 µl of a 50 mg/ml tetramethyl-rhodamine isothiocyanate dextran 70 kDa (TRITC-dextran$_{70}$) and precipitated in the acetone/DMF solution. TRITC-dextran loaded GNPs have been dispersed in fluorescein amine labelled PLGA (FA-PLGA), produced by Dr. René Rietscher according to literature[186]. As a reference pure FA-PLGA NPs and TRITC-dextran loaded GNPs in unlabeled PLGA have been used. For CLSM analysis particles have been diluted 1:10 and 920 µl NP dispersion

was incorporated in 80 µg of an agarose gel. For visualization an argon laser with a wavelength of 488 nm and a helium-neon laser with a wavelength of 543 nm respectively have been used.

6.2.5.2 Transmission Electron Microscopy

Transmission electron microscopy makes use of electrons penetrating through the specimen. Electron sources are usually LaB6 rods or tungsten filaments. The acceleration voltage ranges from 60 keV to 3 MeV. The electron beam generation is the same as described for SEM in chapter 5.2.4. For imaging very thin samples are necessary. The electron beam is bundled before hitting the sample so electrons are imping in parallel to each other. On the way through the specimen the electron beam interacts with the sample. When the beam encounters an atom it is scattered, if no atoms are encountered it goes straight through the sample. The scattering is dependent on the atom´s electron density and the specimen thickness. An aperture filters electrons which are scattered to a greater value. As scattered electrons are removed from the beam, areas of higher electron scattering occur dark, whereas bright areas are regions without or with only low scattering. This imaging mode is called bright field (BF).
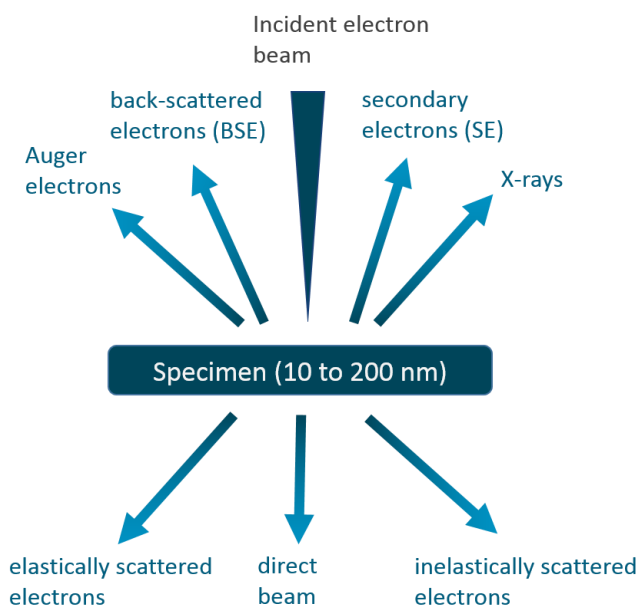
Figure 6-9: Scattering possibilities of electrons after interacting with the specimen

If the aperture is moved to the side, unscattered electrons are removed and scattered electrons are detected we talk about dark field imaging. For amorphous substances no additional information can be received. Just the bright and dark areas are inverted.

Electron scattering is not only influenced by the atom density. Depending on where the beam encounters the atom the scattering has different characteristics. Figure 6-9 illustrates the possibilities how electron scattering can occur. Elastically scattered electrons do not undergo any energy loss whereas inelastically scattered electrons lose energy. This loss is specific for the element the electron beam is in interaction with and the region of the atom where the electron beam is hitting the atom. Secondary electrons and back scattered electrons interact relatively close to the surface and are used in SEM. Electrons going through the specimen are scattered either elastically, without any energy loss, and used for imaging in TEM in the BF mode or inelastically, with an element specific energy loss, used in electron energy loss spectroscopy (EELS) and energy filtered TEM (EFTEM).[187]

6.2.5.3 Cryo-TEM for Structure Analysis

In cryo-TEM NPs can be imaged in their frozen-hydrated state and so can be depicted in the way they are present in suspension. Frozen samples are very beam sensitive. To prevent sample damage a low electron dose is required. For polymers which are not packed in a dense manner, the contrast can be relatively low. Nevertheless, it is possible to see differences in the electron density.[188] These differences are supposed to distinguish between gelatin and PLGA. As reference systems, pure PLGA and pure gelatin NPs have been used as well as a mixture of the two formulations. For imaging 3 µl nanosuspension were dropped on a holey-carbon film on a copper grid and stamped for 2 sec to the grid (Plano S147-4). Excessive water is removed during plotting. The specimen was immersed into -165°C cold liquid ethane, with a Gatan CP3 cryoplunger, to freeze it within a time as short as possible to obtain an amorphous state. Samples have been kept at liquid nitrogen and transferred to a Gatan 914 cryo-TEM holder. A JOEL JEM 2100 TEM with a LaB6-cathode and a Gatan Orius SC100 camera was used to image samples at a temperature of -170°C with an acceleration voltage of 200 kV in the bright field mode. The electron dose was set to 32 pA/cm². Images have been taken in a time series to capture the transformation process of the materials during the exposure to the electron beam. Particle diameter and shell thickness are measured with ImageJ.

6.2.5.4 Energy filtered TEM

As described in 6.2.5.2 electrons scattered inelastically by the specimen undergo an energy loss. The scattered beam can be split in an electric prism according to the energy of the electrons. In this way, electrons with the same energy occur at the same area at so-called energy selective levels. In EELS these levels are captured by a charge couple device (CCD) camera and the brightness can be read out. This is then displayed in an EEL spectrum. The "zero-loss-peak" is representing elastically scattered electrons and its maximum is set to "0" at the abscissa. The "zero-loss" area is followed by the low loss area which ranges from 0 eV to 100 eV. All energy losses above 100 eV occur when inner shell electrons are ionized. In this area the intensity is very low, therefore the aperture has to be enlarged and the measurement time needs to be prolonged. To avoid damage to the camera the zero-loss-peak and the low-loss-area are usually cut off. In the core-loss area the energy is, in contrast to the low loss area, not only specific for the element they are also specific for the orbital the ionized electron was located in before ionization. The EEL-spectra shown in this thesis are representing the core-loss area. An example for the core-loss region of an EEL spectrum for crosslinked GNPs is shown in Figure 6-10.
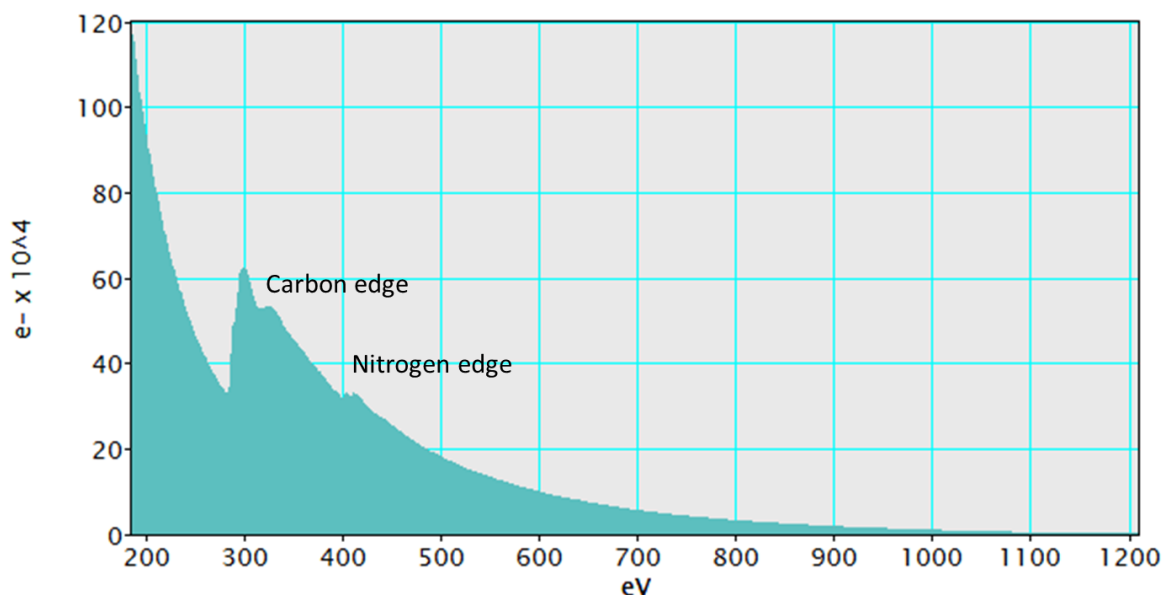
Figure 6-10: Core-loss area of an electron energy loss spectrum of crosslinked gelatin nanoparticles showing the carbon and nitrogen edges.

Images generated in the energy filtered TEM mode make use of the energy loss of inelastically scattered electrons. After passing the specimen, scattered electrons need to be focused to bring them in the same angle in the electronic prism, where the electrons

are separated according to their energy. In front of the detector a filtering slit is placed that allows only electrons of certain energy to pass and subsequently be imaged element specific. To eliminate the background signal at least two pictures are taken, one directly before the edge of the element of interest and the other one at, or immediately after, the edge. The resulting image shows exactly if the corresponding element is present at a certain place or not. By comparing different images, the material composition and in this experiment the polymer, whether it contains nitrogen, which indicates gelatin or carbon or oxygen, which are present in both polymers. For EFTEM analysis 3 µl of the nanosuspension was dropped on a holey-carbon film and, after complete drying at room temperature, transferred to a JOEL JEM 2100 TEM. At an acceleration voltage of 200 kV energy filtered images of the elements carbon, nitrogen and oxygen have been taken with a Gatan image filter (GIF 2002) and a 2048x2048 pixel slow-scan camera (Gatan model 850). As reference system pure gelatin particles have been investigated.

6.3   Results and Discussion

6.3.1   Formulation Development of GNPs in PLGA

The aim of the experiments described in this chapter was a core-shell formulation of GNPs stabilized by PLGA without crosslinking to be used as formulation platform for the delivery of hydrophilic macromolecular APIs. Therefore, the hydrophilic gelatin part should show a constant and sustained release so the embedded drug will be available over a prolonged time range. In addition, the gelatin proportion should be as high as possible.

6.3.1.1   Development of a Suitable Formulation

The starting point of the formulation development was the study with GE100-NiNOS, which are GNPs stabilized with Eudragit® E100.[189] The first system proving the possibility to conserve the shape of GNPs without crosslinking. As Eudragit® E100 is not suitable for many applications the system needs to be developed further. Therefore, different combinations of solvents and stabilizers have been tested all meeting the requirements described in chapter 6.2.2.5.
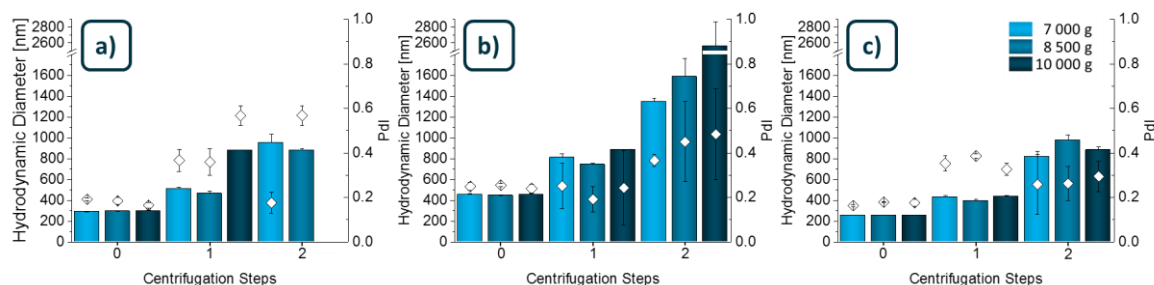
Figure 6-11: Hydrodynamic diameters and PdIs of GNPs in PLGA with DDA as stabilizer in dependency of the homogenization time a) one minute, b) three minutes and c) 5 minutes and the number of centrifugation steps for purification.

The formulation of which the hydrodynamic diameters and PdIs are presented in Figure 6-11 have been produced with DMSO to dissolve gelatin which was then precipitated in acetone:DMF 1:1 with DDA as stabilizer. PLGA was dissolved in ethyl acetate. The particles obtained show hydrodynamic diameters around 250 nm and a PdI between 0.15 and 0.2 with a tendency to smaller sizes with a narrower particle size distribution. These parameters are well suitable for the formulation. Looking at the sizes and PdIs after already the first centrifugation step NPs size and PdI are rising even with a relative low centrifugation speed of 7,000 g indicating agglomeration. A homogenization time of 5 min

was chosen as NPs showed the smallest hydrodynamic diameter with a good PdI. Longer homogenization did not lead to smaller particles or PdIs. NPs showed a round shape and a smooth surface but have not been stable in SEM for imaging. The gelatin content was around 9.04 % with a high gelatin burst release of 28.02 %. In the following formulation development the improvement of these parameters was addressed. In a first step the influence of the nonsolvent was investigated. Acetone and DMF with DDA as stabilizer have the function of the nonsolvent solution. As can be seen in Table 6-1, the sizes were increased to hydrodynamic diameters of 309 nm and 418 nm with a good particle size distribution for acetone. The encapsulation efficiency and load of gelatin was decreasing for pure nonsolvents. This means a smaller hydrophilic compartment in the formulation. At the same time, the gelatin burst release increased. As the hydrophilic proportion should be increased for a potentially higher drug loading, the first formulation with acetone:DMF in an equal ratio was used as nonsolvent again. Now the stabilizer was changed to Pluronic®F68 as described in chapter 6.2.2.5. The sizes and PdIs have been still in the range aimed for and the ζ-potential was approximately -20 mV, which is a strong enough surface charge for a stable particle formulation. Looking at the gelatin entrapment the new formulation shows clear advantages over the former ones. Here an entrapment efficiency of 64.4 % could be achieved. The load of 12.02 % is still expandable but is improved in comparison to the former formulations. Looking at the release characteristics a burst release of less than 30 % can be detected. The further release characteristics are addressed later in this paragraph. To complete the study, Pluronic® F68 was as well tested with pure acetone as antisolvent. This formulation row shows the same tendency as when DDA was used for stabilization. Therefore, the combination of acetone and DMF together with poloxamer 188 was set as standard for further investigations.

Nonsolvent	Stabilizer	Hydrodynamic diameter [nm]	PdI	ζ-Potential [mV]	Gelatin Load [%]	Gelatin Entrapment [%]
Acetone:DMF	DDA	247.62 ± 42.68	0.153 ± 0.033	-17.07 ± 1.02	9.04 ± 2.52	49.78 ± 10.33
Acetone	DDA	309.9 ± 8.72	0.152 ± 0.018	- 17.77 ± 2.71	3.50 ± 0.54	26.20 ± 11.04
DMF	DDA	418.13 ± 7.96	0.338 ± 0.011	-17.27 ± 1.45	3.80 ± 0.63	18.97 ± 5.36
Acetone:DMF	Pluronic F 68	272.61 ± 10.38	0.139 ± 0.012	- 19.02 ± 0.88	12.02 ± 4.45	64.4 ± 12.18
Aceton	Pluronic F 68	253.9 ± 4.0	0.16 ± 0.023	-19.83 ± 1.65	-	53.12 ± 8.67

Table 6-1: Formulation development with different nonsolvents and stabilizers. Acetone and DMF in an equal mixture together with poloxamer 188 showed the best results in all tests and therefore was set as standard formulation.

This standard formulation shows perfectly spherical NPs in SEM and SPM investigations. The results of the visualization experiments are presented in Figure 6-12. Particle size determined in SEM, with a diameter of 135.75 ± 23.07 nm, is smaller than measured with DLS. This is according to the expectations and can be explained because in DLS the hydrodynamic diameter is determined which includes the surrounding solvation shell. As a second reason, particle shrinkage during drying has to be considered.
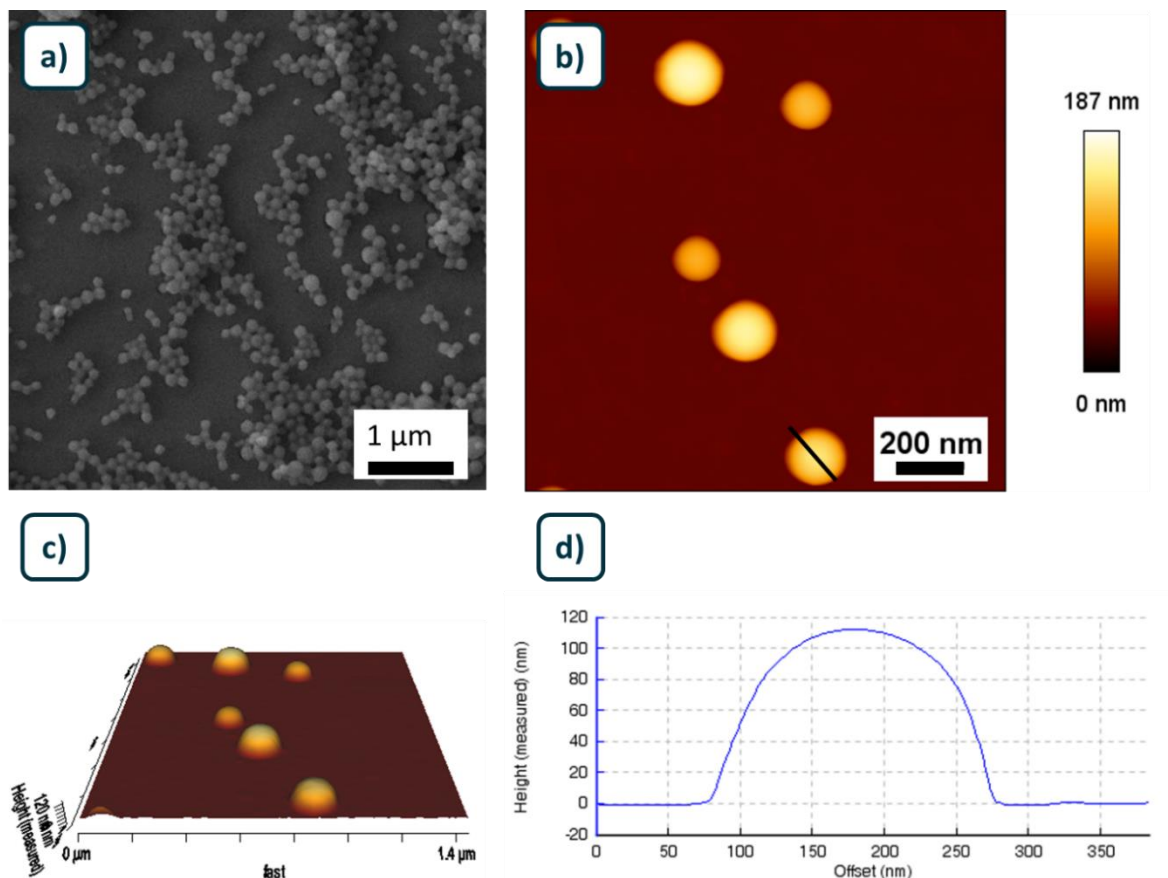

Figure 6-12: Images of GNPs in PLGA standard formulation in SEM a) and displayed in a closer view in SPM height 2D image in b) with the belonging 3D height image in c) and a cross-section in d). The cut through the NPs for the cross section is marked in b). It shows the spherical particle shape with a diameter of around 175 nm and a height of 115 nm.

The SPM height images and the cross-section presented in Figure 6-12 b)-d) have been taken in dry conditions and underline the particle shape and the smooth surface. Particles do not show any dents or holes. The selected particle shows a diameter of approximately 175 nm with a height of 115 nm in the cross-section. Compared with cGNPs captured in air the new formulation shows a very slight collapse only. Release profiles and encapsulation efficiency was investigated by BCA assay. The gelatin release profiles of the three formulations with the most promising encapsulation efficacy and load of gelatin have been determined over 6 days. The result is presented in Figure 6-13. Both DDA-

stabilized formulations showed a high burst release of 100 % and 60 % respectively. With acetone:DMF as nonsolvent (60 % burst release) after 6 days 10 % more are released in comparison to the start of the experiment. Acetone and DMF in equal proportions with poloxamer 188 for stabilization showed only a burst release of less than 30 %. Gelatin is released continuously over 6 days. After this period 60 % is released from the system, so 40 % are still remaining and building the matrix for a sustained drug release. In combination with the determined physicochemical parameters this properties are well suited for a drug delivery platform system for the delivery of hydrophilic APIs and set as the standard formulation described in chapter 6.2.2.6.
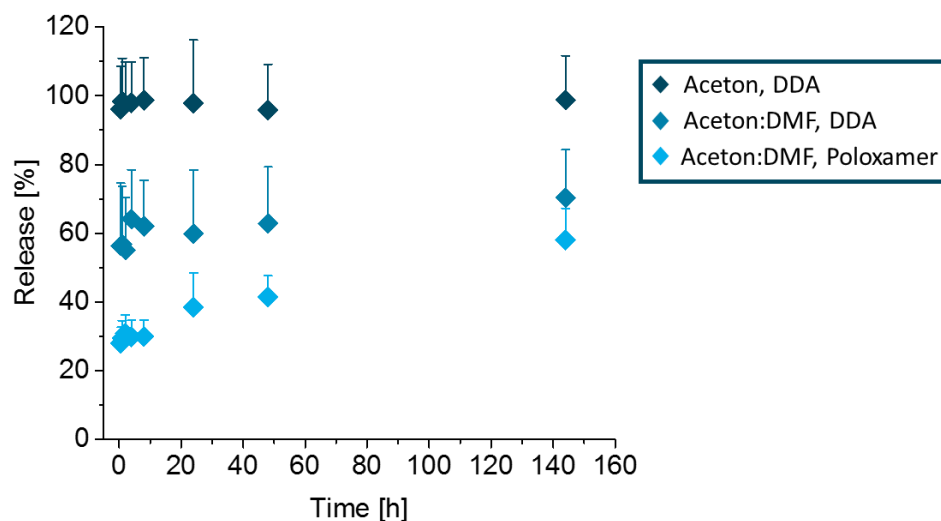
Figure 6-13: Gelatin release of GNPs in PLGA with different nonsolvents and stabilizer over 6 days. Gelatin content is determined by BCA assay.

Based on the standard formulation, investigations, aiming for a simplified process, have been performed. The gelatin load and release should be at least the same compared to the standard formulation. Therefore, the preheating of gelatin in water was skipped and DMSO as solvent was mixed with water or completely replaced. In a second step gelatin was dissolved in water with adjusted pH values of pH 6, 4 and 3. The aim was to enhance the electrostatic interaction between negatively charged PLGA and positively charged gelatin at pH values lower than the IEP. All further investigations have been tested against the standard formulation. Size and particle size distribution of the resulting NP formulation are shown in Figure 6-14. Except of the equal mixture of DMSO and deionized water all hydrodynamic diameters range around 250 nm.
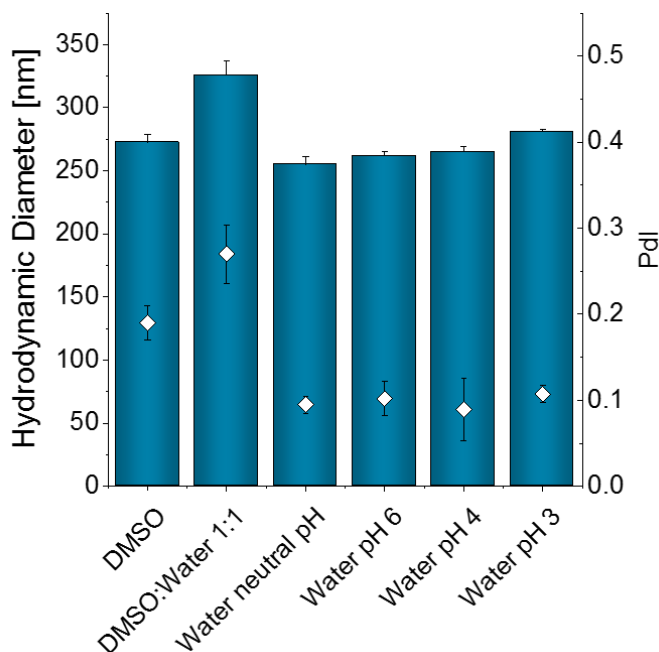
Figure 6-14; Sizes and PdI of GNPs in PLGA prepared with different gelatin solvents. Most formulations showed a hydrodynamic diameters around 250 nm and a narrow particle size distribution with a PdI below 0.2.

Regarding the proportion of the gelatin compartment no benefit could be achieved. In the opposite, the gelatin load decreased. The highest loading was 2.7 % when gelatin was dissolved with deionized water and an adjusted pH of 4. This was slightly better than pH 6 (gelatin load of 2.05 %) what supports the hypothesis that the oppositely charged gelatin shows more interaction with PLGA. Nevertheless, the best results could be achieved when gelatin was dissolved in DMSO. As no benefits where obtained, the solvent combination was kept as in the standard formulation.

6.3.1.2 Varying the Gelatin to PLGA Ratio

An enhanced hydrophilic reservoir for the encapsulation of a high amount of drug was, as mentioned, the aim of this study. Therefore, the ratio of the raw materials was changed to a higher amount of gelatin than in the standard formulation. The evaluation included hydrodynamic diameter, PdI, ζ-potential, gelatin load, entrapment and release. Results are summarized in Table 6-2. Hydrodynamic diameters, PdI and ζ-potential stay nearly the same for all variations. The same holds true for the entrapment efficiency, which ranges from 63 to 71 %. In contrast, the gelatin load increased with the increasing proportion of gelatin used and reaches a share of nearly 45 % in the formulation with the highest used gelatin amount. Gelatin showed a relative high burst release of 45 % and 57 % respectively after half an hour. After one hour 54 % of the gelatin from the formulation

made by a ratio of 1:1.25 is released and 65 % of the ratio 1:0.625. As the delivery system is based on gelatin this means after one hour only 46 % or 35 % respectively of the hydrophilic compartment is left. For the standard formulation was still around 70 % gelatin left after the same time.

Gelatin to PLGA Ratio	Hydrodynamic diameter [nm]	PdI	ζ-Potential [mV]	Gelatin Load [%]	Gelatin Entrapment [%]
1:5	219.67 ± 6.92	0.139 ± 0.038	-11.45 ± 0,75	12.55 ± 3,94	64.41 ± 6.17
1:1.25	235.04 ± 16.86	0.122 ± 0.056	- 10.96 ± 1.98	28.59 ± 0.88	63.22 ± 1.93
1:0.625	210.38 ± 14.78	0.118 ± 0.086	- 11.35 ± 2.3	44.32 ± 1.66	71.29± 0.97

Table 6-2: Different gelatin to PLGA ratios and the respective NP characteristics
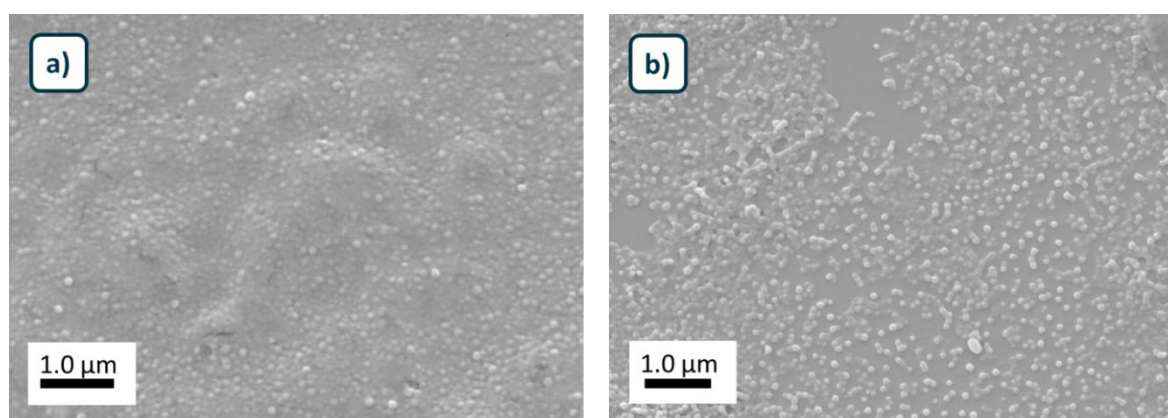
Figure 6-15: SEM image of particles made by a gelatin to PLGA ratio of 1:1.25 in a) and 1:0.625 in b).
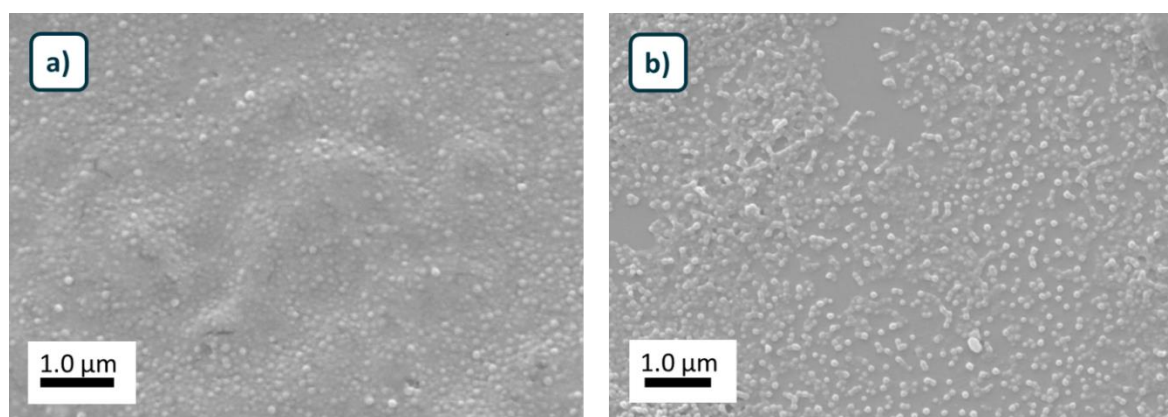
Figure 6-15 it can be seen, that particles keep their morphology with the raising gelatin fraction. NPs are still roundly shaped with a smooth surface and show a homogeneous particle size distribution in both formulations. This supports the values in Table 6-2. It can be summarized that the gelatin proportion can be enhanced with changing the ratio of raw materials while keeping the evaluated physicochemical parameters consistent. The release profile does not provide a sustained release, but could be enough for further processing like PEI coating for gen delivery like the delivery of plasmids where

transfection studies are performed with PEI coated GNPs in PLGA particles (see chapter 6.2.4.2).

6.3.1.3 Comparison between Gelatin A and Gelatin B

Gelatin A NPs exhibit a positive surface charge at neutral pH, which can be explained by the IEP at a pH between 8.0 and 9.0. This means an opposite charge of gelatin and PLGA. Based on the results from chapter 6.3.1.1 the electrostatic interaction should be enhanced and thus the encapsulation of a higher gelatin amount with the same ratio of raw material should be possible. Particle sizes are presented in Figure 6-16 a). They are larger than particles prepared by gelatin B whereas the particle size distribution is approximately the same as for PLGA NPs. This can be due to different reasons such as differences in the molecular weight, in solubility or viscosity. Opposite to the other formulations gelatin A NPs in PLGA exhibit positive ζ-potentials. Due to the IEP of gelatin this might be feasible. However, as gelatin should be packed in PLGA or both polymers building a hybrid NP it was certainly not expected to obtain a positive surface charge as the positively charged gelatin groups have to be at the outside of the particle to achieve a positive ζ-potential.
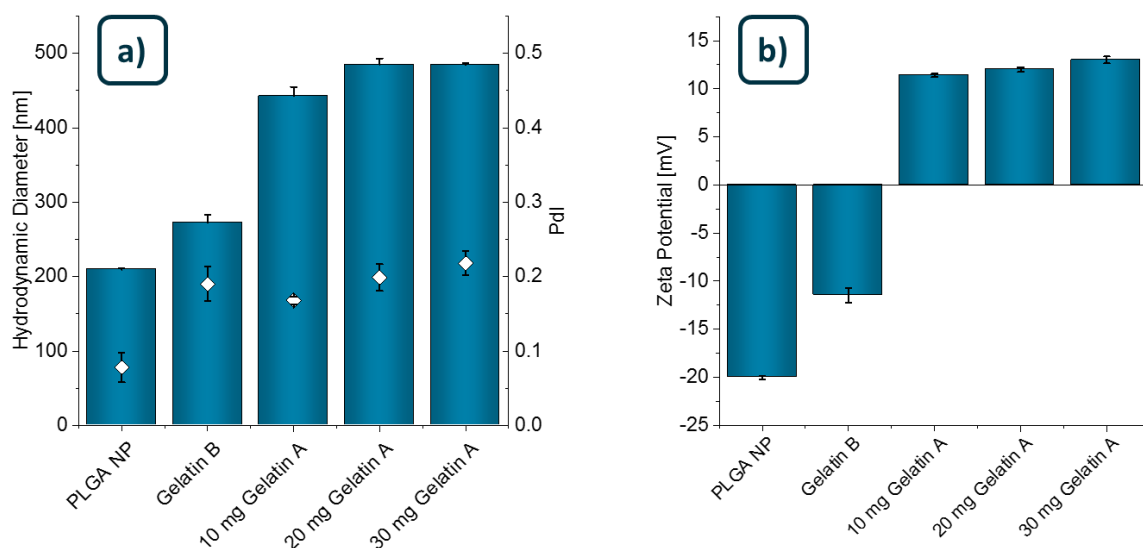
Figure 6-16: Gelatin A NPs in PLGA a) Hydrodynamic diameter and PdI and b) ζ-potential. Both parameters are compared to gelatin B NPs (Gelatin B) in PLGA and pure PLGA NPs.

The hydrophilic proportion is slightly enlarged with a gelatin compartment of approximately 15 %. Release studies have not been performed as the positive ζ-potentials indicated differences to the standard system. Nevertheless, gelatin A has to be

considered for a further formulation development especially in regard of intra cellular delivery such as for nonviral gene transfer. Here a positive surface charge is advantageous and furthermore, positively charged nanosystems show higher transfection rates than their negatively charged counterparts. Therefore particles are often coated with PEI, which brings a, not only charge dependent, cytotoxicity into the formulation.[190] The good *in vitro* safety profile of gelatin A NPs could be already shown in literature.[191] Furthermore, a larger *in vitro* uptake could be demonstrated for cationic gelatin A NPs in comparison to negatively charged GNPs produced by gelatin B.[192] This could be a potential application for the GNP in PLGA prepared with gelatin A and an advantage of gelatin as biopolymer coming with different characteristics, which can expand the spectra of the formulation platform.

6.3.2   Cell Viability Assay

The toxicity of NP formulations is a very important parameter to investigate during formulation development. Here for first insights *in vitro* cell viability was tested with a MTT assay. As a control system, with known good cell viability, PLGA NPs were used. The test results showed a very good tolerance of both NP formulations tested with A549 cells after 4 h. Concentrations from 70 µg/ml to 0.9 mg/ml have been investigated. Values above 80 % cell viability are considered as nontoxic. This is indicated in Figure 6-17 with a green background. Even in high concentrations both formulations are very well tolerated. Whereas the percentage cell viability stays constant for PLGA NPs, cell viability was increasing with decreased GNPs in PLGA concentration. This indicates an advantage of the composite particles over pure PLGA at concentrations lower the 280 µg/ml.
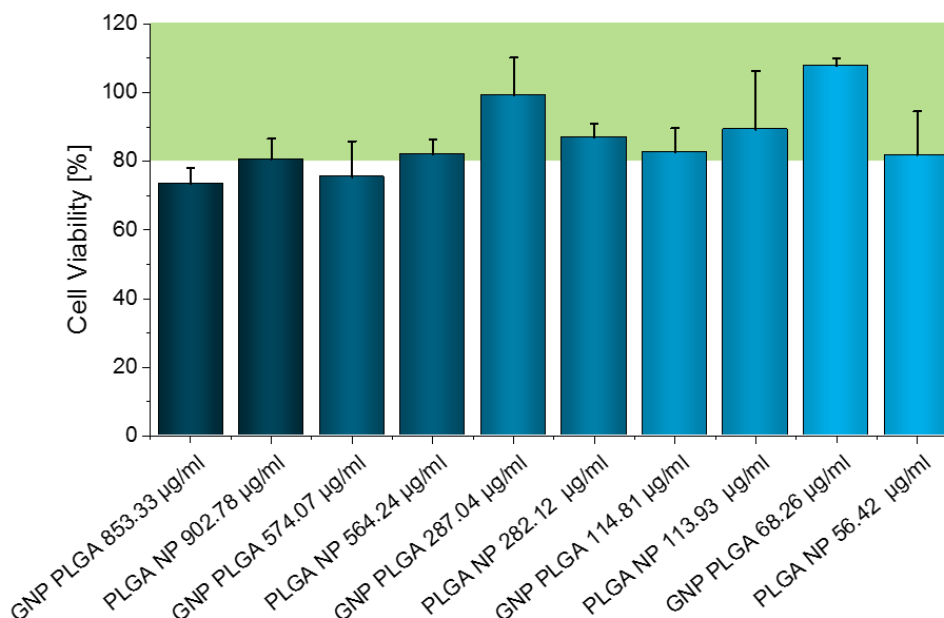
Figure 6-17: Cell viability after 4 h incubation on A549 cells tested by MTT assay. All tested concentrations are in the as nontoxic considered range.

6.3.3 Loading of Drugs

6.3.3.1 Loading of Locked Nucleic Acid

GNPs in PLGA have been loaded with radioactive labeled LNA in three concentrations 20 kcpm, 100 kcpm and 200 kcpm. LNA loaded particles have been investigated for morphology in SEM and SPM. The smooth surface of the round shape of 20 kcpm loaded NPs are visualized in Figure 6-18.
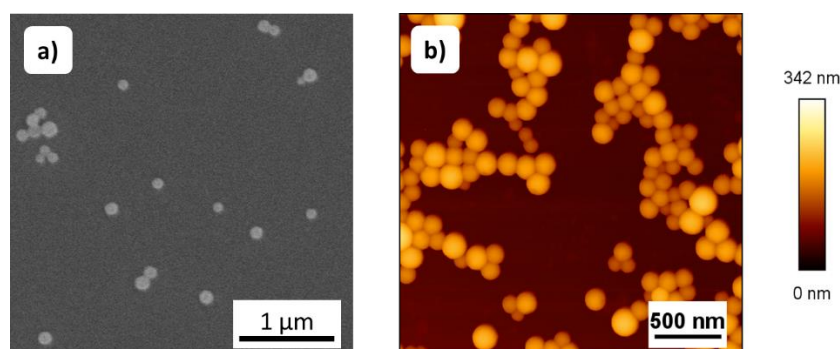
Figure 6-18: Morphology of LNA loaded GNPs in PLGA in SEM (a) and in an SPM height image (b).

Due to safety reasons, radioactive labelled samples could not be measured in the zetasizer. Two non-radioactive formulations with LNA amounts equivalent to the samples with 20 kcpm and 100 kcpm have been used to evaluate hydrodynamic diameters. The size of loaded NPs was around 225 nm and therefore, approximately 50 nm smaller than pure GNPs in PLGA. In comparison to control NPs, PdIs are slightly decreased too. With 0.139 and 0.118 particles show a narrow size distribution. Hydrodynamic diameters and PdIs are summarized in Figure 6-19 b).
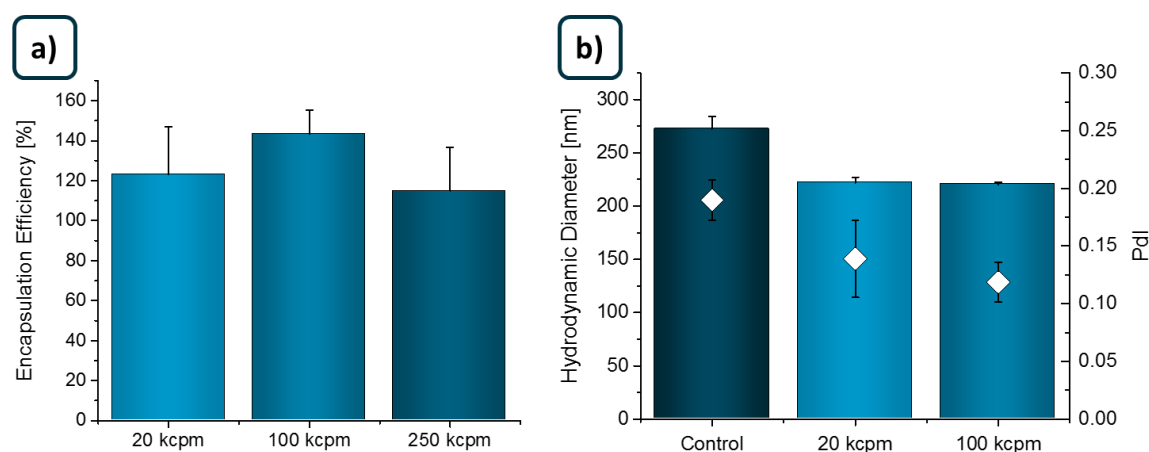
Figure 6-19: a) Encapsulation efficiency of radioactive labelled LNA in GNPs in PLGA in different LNA concentrations and b) hydrodynamic diameters and PdI´s of LNA loaded NP formulations.

The encapsulation efficiency, which is shown in Figure 6-19 a), was evaluated according to equation (9). The encapsulation efficiency of all tested concentrations was over 100 % and showed no significant difference (significance tested with Student's t-test, p > 0.05). Values above 100 % are possible due to the equation, which includes the ratio from drug to polymer used for the production. If, compared to the polymer, a higher percentage of drug goes to the end formulation the encapsulation efficiency increases. In this case the highly hydrophilic LNA goes to a very high percentage to the gelatin particles in the NP formulation. The smooth particle morphology with particle sizes of 225 nm and the very good encapsulation efficiency show the high potential of the formulation for intracellular delivery in gene therapy.

6.3.3.2   Loading and Transfection with eGFP

In cooperation with the IBMT the transfection of plasmid-loaded GNPs in PLGA was tested. The particle system not only protects the plasmid from degradation. In addition, it functions as a nonviral vector system for the delivery into the cell. For a successful transfection study the absence of microbes needs to be ensured. Microbes would contaminate cells and therefore could change their behavior and thus falsify the transfection study. As preliminary tests showed contamination in the particle formulation, the production was changed to aseptic conditions (6.2.4.2).
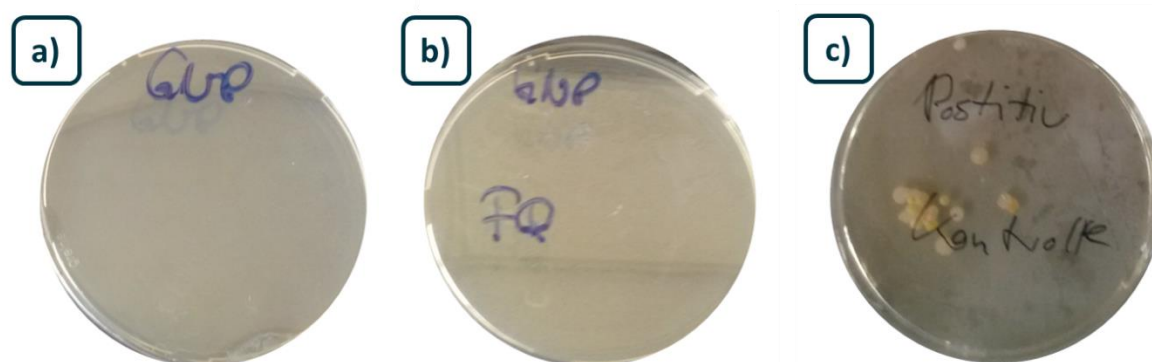
Figure 6-20: Sterility test on agar plates after 120 h of incubation at 37°C a) GNPs in PLGA before freeze drying, b) GNPs in PLGA after freeze drying with sorbitol as cryoprotector and c) a positive control with a contaminated solution.

To prove the absence of bacteria after all production steps, including freeze drying, the formulation was incubated on agar plates and compared with a contaminated positive control and a negative control which was a blank agar plate. Agar plates incubated with plasmid-loaded GNPs in PLGA before and after freeze drying are shown in Figure 6-20 a)

and b) as well as the positive control in Figure 6-20 c). After the successful aseptic particle formation the plasmid-loaded particles have been used for transfection of HEK293T cells with the plasmid coding for eGFP. Green fluorescent protein is a popular readout for transfection studies.
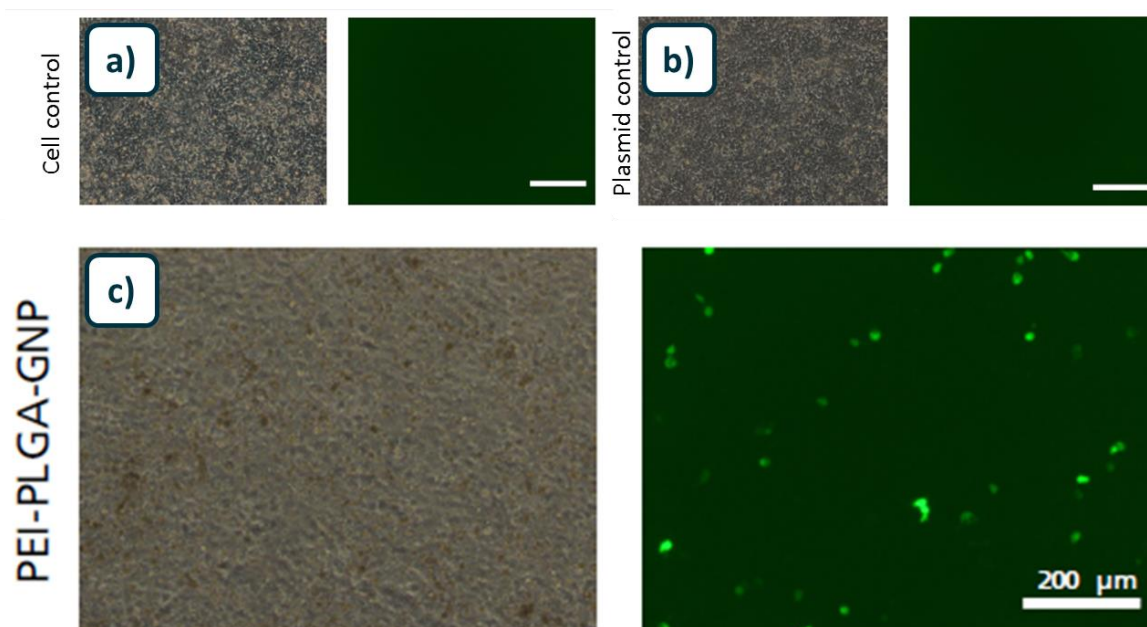
Figure 6-21: Transfection of HEK293T cells with eGFP as well as two controls each consisting of a light microscope and a fluorescent image. Cells without treatment in a) and cells incubated with plasmid without a vector in b). The successful transfection displayed in c) was performed with plasmid-loaded GNPs in PLGA. Scale bars represent 200 μm

As control untreated cells and cells which are only transfected with the blank plasmid were used. Both did not show any green fluorescence. As can be seen in Figure 6-21 cells transfected with the plasmid-loaded PEI layered GNPs in PLGA displayed in c, exhibited green fluorescence. This proves the encapsulation of the plasmid in the particle system as well as the potential of the new formulation platform for the use in intracellular drug delivery. Transfection was studied in two separately produced batches, with the restriction that the batch of the first test introduced contamination to the cells. The transfection rate is lower in the aseptic produced batch shown here and could be enhanced with a further improved formulation. Possible modifications could be an increased plasmid load to ensure all NPs can act as carrier system and thus transfect the cell after internalization. Another important parameter for the successful delivery of the drug is the release after internalization. As liberation was not studied here it can be that either some particles already released the loaded plasmid before they reach the cytoplasm or the release and exhibition of eGFP in the cell is not completed in the time

used in this study. Therefore, the release could be evaluated in different media mimicking the conditions in different cell compartments. Nevertheless, for a first insight in the use of the new platform in intracellular transfection the results are promising and should be further investigated in upcoming studies.

6.3.3.3 Fluorescein-labelled Dextran

A model compound to mimic the drug load was planned to encapsulate. Requirements, which had to be met, have been an easy analytical set up to detect and quantify the loading and the simple possibility to change the molecular weight. Therefore, the compound of choice was FITC-dextran. After the production procedure and freeze drying the particles they have been analyzed for load and entrapment efficiency. An entrapment efficiency of only 0.659 % for FITC-dextran$_{70}$ could be calculated. With an efficiency of 0.59 % for FITC-dextran$_{70}$ in PLGA no real difference could be detected. This is in contrast with the expectations as gelatin should encapsulate the hydrophilic FITC-dextran$_{70}$ to a significant higher extent than PLGA. The same result is achieved regarding to the load which was around 0.11µg per mg NP formulation no matter if FITC-dextran$_{70}$ was encapsulated in GNPs in PLGA or pure PLGA NPs. The low loading can have different reasons at one hand the drug could already be diffused out during the solvent evaporation step or while cleaning the NPs and on the other hand it could be because of the relative low hydrophilic compartment which only covers 12.5 % of the whole system. After the promising results of the encapsulation of LNA and the transfection studies described above this low loading was not expected. In addition, a delivery system, capable to load a high amount of hydrophilic macromolecules, was aimed for. Therefore, these results were not satisfying. As the gelatin content of the current formulation is only around 12 %, the inner structure of the system should be exactly known, before more time and resources are invested for an enhanced loading. Therefore, the FITC-dextran experiments were stopped at this point and the further research concentrated on the investigation of the exact structure.

6.3.4 *Further Analytics for Structure Analysis*

The knowledge about the exact polymer distribution in the NP belongs to a complete characterization. The next chapter is about different methods for the investigation of the inner structure of the platform formulation for the delivery of hydrophilic macromolecules. The methods range from colocalization of polymers to show both, gelatin and PLGA, are actually forming the NPs to an element specific imaging in energy filtered TEM using nitrogen as differentiation between gelatin and the other materials.

6.3.4.1 *Confocal Structure Analysis*

The first method was about the colocalization of gelatin and PLGA. The polymers are colored with different fluorescent dyes and excited with lasers at the appropriate wavelengths. The hydrophilic gelatin was loaded with TRITC-dextran$_{70}$ and PLGA was covalently coupled to fluoresceinamine. To enable the investigation in colocalization, particles are immobilized in an agarose gel. In Figure 6-22 the two channels are displayed separately in the top row and overlaid in the bottom row. The red channel shown in a) display the distribution of TRITC-dextran$_{70}$ and the green channel in b) is representing FA-PLGA. It is obvious that in areas with a green signal the TRITC-dextran$_{70}$ can be detected too. In c) both channels are overlaid and show the colocalization of gelatin and PLGA by a slight change in color. With these experiments, it was possible to proof that the new formulation consists of both used polymers and they are perfectly colocalized. The exact distribution is not accessible by CLSM as the resolution is limited to approximately 200 nm. Therefore, TEM analysis followed to gain more insights due to the higher resolution.
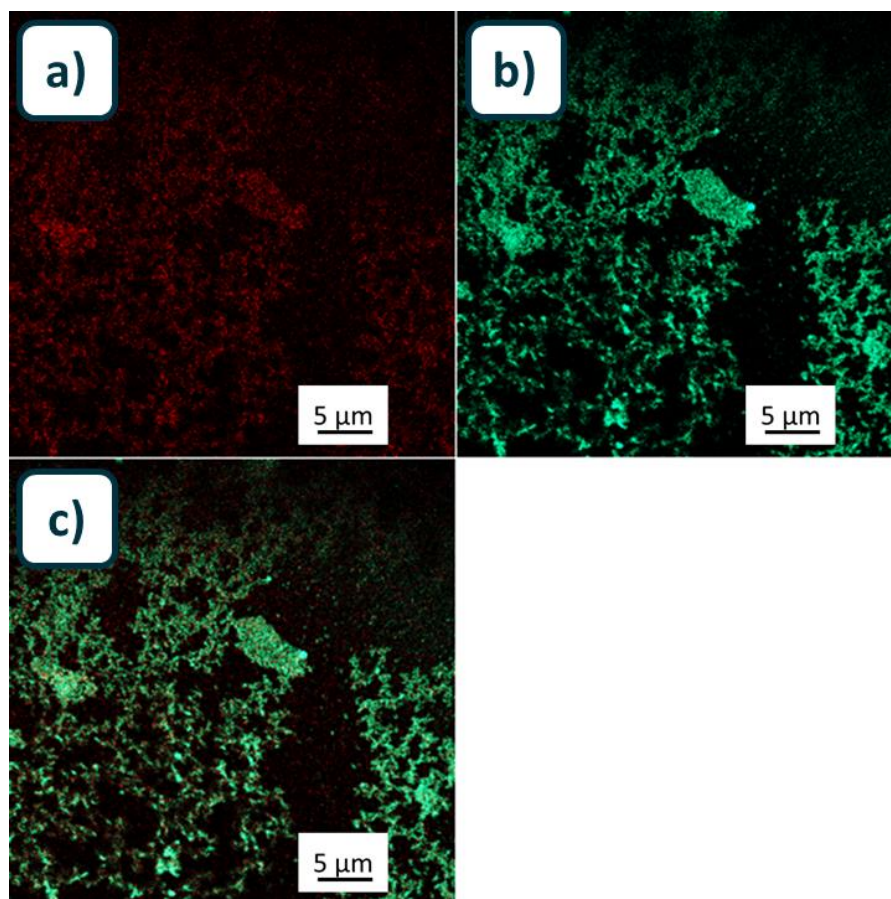
Figure 6-22: CLSM images of TRITC-dextran$_{70}$ GNPs in FA-PLGA. A) TRITC-dextran$_{70}$ in red, b) FA-PLGA in green and both channels overlaying in c). The images show a good colocalization between the two dyes.

6.3.4.2   Cryo-TEM for Structure Analysis

To increase the resolution, NPs have been examined in cryo-TEM. Particles are imaged in a thin layer of polymorph ice. The formulation was examined in time intervals to investigate the alteration caused by the energy brought to the system during the measurement. NPs reaction to the energy was compared to pure PLGA particles and to crosslinked gelatin NPs as well as a mixture of both materials and to identify the behavior of the materials in the electron beam.
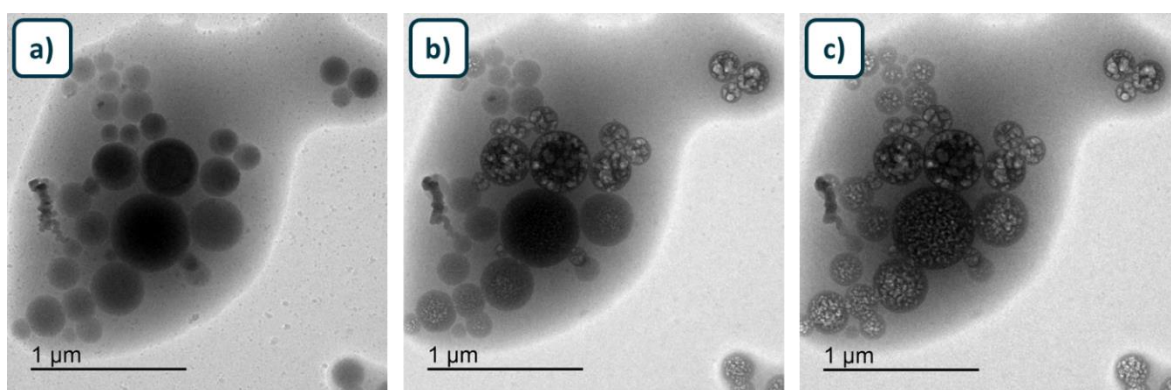
Figure 6-23: a) to c) represent a mixture of cGNPs and PLGA NPs in a time series in cryo-TEM. Particles show different sensitivity to the electron beam and the degradation patterns vary between the populations.

In Figure 6-23 a mix of PLGA NPs and cGNPs is imaged and observed over time of a few minutes in the electron beam. In a), which is the first image taken, all particles look similar with the difference that some of the particles have a higher contrast to the background than others and thus appear darker. In b) a fraction of the imaged particles is already degraded by the high energy whereas the other population is still intact. In c) all particles underwent a modification.
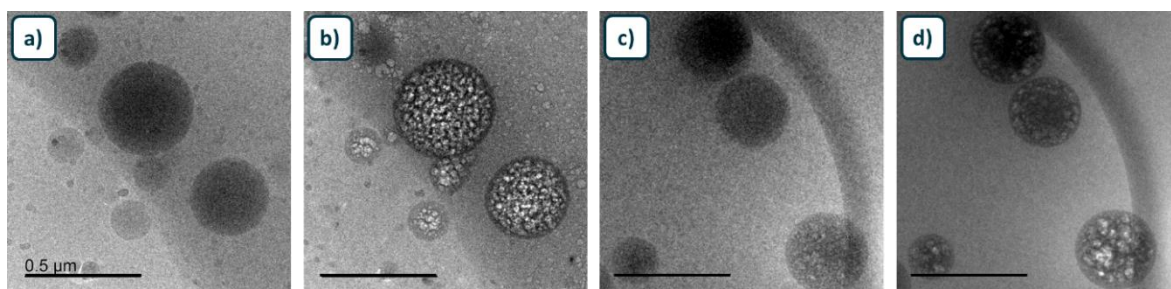
Figure 6-24: Crosslinked gelatin NPs to the right immediately after focusing (a)) and after degradation (b)) and to the right (c) and d)) PLGA NPs showing fast degradation with the formation of large bubbles. Scale bars are representing 0.5 µm.

However, the disintegration pattern is rather different. The darker NPs from the first image show less resistance to the electron beam in addition the degradation pattern is

rougher and less ordered then for the other particle fraction. If the NPs are compared in single analysis as shown in Figure 6-24 the degradation pattern observed in the mixture, can be assigned to the different particles. cGNPs, shown in image a) and b), degrade in a fine structure and resists the electron beam relatively long. PLGA NPs in contrast form larger bubbles and start to degrade within seconds. This can be seen in c) and d). Polymers react differently to the energy brought into the system by an electron beam. Polymers with conjugated systems, such as aromatics, are more resistant than aliphatic structures.[193] This can be explained because the excitation energy can be distributed by delocalized electrons. Furthermore, especially C-O-C bonds are broken easily. Both polymers investigated do not have a large delocalized electron system, nevertheless, with a small fraction of aromatic amino acids, like phenylalanine, the degradation of gelatin could be hindered slightly. The obtained small fragments diffuse out due to the high vacuum. In terms of thin samples, depressions arise. In thicker specimens bubbles are formed due to the polymer scission.[193] Under electron beam radiation the polymer backbone is broken and free radicals occur because of the interaction between the polymers and the electron beam. These radicals can either interact with each other or initiate further reactions and thus enhance the breakages. Semi-crystalline polymers, like gelatin, exhibit two regions an amorphous one and a crystalline part. In crystalline phases polymer chains are packed closer and are more oriented. Therefore, they are less accessible to free radicals. In addition, radicals can even be trapped there. This so-called cage effect reduces the number of radical scissions and rises the stability against electron beam radiation.[194] An additional effect stabilizing cGNPs in comparison to PLGA might be the covalent crosslinking. Even after backbone scission, the polymer fragment cannot diffuse out of the particle as it is still bound covalently through the sight chain.
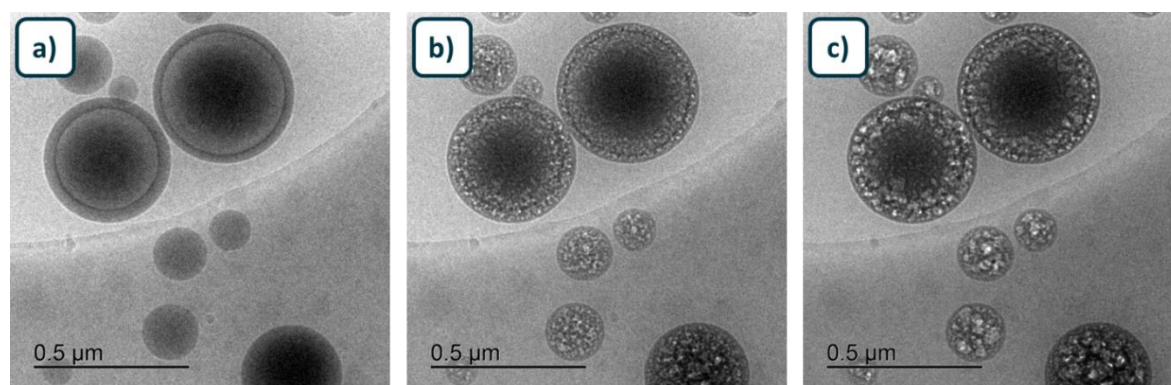
Figure 6-25: Cryo-TEM images of GNPs in PLGA showing core-shell-structure for particles of a size greater than 350 nm.

The composite particles made by GNPs and PLGA are imaged under the same conditions. As can be seen in Figure 6-25 NPs greater than 350 nm formed a clear shell with a thickness of 30 to 40 nm. The core-shell-structure stayed intact even after degradation in the electron beam. For smaller particles the shell is either too small to detect or it is not formed. From the degradation pattern it is not possible to assign which of the materials forms the shell and which one is positioned in the core. This might be because gelatin is not crosslinked here and therefore for sure reacts differently in the electron beam then the crosslinked reference particles. On the other hand the shell layer is relatively thin, so the exact degradation pattern is not accessible. At this point, it can be summarized that the polymer distribution striven for, the core-shell-model, is achieved for particles greater than 350 nm.

6.3.4.3 Energy filtered TEM

To assign which of the used polymers is forming the shell and which one is placed in the NP core, particles have been investigated in EFTEM. Because of the ice the contrast in cryo-TEM was too low to obtain a high enough contrast. Hence EFTEM was performed with dried samples at room temperature. Crosslinked GNPs have been used as reference system.
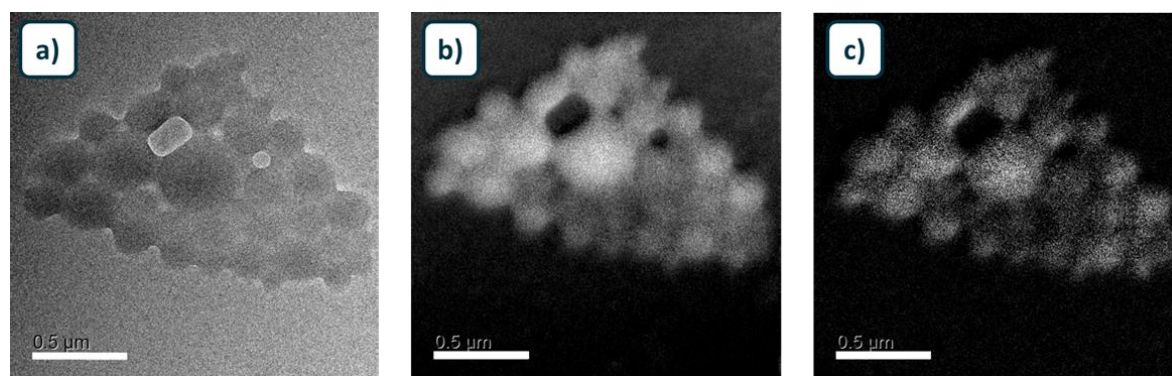
Figure 6-26: EFTEM images of cGNPs a) in the bright field mode, b) the carbon map and c) the nitrogen map showing the distribution of the two elements. Scale bars are representing 0.5 μm.

Figure 6-26 a) shows cGNPs in a BF-TEM image. Particles exhibit a low contrast to the background, as no enhancing staining was used and they melted in the electron beam. Nevertheless, the round shape was still visible. Except the one larger particle in the middle NPs show good particles size distribution. In b) and c) the carbon map and the nitrogen respectively are displayed. Both elements were distributed homogenously throughout the whole particle. In elementary analysis of gelatin the chemical composition

is determined to be carbon 50.5 %, oxygen 25.2 % whereas nitrogen only contributed with 17.0 % and hydrogen 6.8 %. This results in a brighter representation of carbon [195] in the EFTEM image. Switching from pure gelatin NPs to the composite particles we already know from cryo-TEM investigations we can expect a core-shell system at least for NPs with a diameter larger than 350 nm. Comparing the BF-image in Figure 6-27 a) and f) with the one from cGNP NPs in Figure 6-26, the formulation consisting of gelatin and PLGA occurs darker with a higher contrast to the background. This corresponds to results from cryo-TEM investigations where PLGA NPs showed the higher electron density. Looking at the BF images of GNPs in PLGA a difference in the electron density is visible. Going further to the carbon maps b) and g) particles occur very bright due to the high carbon percentage especially in PLGA. Carbon is distributed equally in all particles the same holds true for oxygen c) and h) with the deviation that oxygen is less present in both polymers. The nitrogen maps (Figure 6-27 d) and e)) attracts the highest interest as this is the element distinguishing the used substances, as it is only present in gelatin. As we know, gelatin makes up approximately 12 % in the used formulation and from this only a fraction of 17 % is nitrogen. Thus it is not surprising that nitrogen maps were relatively dark. Unfortunately, the images lost sharpness too. However, it was still clearly visible that for the particles showing the high electron density in the BF mode nitrogen showed circles and a very dark core. This means the outer layer is built by gelatin surrounding a PLGA NPs. The others, mostly smaller particles did not show this obvious core shell model but still consisted partly of gelatin. Either the resolution was too low to define the core shell structure or the smaller particles actually exhibit a mixture throughout the whole particle. As Figure 6-27 e) shows a big particle, which seems to have a homogenous gelatin distribution this seems to be more likely for the small particles too.
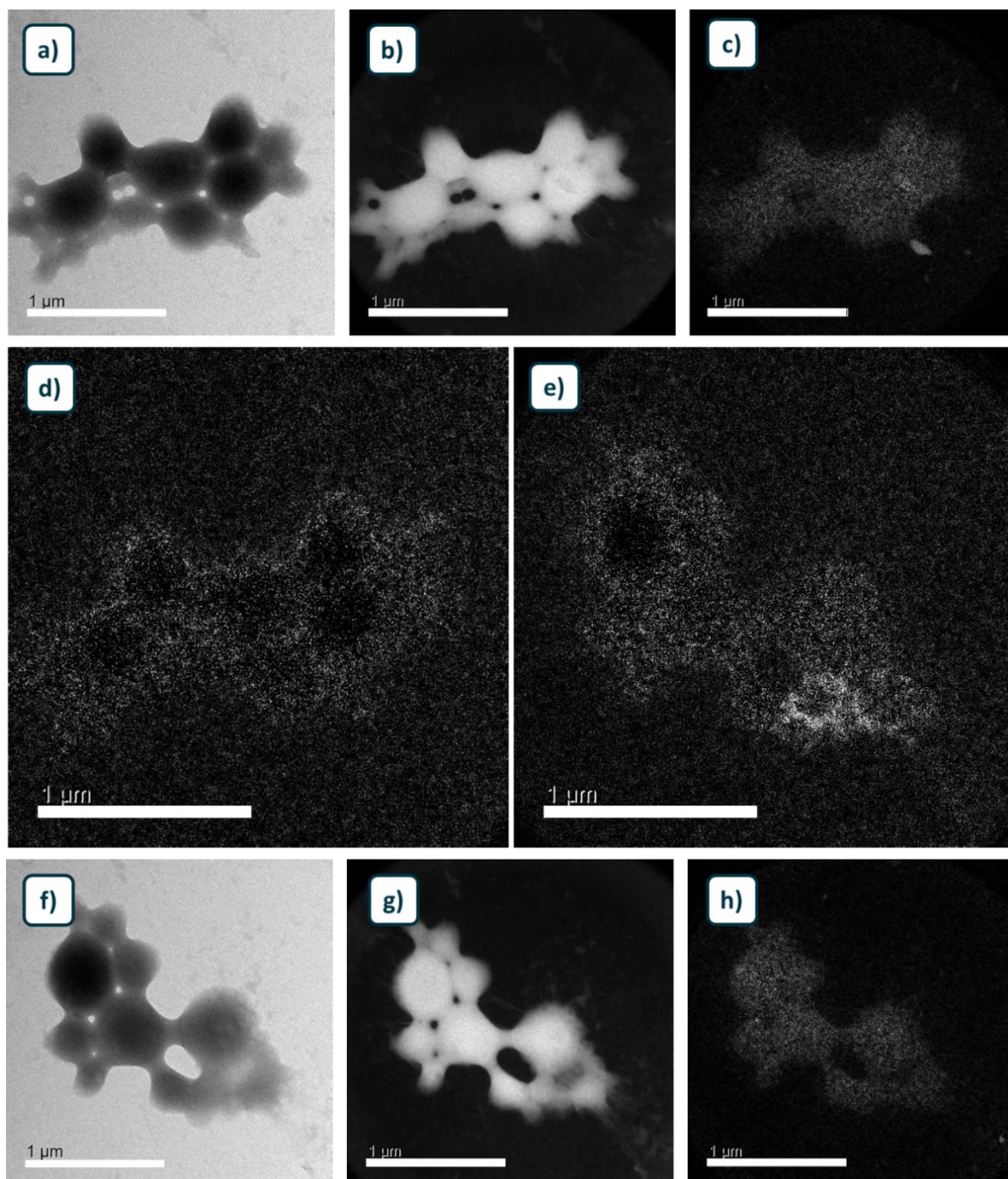
Figure 6-27: EFTEM Images of GNPs in PLGA of two representative areas on the sample grid. Showing the brightfield image in a) and f). b) and g) represent the carbon distribution. Oxygen map images are c) and h) and nitrogen, the element distinguishing the polymers is shown in d) and e).

The knowledge about the formulation gained in EFTEM studies have been reviewed with a pH titration curve measuring the ζ-potential. Hence gelatin as polypeptide exhibits a type dependent isoelectric point, the polarity of NPs with a gelatin shell should inverse in dependency to the pH. Values ranging from 8 to 3 have been tested. In Figure 6-28 they are plotted to the corresponding ζ-potential.
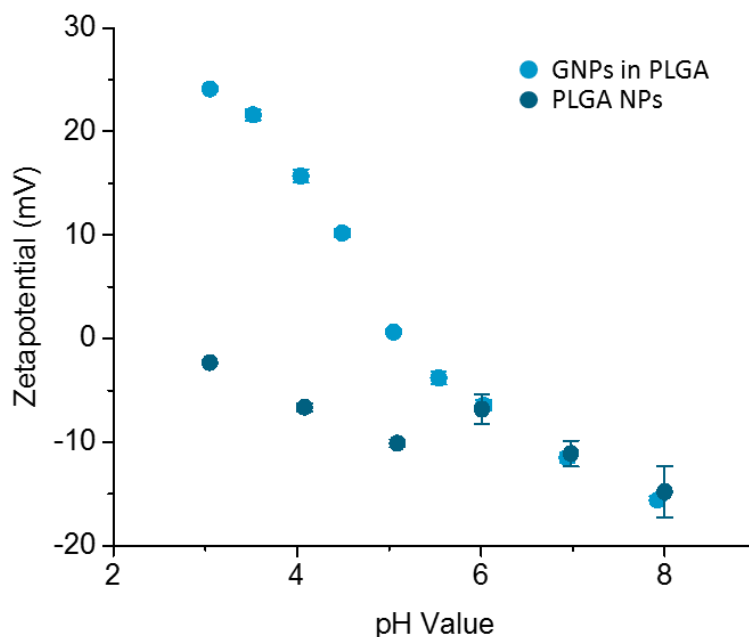
Figure 6-28: pH dependent ζ-potential of GNPs in PLGA particles showing the inversion from negative to positive signs with an IEP between pH 5 to 6. The blue line represents PLGA NPs changing the ζ-potential but not turning the sign.

The ζ-potential increased from – 20 mV to + 25 mV with a decreasing pH. From the graph an IEP (at neutral surface charge) around pH 5.5 was determined. PLGA NPs and cGNPs were used as reference. PLGA in blue changed the surface charge too but did not get neutral or positive. cGNPs changed the charge in the same way as GNPs in PLGA. These results support the findings from the EFTEM investigations. During the production process gelatin seems to be dissolved again and rearranged surrounding the PLGA NPs. The most probable step for this phase inversion is the solvent evaporation time. Gelatin can be dissolved by the aqueous PVA solution and thus diffuses out of the NPs formulation before the PLGA droplet hardens due to the solvent evaporation. In this way, most of the particles form solid PLGA NPs with a gelatin shell. This could explain as well the high burst release of approximately 30 % and the low loading capacity for FITC-dextrans too.

6.4   Conclusion

It was possible to design a crosslinking free carrier system based on gelatin and PLGA, which is exclusively composed by biodegradable, biocompatible and non-toxic materials. This is important for the delivery of the growing amount of biotherapeutics. The obtained NPs have a narrow size distribution with a mean hydrodynamic diameter of 250 nm and a negative surface charge of approximately -20 mV at neutral pH. The new hydrophilic platform technology could be proven to be nontoxic in cell viability studies. Furthermore, by the variation of the used gelatin amount, the hydrophilic part can be tuned. For LNA very good encapsulation efficiencies could be achieved. In further studies, with plasmid coding for eGFP loaded NPs, the suitability of the system as non-viral transfection vector could be demonstrated. Here is a great potential for the delivery system even though, it was in the end proven to be composed by a PLGA core surrounded by a gelatin shell. The encapsulation of larger molecules, like FITC-dextran$_{70}$, was unfortunately not sufficient. For the purpose of a non-viral transfection vector the achieved loading was high enough, what can be seen from the results described in chapter 6.3.3.2. In confocal laser microscopy studies with fluorescently labelled materials a colocalization could be shown. However, the resolution of CLSM is not high enough for a detailed material separation. The use of the innovative EFTEM technique enabled the exact structure determination. To our knowledge EFTEM was used for the first time to exactly investigate the distribution of two organic polymers in the nanometer scale. In this way, the phase inversion during the preparation process was detected and underlined by the investigation of a pH dependent ζ-potential measurement. By the establishment of the unique analytical method combination a further development of the platform and the investigation in possibilities to force the gelatin to stay inside the PLGA NPs can be envisaged. Even though the polymer distribution is exactly opposite to what was intended, it could be shown as effective carrier for transfection studies.

7 Outlook

7.1 Elasticity of Crosslinked Gelatin Nanoparticles

The change in the elastic moduli over the storage time should be further investigated. For the development of an applicable GNP formulation the hardening has to be monitored over a longer time. The question which should be addressed in this regard is, if after a certain time Young's moduli stay constant and a plateau is reached, or not. This should have an impact on the *in vivo* fate after usual storage times between preparation and application. A second parameter, which can be considered to be examined, is the influence of the storage conditions. It could be shown, that hardening of gelatin gels takes place at a faster rate at lower temperatures.[196] Storage at room temperature might slow down the increase of Young´s moduli and therefore, slow down the hardening process. In order to investigate the influence of shorter crosslinking times alternative purification methods need to be established. The agglomeration after centrifugation of cGNPs, prepared with crosslinking of less than three hours, could be prevented by the use of cross flow filtration or dialysis. The irreversible formation of aggregates might come from the softness of these particles, which could be very interesting in terms of the design of long circulating cGNPs. A comparison with GNPs crosslinked only in the area of an outer shell, like it could be achieved in our laboratory with N,N'-diisopropylcarbodiimide would be of interest. By the limitation of the crosslinking to the outside of the particles, it is assumable to form softer particles, than by crosslinking the whole particle matrix. In regard to the interaction of cells with cGNPs shorter and longer incubation times should be examined as well as a collection of more data per time point. When enough time points are measured in a quantitative way, the calculation of *in vitro* kinetics and a correlation to the measured Young´s moduli could be very interesting. Macrophage uptake would be an important information to obtain, as many particle systems are cleaned from the blood circulation by cells of the MPS.[108] After these experiments, by which the knowledge of the mechanical properties and their influences to *in vitro* systems can be increased, the evaluation of the *in vivo* fate of soft and hard NPs would be a very interesting aspect.

7.2   Gelatin Nanoparticles in PLGA

The resulting NPs system, having PLGA NPs coated by gelatin can be further investigated, like for example for the co- delivery of hydrophobic and hydrophilic drugs. This is an increasing trend, especially used in cancer treatment.[197] Another possible benefit of the gelatin core is the formation of a softer particle system. This could be investigated by the nanoindentation method with SPM, which is described in detail in chapter 5.2.5.3. Softer particles in general prolong the half-life time and alter the NP distribution into organs.[9] In addition, gelatin could provide the possibility of a chemical modification by the functional groups, and in this way could be used for an active drug targeting. Another possibility is a further formulation development with the aim to actually achieve GNPs coated by PLGA and monitored by the established analytical methods. By the use of co-solvents PLGA could be forced to form a solid shell around the GNPs before the formation of the emulsion. Pentane, an antisolvent for PLGA, could be used for this approach. First preliminary experiments showed the potential of this attempt. ζ-potential still turned positive at lower pH values, but much less than for NPs prepared by the standard protocol. A challenging part in this approach is to maintain the size range constant. Samples prepared in this way had a very broad size distribution and were interspersed with microparticles of several tenths of micrometers. A second possibility would be the exchange of the emulsifying step by a second precipitation. In this way first gelatin would be precipitated and, after mixing the freshly prepared GNPs with dissolved PLGA, they would be co precipitated. When the second solvent is chosen in a way that gelatin is insoluble too, GNPs should be stable and the phase inversion could be hindered. Changing the temperature and transferring the process into an ice bath could prevent the liberation of gelatin. By gelling the freshly prepared particles they could be solidified until a stable PLGA layer is formed, which is stabilizing them in a sufficient way. To evaluate the interaction between gelatin and PLGA it would be a possibility to go one step back and investigate in the coating of cGNPs. This could be interesting as well in regard to an altered release compared with blank cGNPs. A hydrophobic shell should prolong the release of hydrophilic drugs in a significant way. This results in larger application intervals what is beneficial in terms of patient's compliance.

8   Literature

1.   Thomas, S. E.; Mendes, V.; Kim, S. Y.; Malhotra, S.; Ochoa-Montaño, B.; Blaszczyk, M.; Blundell, T. L. Structural Biology and the Design of New Therapeutics: From HIV and Cancer to Mycobacterial Infections. *Journal of Molecular Biology* **2017,** *429* (17), 2677-2693.

2.   Pavlou, A. K.; Reichert, J. M. Recombinant protein therapeutics?success rates, market trends and values to 2010. *Nature Biotechnology* **2004,** *22* (12), 1513-1519.

3.   Shadab, M.; Haque, S.; Sheshala, R.; Meng, L.; Meka, V.; Ali, J. Recent advances in non-invasive delivery of macromolecules using nanoparticulate carriers system. *Current Pharmaceutical Design* **2016,** *22* (999), 1-1.

4.   Grabowski, H. Follow-on biologics: data exclusivity and the balance between innovation and competition. *Nature Reviews Drug Discovery* **2008,** *7* (6), 479-488.

5.   Mitragotri, S.; Burke, P. A.; Langer, R. Overcoming the challenges in administering biopharmaceuticals: formulation and delivery strategies. *Nature Reviews Drug Discovery* **2014,** *13* (9), 655-672.

6.   Blanco, E.; Shen, H.; Ferrari, M. Principles of nanoparticle design for overcoming biological barriers to drug delivery. *Nature Biotechnology* **2015,** *33* (9), 941-951.

7.   United Stades Food and Drug Administration; Select Committee on GRAS Substances (SCOGS) Opinion: Gelatin. In *ID Code: 9000-70-8*, Administration, U. S. F. a. D., Ed., **1975**; Vol. SCOGS-Report Number: 58.

8.   Elzoghby, A. O. Gelatin-based nanoparticles as drug and gene delivery systems: Reviewing three decades of research. *Journal of Controlled Release* **2013,** *172* (3), 1075-1091.

9.   Anselmo, A. C.; Zhang, M.; Kumar, S.; Vogus, D. R.; Menegatti, S.; Helgeson, M. E.; Mitragotri, S. Elasticity of Nanoparticles Influences Their Blood Circulation, Phagocytosis, Endocytosis, and Targeting. *ACS Nano* **2015,** *9* (3), 3169-3177.

10.   Khan, S. A.; Schneider, M. Stabilization of Gelatin Nanoparticles Without Crosslinking. *Macromolecular Bioscience* **2014,** *14* (11), 1627-1638.

11.   Evaluate Ltd. Evaluate Pharma World Preview 2016, Outlook to 2022. **2016,** *9*, 1-49.

12.   Zelikin, A. N.; Ehrhardt, C.; Healy, A. M. Materials and methods for delivery of biological drugs. *Nature Chemistry* **2016,** *8* (11), 997-1007.

13.   Yildirimer, L.; Thanh, N. T. K.; Loizidou, M.; Seifalian, A. M. Toxicology and clinical potential of nanoparticles. *Nano Today* **2011,** *6* (6), 585-607.

14.   Brayden, D. J.; O'Mahony, D. J. Novel oral drug delivery gateways for biotechnology products: polypeptides and vaccines. *Pharmaceutical Science & Technology Today* **1998,** *1* (7), 291-299.

15.   Hunter, J.; Hirst, B. H. Intestinal secretion of drugs. The role of P-glycoprotein and related drug efflux systems in limiting oral drug absorption. *Advanced Drug Delivery Reviews* **1997,** *25* (2-3), 129-157.

16.   Fromm, M. F. P-glycoprotein: a defense mechanism limiting oral bioavailability and CNS accumulation of drugs. *Int. Journal of Clinical Pharmacology and Therapeutics* **2000,** *38* (02), 69-74.

17.   Pawar, V. K.; Meher, J. G.; Singh, Y.; Chaurasia, M.; Surendar Reddy, B.; Chourasia, M. K. Targeting of gastrointestinal tract for amended delivery of protein/peptide therapeutics: Strategies and industrial perspectives. *Journal of Controlled Release* **2014,** *196*, 168-183.

18.   Choonara, B. F.; Choonara, Y. E.; Kumar, P.; Bijukumar, D.; du Toit, L. C.; Pillay, V. A review of advanced oral drug delivery technologies facilitating the protection and absorption of protein and peptide molecules. *Biotechnology Advances* **2014,** *32* (7), 1269-1282.

19.   Renukuntla, J.; Vadlapudi, A. D.; Patel, A.; Boddu, S. H. S.; Mitra, A. K. Approaches for enhancing oral bioavailability of peptides and proteins. *International Journal of Pharmaceutics* **2013,** *447* (1-2), 75-93.

20.   Kanitakis, J. Anatomy, histology and immunohistochemistry of normal human skin. *Eur J Dermatol* **2002,** *12* (4), 390-9; quiz 400-1.

21.   Hwa, C.; Bauer, E. A.; Cohen, D. E. Skin biology. *Dermatologic Therapy* **2011,** *24* (5), 464-470.

22.   Babu, S. S.; Saeki, A.; Seki, S.; Mohwald, H.; Nakanishi, T. Millimeter-sized flat crystalline sheet architectures of fullerene assemblies with anisotropic photoconductivity. *Phys Chem Chem Phys* **2011,** *13* (11), 4830-4.

23.   Morales, J. O.; Fathe, K. R.; Brunaugh, A.; Ferrati, S.; Li, S.; Montenegro-Nicolini, M.; Mousavikhamene, Z.; McConville, J. T.; Prausnitz, M. R.; Smyth, H. D. C. Challenges

and Future Prospects for the Delivery of Biologics: Oral Mucosal, Pulmonary, and Transdermal Routes. *The AAPS Journal* **2017,** *19* (3), 652-668.

24.   Heisig, M.; Lieckfeldt, R.; Wittum, G.; Mazurkevich, G.; Lee, G. Non Steady-state Descriptions of Drug Permeation Through Stratum Corneum. I. The Biphasic Brick-and-Mortar Model. *Pharmaceutical Research* **1996,** *13* (3), 421-426.

25.   Lampe, M. A.; Burlingame, A. L.; Whitney, J.; Williams, M. L.; Brown, B. E.; Roitman, E.; Elias, P. M. Human stratum corneum lipids: characterization and regional variations. *J Lipid Res* **1983,** *24* (2), 120-30.

26.   Palmer, B.; DeLouise, L. Nanoparticle-Enabled Transdermal Drug Delivery Systems for Enhanced Dose Control and Tissue Targeting. *Molecules* **2016,** *21* (12), 1719.

27.   Prausnitz, M. R.; Mitragotri, S.; Langer, R. Current status and future potential of transdermal drug delivery. *Nature Reviews Drug Discovery* **2004,** *3* (2), 115-124.

28.   Sen, A.; Daly, M. E.; Hui, S. W. Transdermal insulin delivery using lipid enhanced electroporation. *Biochimica et Biophysica Acta (BBA) - Biomembranes* **2002,** *1564* (1), 5-8.

29.   Mitragotri, S.; Kost, J. Transdermal Delivery of Heparin and Low-Molecular Weight Heparin Using Low-Frequency Ultrasound. *Pharmaceutical Research* **2001,** *18* (8), 1151-1156.

30.   Dahlan, A.; Alpar, H. O.; Stickings, P.; Sesardic, D.; Murdan, S. Transcutaneous immunisation assisted by low-frequency ultrasound. *International Journal of Pharmaceutics* **2009,** *368* (1-2), 123-128.

31.   Kochhar, C.; Imanidis, G. In vitro transdermal iontophoretic delivery of leuprolide under constant current application. *Journal of Controlled Release* **2004,** *98* (1), 25-35.

32.   Song, Y.; Hemmady, K.; Puri, A.; Banga, A. K. Transdermal delivery of human growth hormone via laser-generated micropores. *Drug Delivery and Translational Research* **2017**.

33.   Prausnitz, M. R. Engineering Microneedle Patches for Vaccination and Drug Delivery to Skin. *Annual Review of Chemical and Biomolecular Engineering* **2017,** *8* (1), 177-200.

34.   Patzelt, A.; Lademann, J. Drug delivery to hair follicles. *Expert Opinion on Drug Delivery* **2013,** *10* (6), 787-797.

35.　Barua, S.; Mitragotri, S. Challenges associated with penetration of nanoparticles across cell and tissue barriers: A review of current status and future prospects. *Nano Today* **2014,** *9* (2), 223-243.

36.　Santander-Ortega, M. J.; Stauner, T.; Loretz, B.; Ortega-Vinuesa, J. L.; Bastos-González, D.; Wenz, G.; Schaefer, U. F.; Lehr, C. M. Nanoparticles made from novel starch derivatives for transdermal drug delivery. *Journal of Controlled Release* **2010,** *141* (1), 85-92.

37.　Cevc, G.; Chopra, A. Deformable (Transfersome®) Vesicles for Improved Drug Delivery into and Through the Skin. **2016**, 39-59.

38.　Bajaj, P.; Harris, J. F.; Huang, J.-H.; Nath, P.; Iyer, R. Advances and Challenges in Recapitulating Human Pulmonary Systems: At the Cusp of Biology and Materials. *ACS Biomaterials Science & Engineering* **2016,** *2* (4), 473-488.

39.　Labiris, N. R.; Dolovich, M. B. Pulmonary drug delivery. Part I: Physiological factors affecting therapeutic effectiveness of aerosolized medications. *British Journal of Clinical Pharmacology* **2003,** *56* (6), 588-599.

40.　Ruge, C. A.; Kirch, J.; Lehr, C.-M. Pulmonary drug delivery: from generating aerosols to overcoming biological barriers—therapeutic possibilities and technological challenges. *The Lancet Respiratory Medicine* **2013,** *1* (5), 402-413.

41.　Scheuch, G.; Kohlhaeufl, M. J.; Brand, P.; Siekmeier, R. Clinical perspectives on pulmonary systemic and macromolecular delivery. *Advanced Drug Delivery Reviews* **2006,** *58* (9-10), 996-1008.

42.　Wan, F.; Møller, E. H.; Yang, M.; Jørgensen, L. Formulation technologies to overcome unfavorable properties of peptides and proteins for pulmonary delivery. *Drug Discovery Today: Technologies* **2012,** *9* (2), e141-e146.

43.　Sturm, R.; Hofmann, W. A theoretical approach to the deposition and clearance of fibers with variable size in the human respiratory tract. *Journal of Hazardous Materials* **2009,** *170* (1), 210-218.

44.　Werle, M.; Bernkop-Schnürch, A. Strategies to improve plasma half life time of peptide and protein drugs. *Amino Acids* **2006,** *30* (4), 351-367.

45.　Gottesman, M. M.; Pastan, I.; Ambudkar, S. V. P-glycoprotein and multidrug resistance. *Current Opinion in Genetics & Development* **1996,** *6* (5), 610-617.

46.   Schmidt, K. S. Application of locked nucleic acids to improve aptamer in vivo stability and targeting function. *Nucleic Acids Research* **2004,** *32* (19), 5757-5765.

47.   Mout, R.; Rotello, V. Cytosolic and Nuclear Delivery of CRISPR/Cas9-ribonucleoprotein for Gene Editing Using Arginine Functionalized Gold Nanoparticles. *Bio-Protocol* **2017,** *7* (20).

48.   Pinto, M. P.; Arce, M.; Yameen, B.; Vilos, C. Targeted brain delivery nanoparticles for malignant gliomas. *Nanomedicine* **2017,** *12* (1), 59-72.

49.   Swaminathan, J.; Ehrhardt, C. Liposomal delivery of proteins and peptides. *Expert Opinion on Drug Delivery* **2012,** *9* (12), 1489-1503.

50.   Battaglia, L.; Gallarate, M. Lipid nanoparticles: state of the art, new preparation methods and challenges in drug delivery. *Expert Opinion on Drug Delivery* **2012,** *9* (5), 497-508.

51.   Liechty, W. B.; Kryscio, D. R.; Slaughter, B. V.; Peppas, N. A. Polymers for Drug Delivery Systems. *Annual Review of Chemical and Biomolecular Engineering* **2010,** *1* (1), 149-173.

52.   Barichello, J. M.; Morishita, M.; Takayama, K.; Nagai, T. Encapsulation of Hydrophilic and Lipophilic Drugs in PLGA Nanoparticles by the Nanoprecipitation Method. *Drug Development and Industrial Pharmacy* **1999,** *25* (4), 471-476.

53.   Hamidi, M.; Azadi, A.; Rafiei, P. Hydrogel nanoparticles in drug delivery. *Advanced Drug Delivery Reviews* **2008,** *60* (15), 1638-1649.

54.   Joshy, K. S.; Susan, M. A.; Snigdha, S.; Nandakumar, K.; Laly, A. P.; Sabu, T. Encapsulation of zidovudine in PF-68 coated alginate conjugate nanoparticles for anti-HIV drug delivery. *International Journal of Biological Macromolecules* **2017**.

55.   Ragelle, H.; Riva, R.; Vandermeulen, G.; Naeye, B.; Pourcelle, V.; Le Duff, C. S.; D'Haese, C.; Nysten, B.; Braeckmans, K.; De Smedt, S. C.; Jérôme, C.; Préat, V. Chitosan nanoparticles for siRNA delivery: Optimizing formulation to increase stability and efficiency. *Journal of Controlled Release* **2014,** *176*, 54-63.

56.   Elzoghby, A. O.; Samy, W. M.; Elgindy, N. A. Protein-based nanocarriers as promising drug and gene delivery systems. *Journal of Controlled Release* **2012,** *161* (1), 38-49.

57.   Marty, J. J.; Oppenheim, R. C.; Speiser, P. Nanoparticles--a new colloidal drug delivery system. *Pharm Acta Helv* **1978,** *53* (1), 17-23.

58.   Babel, W. Gelatin - A versatile biopolymer. *Chem Unserer Zeit* **1996,** *30* (2), 86-95.

59.   *Council of Europe; European Pharmacopoeia Commission; European Directorate for the Quality of Medicines & Healthcare; European pharmacopoeia*: Strasbourg : Council Of Europe : European Directorate for the Quality of Medicines and Healthcare, **2014**; Vol. 8.

60.   Miller, J. H.; Lewontin, R. C.; Gelbart, W. M.; Griffiths, A. J. F. *Molecular Cell Biology 4th Edition* Macmillan Higher Education **2002**.

61.   Thomas-Rueddel, D. O.; Vlasakov, V.; Reinhart, K.; Jaeschke, R.; Rueddel, H.; Hutagalung, R.; Stacke, A.; Hartog, C. S. Safety of gelatin for volume resuscitation—a systematic review and meta-analysis. *Intensive Care Medicine* **2012,** *38* (7), 1134-1142.

62.   Razieh Kamali-Jamil, M. S., Zohreh-Azita Sadigh, Mohammad Taqavian, Mohammad-Kazem Shahkarami, Fatemeh Esna-Ashari, Reza Shahbazi, Ashraf Mohammadi, Abolhasan Foroughi, Bizhan Romani. The Effect of Various Stabilizers on Preserving Immunogenicity of Lyophilized Mumps Vaccines. *Journal of Research in Health Sciences* **2017,** *17* (4).

63.   Goings, G. E.; Kozlowski, D. A.; Szele, F. G. Differential activation of microglia in neurogenic versus non-neurogenic regions of the forebrain. *Glia* **2006,** *54* (4), 329-342.

64.   Mäder, K.; Allhenn, D. *Innovative Arzneiformen: ein Lehrbuch für Studium und Praxis ; mit 59 Tabellen*; Wiss. Verlag-Ges. **2010**.

65.   Krause, H. J.; Rohdewald, P. Preparation of gelatin nanocapsules and their pharmaceutical characterization. *Pharmaceutical Research* **1985,** *02* (5), 239-243.

66.   Coester, C. J.; Langer, K.; Van Briesen, H.; Kreuter, J. Gelatin nanoparticles by two step desolvation a new preparation method, surface modifications and cell uptake. *Journal of Microencapsulation* **2008,** *17* (2), 187-193.

67.   Ofokansi, K.; Winter, G.; Fricker, G.; Coester, C. Matrix-loaded biodegradable gelatin nanoparticles as new approach to improve drug loading and delivery. *European Journal of Pharmaceutics and Biopharmaceutics* **2010,** *76* (1), 1-9.

68.   Bajpai, A. K.; Choubey, J. Design of gelatin nanoparticles as swelling controlled delivery system for chloroquine phosphate. *Journal of Materials Science: Materials in Medicine* **2006,** *17* (4), 345-358.

69.   Lu, Z. Paclitaxel-Loaded Gelatin Nanoparticles for Intravesical Bladder Cancer Therapy. *Clinical Cancer Research* **2004,** *10* (22), 7677-7684.

70. Gupta, A. K.; Gupta, M.; Yarwood, S. J.; Curtis, A. S. G. Effect of cellular uptake of gelatin nanoparticles on adhesion, morphology and cytoskeleton organisation of human fibroblasts. *Journal of Controlled Release* **2004,** *95* (2), 197-207.

71. Kim, K. J.; Byun, Y. Preparation and characterizations of self-assembled PEGylated gelatin nanoparticles. *Biotechnology and Bioprocess Engineering* **1999,** *4* (3), 210-214.

72. Li, W.-M.; Liu, D.-M.; Chen, S.-Y. Amphiphilically-modified gelatin nanoparticles: Self-assembly behavior, controlled biodegradability, and rapid cellular uptake for intracellular drug delivery. *Journal of Materials Chemistry* **2011,** *21* (33), 12381.

73. Lee, E. J.; Khan, S. A.; Lim, K. H. Gelatin Nanoparticle Preparation by Nanoprecipitation. *Journal of Biomaterials Science, Polymer Edition* **2011,** *22* (4-6), 753-771.

74. Fessi, H.; Puisieux, F.; Devissaguet, J. P.; Ammoury, N.; Benita, S. Nanocapsule formation by interfacial polymer deposition following solvent displacement. *International Journal of Pharmaceutics* **1989,** *55* (1), R1-R4.

75. Galindo-Rodríguez, S. A.; Puel, F.; Briançon, S.; Allémann, E.; Doelker, E.; Fessi, H. Comparative scale-up of three methods for producing ibuprofen-loaded nanoparticles. *European Journal of Pharmaceutical Sciences* **2005,** *25* (4-5), 357-367.

76. Vitale, S. A.; Katz, J. L. Liquid Droplet Dispersions Formed by Homogeneous Liquid–Liquid Nucleation: "The Ouzo Effect". *Langmuir* **2003,** *19* (10), 4105-4110.

77. Lepeltier, E.; Bourgaux, C.; Amenitsch, H.; Rosilio, V.; Lepetre-Mouelhi, S.; Zouhiri, F.; Desmaële, D.; Couvreur, P. Influence of the nanoprecipitation conditions on the supramolecular structure of squalenoyled nanoparticles. *European Journal of Pharmaceutics and Biopharmaceutics* **2015,** *96*, 89-95.

78. Stainmesse, S.; Orecchioni, A.-M.; Nakache, E.; Puisieux, F.; Fessi, H. Formation and stabilization of a biodegradable polymeric colloidal suspension of nanoparticles. *Colloid and Polymer Science* **1995,** *273* (5), 505-511.

79. Karnik, R.; Gu, F.; Basto, P.; Cannizzaro, C.; Dean, L.; Kyei-Manu, W.; Langer, R.; Farokhzad, O. C. Microfluidic Platform for Controlled Synthesis of Polymeric Nanoparticles. *Nano Letters* **2008,** *8* (9), 2906-2912.

80. Taheri Qazvini, N.; Zinatloo, S. Synthesis and characterization of gelatin nanoparticles using CDI/NHS as a non-toxic cross-linking system. *Journal of Materials Science: Materials in Medicine* **2010,** *22* (1), 63-69.

81.   Choubey, J.; Bajpai, A. K. Investigation on magnetically controlled delivery of doxorubicin from superparamagnetic nanocarriers of gelatin crosslinked with genipin. *Journal of Materials Science: Materials in Medicine* **2010,** *21* (5), 1573-1586.

82.   Khan, H.; Shukla, R. N.; Bajpai, A. K. Genipin-modified gelatin nanocarriers as swelling controlled drug delivery system for in vitro release of cytarabine. *Materials Science and Engineering: C* **2016,** *61*, 457-465.

83.   Broderick, E. P.; O'Halloran, D. M.; Rochev, Y. A.; Griffin, M.; Collighan, R. J.; Pandit, A. S. Enzymatic stabilization of gelatin-based scaffolds. *Journal of Biomedical Materials Research* **2005,** *72B* (1), 37-42.

84.   Farris, S.; Song, J.; Huang, Q. Alternative Reaction Mechanism for the Cross-Linking of Gelatin with Glutaraldehyde. *Journal of Agricultural and Food Chemistry* **2010,** *58* (2), 998-1003.

85.   Cai, B.; Rao, L.; Ji, X.; Bu, L.-L.; He, Z.; Wan, D.; Yang, Y.; Liu, W.; Guo, S.; Zhao, X.-Z. Autofluorescent gelatin nanoparticles as imaging probes to monitor matrix metalloproteinase metabolism of cancer cells. *Journal of Biomedical Materials Research Part A* **2016,** *104* (11), 2854-2860.

86.   Thakral, S.; Thakral, N. K.; Majumdar, D. K. Eudragit®: a technology evaluation. *Expert Opinion on Drug Delivery* **2012,** *10* (1), 131-149.

87.   Wang, H.; Boerman, O. C.; Sariibrahimoglu, K.; Li, Y.; Jansen, J. A.; Leeuwenburgh, S. C. G. Comparison of micro- vs. nanostructured colloidal gelatin gels for sustained delivery of osteogenic proteins: Bone morphogenetic protein-2 and alkaline phosphatase. *Biomaterials* **2012,** *33* (33), 8695-8703.

88.   Danhier, F.; Pourcelle, V.; Marchand-Brynaert, J.; Jérôme, C.; Feron, O.; Préat, V. Targeting of Tumor Endothelium by RGD-Grafted PLGA-Nanoparticles. **2012,** *508*, 157-175.

89.   Youngren-Ortiz, S. R.; Hill, D. B.; Hoffmann, P. R.; Morris, K. R.; Barrett, E. G.; Forest, M. G.; Chougule, M. B. Development of Optimized, Inhalable, Gemcitabine-Loaded Gelatin Nanocarriers for Lung Cancer. *Journal of Aerosol Medicine and Pulmonary Drug Delivery* **2017,** *30* (5), 299-321.

90.   Nayak, D.; Boxi, A.; Ashe, S.; Thathapudi, N. C.; Nayak, B. Stavudine loaded gelatin liposomes for HIV therapy: Preparation, characterization and in vitro cytotoxic evaluation. *Materials Science and Engineering: C* **2017,** *73*, 406-416.

91.   Mahor, A.; Prajapati, S. K.; Verma, A.; Gupta, R.; Iyer, A. K.; Kesharwani, P. Moxifloxacin loaded gelatin nanoparticles for ocular delivery: Formulation and in - vitro , in - vivo evaluation. *Journal of Colloid and Interface Science* **2016,** *483*, 132-138.

92.   Esmaeili, A.; Mousavi, S. N. Synthesis of a novel structure for the oral delivery of insulin and the study of its effect on diabetic rats. *Life Sciences* **2017,** *186*, 43-49.

93.   Sudheesh, M. S.; Vyas, S. P.; Kohli, D. V. Nanoparticle-based immunopotentiation via tetanus toxoid-loaded gelatin and aminated gelatin nanoparticles. *Drug Delivery* **2011,** *18* (5), 320-330.

94.   Chou, L. Y. T.; Ming, K.; Chan, W. C. W. Strategies for the intracellular delivery of nanoparticles. *Chem. Soc. Rev.* **2011,** *40* (1), 233-245.

95.   Yameen, B.; Choi, W. I.; Vilos, C.; Swami, A.; Shi, J.; Farokhzad, O. C. Insight into nanoparticle cellular uptake and intracellular targeting. *Journal of Controlled Release* **2014,** *190*, 485-499.

96.   Canton, I.; Battaglia, G. Endocytosis at the nanoscale. *Chemical Society Reviews* **2012,** *41* (7), 2718.

97.   Stan, R. V. Structure of caveolae. *Biochimica et Biophysica Acta (BBA) - Molecular Cell Research* **2005,** *1746* (3), 334-348.

98.   Oh, P.; Borgström, P.; Witkiewicz, H.; Li, Y.; Borgström, B. J.; Chrastina, A.; Iwata, K.; Zinn, K. R.; Baldwin, R.; Testa, J. E.; Schnitzer, J. E. Live dynamic imaging of caveolae pumping targeted antibody rapidly and specifically across endothelium in the lung. *Nature Biotechnology* **2007,** *25* (3), 327-337.

99.   Lim, J. P.; Gleeson, P. A. Macropinocytosis: an endocytic pathway for internalising large gulps. *Immunology and Cell Biology* **2011,** *89* (8), 836-843.

100.   Kerr, M. C.; Teasdale, R. D. Defining Macropinocytosis. *Traffic* **2009,** *10* (4), 364-371.

101.   Fornetti, J.; Flanders, K. C.; Henson, P. M.; Tan, A. C.; Borges, V. F.; Schedin, P. Mammary epithelial cell phagocytosis downstream of TGF-β3 is characterized by adherens junction reorganization. *Cell Death & Differentiation* **2015,** *23* (2), 185-196.

102.   Boochoon, K. S.; Manarang, J. C.; Davis, J. T.; McDermott, A. M.; Foster, W. J. The influence of substrate elastic modulus on retinal pigment epithelial cell phagocytosis. *Journal of Biomechanics* **2014,** *47* (12), 3237-3240.

103. Segal, G.; Lee, W.; Arora, P. D.; McKee, M.; Downey, G.; McCulloch, C. A. G. Involvement of actin filaments and integrins in the binding step in collagen phagocytosis by human fibroblasts. *Journal of Cell Science* **2001,** *114* (1), 119-129.

104. Aderem, A.; Underhill, D. M. Mechanisms of Phagocytosis in Macrophages. *Annual Review of Immunology* **1999,** *17* (1), 593-623.

105. Hoshyar, N.; Gray, S.; Han, H.; Bao, G. The effect of nanoparticle size on in vivo pharmacokinetics and cellular interaction. *Nanomedicine* **2016,** *11* (6), 673-692.

106. Soo Choi, H.; Liu, W.; Misra, P.; Tanaka, E.; Zimmer, J. P.; Itty Ipe, B.; Bawendi, M. G.; Frangioni, J. V. Renal clearance of quantum dots. *Nature Biotechnology* **2007,** *25* (10), 1165-1170.

107. Caster, J. M.; Yu, S. K.; Patel, A. N.; Newman, N. J.; Lee, Z. J.; Warner, S. B.; Wagner, K. T.; Roche, K. C.; Tian, X.; Min, Y.; Wang, A. Z. Effect of particle size on the biodistribution, toxicity, and efficacy of drug-loaded polymeric nanoparticles in chemoradiotherapy. *Nanomedicine: Nanotechnology, Biology and Medicine* **2017,** *13* (5), 1673-1683.

108. Albanese, A.; Tang, P. S.; Chan, W. C. W. The Effect of Nanoparticle Size, Shape, and Surface Chemistry on Biological Systems. *Annual Review of Biomedical Engineering* **2012,** *14* (1), 1-16.

109. Perrault, S. D.; Walkey, C.; Jennings, T.; Fischer, H. C.; Chan, W. C. W. Mediating Tumor Targeting Efficiency of Nanoparticles Through Design. *Nano Letters* **2009,** *9* (5), 1909-1915.

110. Stylianopoulos, T. EPR-effect: utilizing size-dependent nanoparticle delivery to solid tumors. *Therapeutic Delivery* **2013,** *4* (4), 421-423.

111. Moghimi, S. M.; Hunter, A. C.; Andresen, T. L. Factors Controlling Nanoparticle Pharmacokinetics: An Integrated Analysis and Perspective. *Annual Review of Pharmacology and Toxicology* **2012,** *52* (1), 481-503.

112. Champion, J. A.; Katare, Y. K.; Mitragotri, S. Particle shape: A new design parameter for micro- and nanoscale drug delivery carriers. *Journal of Controlled Release* **2007,** *121* (1-2), 3-9.

113. Sharma, G.; Valenta, D. T.; Altman, Y.; Harvey, S.; Xie, H.; Mitragotri, S.; Smith, J. W. Polymer particle shape independently influences binding and internalization by macrophages. *Journal of Controlled Release* **2010,** *147* (3), 408-412.

114.   Kinnear, C.; Moore, T. L.; Rodriguez-Lorenzo, L.; Rothen-Rutishauser, B.; Petri-Fink, A. Form Follows Function: Nanoparticle Shape and Its Implications for Nanomedicine. *Chemical Reviews* **2017,** *117* (17), 11476-11521.

115.   Zhang, Y.; Tekobo, S.; Tu, Y.; Zhou, Q.; Jin, X.; Dergunov, S. A.; Pinkhassik, E.; Yan, B. Permission to Enter Cell by Shape: Nanodisk vs Nanosphere. *ACS Applied Materials & Interfaces* **2012,** *4* (8), 4099-4105.

116.   Gratton, S. E. A.; Ropp, P. A.; Pohlhaus, P. D.; Luft, J. C.; Madden, V. J.; Napier, M. E.; DeSimone, J. M. The effect of particle design on cellular internalization pathways. *Proceedings of the National Academy of Sciences* **2008,** *105* (33), 11613-11618.

117.   Decuzzi, P.; Godin, B.; Tanaka, T.; Lee, S. Y.; Chiappini, C.; Liu, X.; Ferrari, M. Size and shape effects in the biodistribution of intravascularly injected particles. *Journal of Controlled Release* **2010,** *141* (3), 320-327.

118.   Huang, X.; Li, L.; Liu, T.; Hao, N.; Liu, H.; Chen, D.; Tang, F. The Shape Effect of Mesoporous Silica Nanoparticles on Biodistribution, Clearance, and Biocompatibilityin Vivo. *ACS Nano* **2011,** *5* (7), 5390-5399.

119.   Niikura, K.; Matsunaga, T.; Suzuki, T.; Kobayashi, S.; Yamaguchi, H.; Orba, Y.; Kawaguchi, A.; Hasegawa, H.; Kajino, K.; Ninomiya, T.; Ijiro, K.; Sawa, H. Gold Nanoparticles as a Vaccine Platform: Influence of Size and Shape on Immunological Responses in Vitro and in Vivo. *ACS Nano* **2013,** *7* (5), 3926-3938.

120.   Kohler, D.; Schneider, M.; Kruger, M.; Lehr, C. M.; Mohwald, H.; Wang, D. Template-assisted polyelectrolyte encapsulation of nanoparticles into dispersible, hierarchically nanostructured microfibers. *Adv Mater* **2011,** *23* (11), 1376-9.

121.   Möhwald, M.; Pinnapireddy, S. R.; Wonnenberg, B.; Pourasghar, M.; Jurisic, M.; Jung, A.; Fink-Straube, C.; Tschernig, T.; Bakowsky, U.; Schneider, M. Aspherical, Nanostructured Microparticles for Targeted Gene Delivery to Alveolar Macrophages. *Advanced Healthcare Materials* **2017,** *6* (20), 1700478.

122.   Thorek, D. L. J.; Tsourkas, A. Size, charge and concentration dependent uptake of iron oxide particles by non-phagocytic cells. *Biomaterials* **2008,** *29* (26), 3583-3590.

123.   Yue, Z.-G.; Wei, W.; Lv, P.-P.; Yue, H.; Wang, L.-Y.; Su, Z.-G.; Ma, G.-H. Surface Charge Affects Cellular Uptake and Intracellular Trafficking of Chitosan-Based Nanoparticles. *Biomacromolecules* **2011,** *12* (7), 2440-2446.

124.   Song, E.; Gaudin, A.; King, A. R.; Seo, Y.-E.; Suh, H.-W.; Deng, Y.; Cui, J.; Tietjen, G. T.; Huttner, A.; Saltzman, W. M. Surface chemistry governs cellular tropism of nanoparticles in the brain. *Nature Communications* **2017,** *8*, 15322.

125.   Conde, J. o.; Dias, J. T.; Grazú, V.; Moros, M.; Baptista, P. V.; de la Fuente, J. M. Revisiting 30 years of biofunctionalization and surface chemistry of inorganic nanoparticles for nanomedicine. *Frontiers in Chemistry* **2014,** *2*.

126.   Lundqvist, M.; Stigler, J.; Cedervall, T.; Berggård, T.; Flanagan, M. B.; Lynch, I.; Elia, G.; Dawson, K. The Evolution of the Protein Corona around Nanoparticles: A Test Study. *ACS Nano* **2011,** *5* (9), 7503-7509.

127.   Prow, T. W.; Ruge, C. A.; Schaefer, U. F.; Herrmann, J.; Kirch, J.; Cañadas, O.; Echaide, M.; Pérez-Gil, J.; Casals, C.; Müller, R.; Lehr, C.-M. The Interplay of Lung Surfactant Proteins and Lipids Assimilates the Macrophage Clearance of Nanoparticles. *PLoS ONE* **2012,** *7* (7), e40775.

128.   Yang, Q.; Jones, S. W.; Parker, C. L.; Zamboni, W. C.; Bear, J. E.; Lai, S. K. Evading Immune Cell Uptake and Clearance Requires PEG Grafting at Densities Substantially Exceeding the Minimum for Brush Conformation. *Molecular Pharmaceutics* **2014,** *11* (4), 1250-1258.

129.   Yang, C.; Gao, S.; Dagnæs-Hansen, F.; Jakobsen, M.; Kjems, J. Impact of PEG Chain Length on the Physical Properties and Bioactivity of PEGylated Chitosan/siRNA Nanoparticles in Vitro and in Vivo. *ACS Applied Materials & Interfaces* **2017,** *9* (14), 12203-12216.

130.   Naidu, P. S. R.; Norret, M.; Smith, N. M.; Dunlop, S. A.; Taylor, N. L.; Fitzgerald, M.; Iyer, K. S. The Protein Corona of PEGylated PGMA-Based Nanoparticles is Preferentially Enriched with Specific Serum Proteins of Varied Biological Function. *Langmuir* **2017,** *33* (45), 12926-12933.

131.   Liu, X.; Jin, Q.; Ji, Y.; Ji, J. Minimizing nonspecific phagocytic uptake of biocompatible gold nanoparticles with mixed charged zwitterionic surface modification. *J. Mater. Chem.* **2012,** *22* (5), 1916-1927.

132.   Ou, H.; Cheng, T.; Zhang, Y.; Liu, J.; Ding, Y.; Zhen, J.; Shen, W.; Xu, Y.; Yang, W.; Niu, P.; Liu, J.; An, Y.; Liu, Y.; Shi, L. Surface-adaptive zwitterionic nanoparticles for prolonged blood circulation time and enhanced cellular uptake in tumor cells. *Acta Biomaterialia* **2017**.

133.   Anselmo, A. C.; Mitragotri, S. Impact of particle elasticity on particle-based drug delivery systems. *Advanced Drug Delivery Reviews* **2017,** *108*, 51-67.

134.   Banquy, X.; Suarez, F.; Argaw, A.; Rabanel, J.-M.; Grutter, P.; Bouchard, J.-F.; Hildgen, P.; Giasson, S. Effect of mechanical properties of hydrogel nanoparticles on macrophage cell uptake. *Soft Matter* **2009,** *5* (20), 3984.

135.   Beningo, K. A.; Wang, Y.-l. Fc-receptor-mediated phagocytosis is regulated by mechanical properties of the target. *Journal of Cell Science* **2002,** *115* (4), 849.

136.   Alexander, J. F.; Kozlovskaya, V.; Chen, J.; Kuncewicz, T.; Kharlampieva, E.; Godin, B. Cubical Shape Enhances the Interaction of Layer-by-Layer Polymeric Particles with Breast Cancer Cells. *Advanced Healthcare Materials* **2015,** *4* (17), 2657-2666.

137.   Sun, J.; Zhang, L.; Wang, J.; Feng, Q.; Liu, D.; Yin, Q.; Xu, D.; Wei, Y.; Ding, B.; Shi, X.; Jiang, X. Tunable Rigidity of (Polymeric Core)-(Lipid Shell) Nanoparticles for Regulated Cellular Uptake. *Advanced Materials* **2015,** *27* (8), 1402-1407.

138.   Yi, X.; Shi, X.; Gao, H. Cellular Uptake of Elastic Nanoparticles. *Physical Review Letters* **2011,** *107* (9).

139.   Merkel, T. J.; Jones, S. W.; Herlihy, K. P.; Kersey, F. R.; Shields, A. R.; Napier, M.; Luft, J. C.; Wu, H.; Zamboni, W. C.; Wang, A. Z.; Bear, J. E.; DeSimone, J. M. Using mechanobiological mimicry of red blood cells to extend circulation times of hydrogel microparticles. *Proceedings of the National Academy of Sciences* **2011,** *108* (2), 586-591.

140.   Zhang, L.; Cao, Z.; Li, Y.; Ella-Menye, J.-R.; Bai, T.; Jiang, S. Softer Zwitterionic Nanogels for Longer Circulation and Lower Splenic Accumulation. *ACS Nano* **2012,** *6* (8), 6681-6686.

141.   Tsoi, K. M.; MacParland, S. A.; Ma, X.-Z.; Spetzler, V. N.; Echeverri, J.; Ouyang, B.; Fadel, S. M.; Sykes, E. A.; Goldaracena, N.; Kaths, J. M.; Conneely, J. B.; Alman, B. A.; Selzner, M.; Ostrowski, M. A.; Adeyi, O. A.; Zilman, A.; McGilvray, I. D.; Chan, W. C. W. Mechanism of hard-nanomaterial clearance by the liver. *Nature Materials* **2016,** *15* (11), 1212-1221.

142.   Bigi, A.; Cojazzi, G.; Panzavolta, S.; Rubini, K.; Roveri, N. Mechanical and thermal properties of gelatin films at different degrees of glutaraldehyde crosslinking. *Biomaterials* **2001,** *22* (8), 763-8.

143.	Usković, V. Dynamic Light Scattering Based Microelectrophoresis: Main Prospects and Limitations. *Journal of Dispersion Science and Technology* **2012,** *33* (12), 1762-1786.

144.	El Hadji Mamour Sakho, E. A., Oluwatobi S. Olwafemi, Sabu Thomas, Nandakumar Kalarikkal. *Thermal and Rheological Measurement Techniques for Nanomaterials Characterization*; 1 ed.; Elsevier **2017**; Vol. 3. p 292.

145.	ISO/TC 24/SC 4, Particle characterization, ISO 22412:2017, Particle size analysis -- Dynamic light scattering (DLS). In *22412:2017*, 2 ed.; ISO, Ed., **2017**, p 34.

146.	Bhattacharjee, S. DLS and zeta potential – What they are and what they are not? *Journal of Controlled Release* **2016,** *235*, 337-351.

147.	Müller, R. H. *Zetapotential und Partikelladung in der Laborpraxis*: Wissenschaftliche Verlagsgesellschaft mbH, **1996**. p 254.

148.	*Malvern Instruments Ltd.; Malvern Zetasizer ZS DLS user manual*; Malvern Instruments Ltd. **2013**; Vol. MANO485 1.1.

149.	Egerton, R. F. *Physical Principles of Electron Microscopy*; Springer Nature: Springer International Publishing Switzerland **2016**; Vol. 2. p 196.

150.	Binnig, G.; Quate, C. F.; Gerber, C. Atomic Force Microscope. *Physical Review Letters* **1986,** *56* (9), 930-933.

151.	Meyer, G.; Amer, N. M. Novel optical approach to atomic force microscopy. *Applied Physics Letters* **1988,** *53* (12), 1045-1047.

152.	Rodríguez, T. R.; García, R. Compositional mapping of surfaces in atomic force microscopy by excitation of the second normal mode of the microcantilever. *Applied Physics Letters* **2004,** *84* (3), 449-451.

153.	Ozkan, A. D.; Topal, A. E.; Dikecoglu, F. B.; Guler, M. O.; Dana, A.; Tekinay, A. B. Probe microscopy methods and applications in imaging of biological materials. *Seminars in Cell & Developmental Biology* **2017**.

154.	Hansma, P. K.; Cleveland, J. P.; Radmacher, M.; Walters, D. A.; Hillner, P. E.; Bezanilla, M.; Fritz, M.; Vie, D.; Hansma, H. G.; Prater, C. B.; Massie, J.; Fukunaga, L.; Gurley, J.; Elings, V. Tapping mode atomic force microscopy in liquids. *Applied Physics Letters* **1994,** *64* (13), 1738-1740.

155.   Newton, R.; Delguste, M.; Koehler, M.; Dumitru, A. C.; Laskowski, P. R.; Müller, D. J.; Alsteens, D. Combining confocal and atomic force microscopy to quantify single-virus binding to mammalian cell surfaces. *Nature Protocols* **2017,** *12* (11), 2275-2292.

156.   Bulychev, S. I.; Alekhin, V. P.; Shorshorov, M. K.; Ternovskii, A. P.; Shnyrev, G. D. Determining Young's modulus from the indentor penetration diagram. *Zavodskaya Laboratoriya* **1975,** *41*, 1409-1412.

157.   Butt, H.-J.; Cappella, B.; Kappl, M. Force measurements with the atomic force microscope: Technique, interpretation and applications. *Surface Science Reports* **2005,** *59* (1-6), 1-152.

158.   Hutter, J. L.; Bechhoefer, J. Calibration of atomic-force microscope tips. *Review of Scientific Instruments* **1993,** *64* (7), 1868-1873.

159.   Benitez, R.; Bolós, V. J.; Toca-Herrera, J. L. afmToolkit: an R Package for Automated AFM Force-Distance Curves Analysis. *The R Journal* **2017**.

160.   Guo, D.; Xie, G.; Luo, J. Mechanical properties of nanoparticles: basics and applications. *Journal of Physics D: Applied Physics* **2014,** *47* (1), 013001.

161.   *JPK Instruments AG, Determining the elastic modulus of biological samples using atomic force microscopy*; Application Note: jpk.com, p 9.

162.   Paddock, S. W. Confocal laser scanning microscopy. *Biotechniques* **1999,** *27* (5), 992-6, 998-1002, 1004.

163.   Djabourov, M. Architecture of gelatin gels. *Contemporary Physics* **1988,** *29* (3), 273-297.

164.   Djabourov, M.; Leblond, J.; Papon, P. Gelation of aqueous gelatin solutions. I. Structural investigation. *Journal de Physique* **1988,** *49* (2), 319-332.

165.   Djabourov, M.; Leblond, J.; Papon, P. Gelation of aqueous gelatin solutions. II. Rheology of the sol-gel transition. *Journal de Physique* **1988,** *49* (2), 333-343.

166.   Martucci, J. F.; Ruseckaite, R. A.; Vázquez, A. Creep of glutaraldehyde-crosslinked gelatin films. *Materials Science and Engineering: A* **2006,** *435-436*, 681-686.

167.   Theimer, W. Struktur und Alterung von Gelatine-Gelen. *Zeitschrift für Naturforschung B* **1960,** *15* (6).

168.   Shi, C.; Ahmad Khan, S.; Wang, K.; Schneider, M. Improved delivery of the natural anticancer drug tetrandrine. *International Journal of Pharmaceutics* **2015,** *479* (1), 41-51.

169.   Sanders, L. M.; Kell, B. A.; McRae, G. I.; Whitehead, G. W. Prolonged Controlled-Release of Nafarelin, a Luteinizing Hormone-Releasing Hormone Analogue, from Biodegradable Polymeric Implants: Influence of Composition and Molecular Weight of Polymer. *Journal of Pharmaceutical Sciences* **1986,** *75* (4), 356-360.

170.   Mittal, G.; Sahana, D. K.; Bhardwaj, V.; Ravi Kumar, M. N. V. Estradiol loaded PLGA nanoparticles for oral administration: Effect of polymer molecular weight and copolymer composition on release behavior in vitro and in vivo. *Journal of Controlled Release* **2007,** *119* (1), 77-85.

171.   Lemoine, D.; Francois, C.; Kedzierewicz, F.; Preat, V.; Hoffman, M.; Maincent, P. Stability study of nanoparticles of poly(ε-caprolactone), poly(d,l-lactide) and poly(d,l-lactide-co-glycolide). *Biomaterials* **1996,** *17* (22), 2191-2197.

172.   Lewis, D. H. Controlled Release of Bioactive Agents from Lactide/Glycolide Polymers. In *Biodegradable Polymers as Drug Delivery Systems*, Mark chasin, R. L., Ed.: Marcel Dekker, New York, **1990**; Vol. 45, pp 1-41.

173.   Yolles, S.; Leafe, T. D.; Woodland, J. H. R.; Meyer, F. J. Long Acting Delivery Systems for Narcotic Antagonists II: Release Rates of Naltrexone from Poly(lactic Acid) Composites. *Journal of Pharmaceutical Sciences* **1975,** *64* (2), 348-349.

174.   Beck, L. R.; Cowsar, D. R.; Lewis, D. H.; Gibson, J. W.; Flowers, C. E. New long-acting injectable microcapsule contraceptive system. *American Journal of Obstetrics and Gynecology* **1979,** *135* (3), 419-426.

175.   Venier-Julienne, M. C.; Vouldoukis, I.; Monjour, L.; Benoit, J. P. In Vitro Study of the Anti-Leishmanial Activity of Biodegradable Nanoparticles. *Journal of Drug Targeting* **2008,** *3* (1), 23-29.

176.   Smith, P. K.; Krohn, R. I.; Hermanson, G. T.; Mallia, A. K.; Gartner, F. H.; Provenzano, M. D.; Fujimoto, E. K.; Goeke, N. M.; Olson, B. J.; Klenk, D. C. Measurement of protein using bicinchoninic acid. *Analytical Biochemistry* **1985,** *150* (1), 76-85.

177.   Paillard-Giteau, A.; Tran, V. T.; Thomas, O.; Garric, X.; Coudane, J.; Marchal, S.; Chourpa, I.; Benoît, J. P.; Montero-Menei, C. N.; Venier-Julienne, M. C. Effect of various additives and polymers on lysozyme release from PLGA microspheres prepared by an s/o/w emulsion technique. *European Journal of Pharmaceutics and Biopharmaceutics* **2010,** *75* (2), 128-136.

178.   Mosmann, T. Rapid colorimetric assay for cellular growth and survival: application to proliferation and cytotoxicity assays. *J Immunol Methods* **1983,** *65* (1-2), 55-63.

179.   Giard, D. J.; Aaronson, S. A.; Todaro, G. J.; Arnstein, P.; Kersey, J. H.; Dosik, H.; Parks, W. P. In vitro cultivation of human tumors: establishment of cell lines derived from a series of solid tumors. *J Natl Cancer Inst* **1973,** *51* (5), 1417-23.

180.   Jepsen, J. S.; Sorensen, M. D.; Wengel, J. Locked nucleic acid: a potent nucleic acid analog in therapeutics and biotechnology. *Oligonucleotides* **2004,** *14* (2), 130-46.

181.   Kawabata, K.; Takakura, Y.; Hashida, M. The fate of plasmid DNA after intravenous injection in mice: involvement of scavenger receptors in its hepatic uptake. *Pharm Res* **1995,** *12* (6), 825-30.

182.   Frieden, M.; Orum, H. Locked nucleic acid holds promise in the treatment of cancer. *Curr Pharm Des* **2008,** *14* (11), 1138-42.

183.   Thomas, M.; Lange-Grunweller, K.; Dayyoub, E.; Bakowsky, U.; Weirauch, U.; Aigner, A.; Hartmann, R. K.; Grunweller, A. PEI-complexed LNA antiseeds as miRNA inhibitors. *RNA Biol* **2012,** *9* (8), 1088-98.

184.   Florea, B. I.; Meaney, C.; Junginger, H. E.; Borchard, G. Transfection efficiency and toxicity of polyethylenimine in differentiated Calu-3 and nondifferentiated COS-1 cell cultures. *AAPS PharmSci* **2015,** *4* (3), 1-11.

185.   Graham, F. L.; Smiley, J.; Russell, W. C.; Nairn, R. Characteristics of a Human Cell Line Transformed by DNA from Human Adenovirus Type-5. *J Gen Virol* **1977,** *36* (Jul), 59-72.

186.   Weiss, B.; Schaefer, U. F.; Zapp, J.; Lamprecht, A.; Stallmach, A.; Lehr, C. M. Nanoparticles made of fluorescence-labelled Poly(L-lactide-co-glycolide): preparation, stability, and biocompatibility. *J Nanosci Nanotechnol* **2006,** *6* (9-10), 3048-56.

187.   Thomas, J.; Gemming, T. *Analytische Transmissionselektronenmikroskopie*; 1 ed.; Springer-Verlag Wien **2013**; Vol. 1.

188.   Stewart, P. L. Cryo-electron microscopy and cryo-electron tomography of nanoparticles. *Wiley Interdiscip Rev Nanomed Nanobiotechnol* **2017,** *9* (2).

189.   Khan, S. A.; Schneider, M. Stabilization of gelatin nanoparticles without crosslinking. *Macromol Biosci* **2014,** *14* (11), 1627-38.

190.   Fröhlich, E. The role of surface charge in cellular uptake and cytotoxicity of medical nanoparticles. *International Journal of Nanomedicine* **2012**, 5577.

191.   Aramwit, P.; Jaichawa, N.; Ratanavaraporn, J.; Srichana, T. A comparative study of type A and type B gelatin nanoparticles as the controlled release carriers for different model compounds. *Materials Express* **2015,** *5* (3), 241-248.

192.   Tseng, C.-L.; Chen, K.-H.; Su, W.-Y.; Lee, Y.-H.; Wu, C.-C.; Lin, F.-H. Cationic Gelatin Nanoparticles for Drug Delivery to the Ocular Surface:In VitroandIn VivoEvaluation. *Journal of Nanomaterials* **2013,** *2013*, 1-11.

193.   Scheirs, J. *Compositional and Failure Analysis of Polymers: A Practical Approach*: John Wiley Sons, Inc., **2000**. p 806.

194.   Loo, J. S. C.; Ooi, C. P.; Boey, F. Y. C. Degradation of poly(lactide-co-glycolide) (PLGA) and poly(l-lactide) (PLLA) by electron beam radiation. *Biomaterials* **2005,** *26* (12), 1359-1367.

195.   *Academy of Pharmaceutical Sciences, Pharmaceutical Society of Great Britain, Handbook of pharmaceutical excipients*; American Pharmaceutical Association **1986**.

196.   Normand, V.; Muller, S.; Ravey, J.-C.; Parker, A. Gelation Kinetics of Gelatin: A Master Curve and Network Modeling. *Macromolecules* **2000,** *33* (3), 1063-1071.

197.   Garbuzenko, O. B.; Winkler, J.; Tomassone, M. S.; Minko, T. Biodegradable Janus Nanoparticles for Local Pulmonary Delivery of Hydrophilic and Hydrophobic Molecules to the Lungs. *Langmuir* **2014,** *30* (43), 12941-12949.

9   List of used Chemicals

Chemical Name	Comment	Supplier
4´,6-Diamidino-2-phylindol	DAPI	Sigma, Aldrich GmbH, Selze, Germany
A459 cells		ATCC, LGC Standards GmbH, Wesel
Acetone	Analytical reagent grade	Fischer Chemical Ltd., Loughborough, U.K.
Caso-Agar		Carl Roth GmbH + Co. KG, Karlsruhe, Germany
Dimethylformamide		Sigma Aldrich GmbH, Steinheim, Germany
Dimethylsulfoxid		Sigma-Aldrich Chemie GmbH, Steinheim, Germany
Dodecylamine		Sigma Aldrich GmbH, Steinheim, Germany
D-sorbitol		Sigma Aldrich GmbH, Steinheim, Germany
Dulbecco´s Modified Eagle Medium	DMEM	Gibco - Thermo Fisher, Carlsbad, US
EndoFree Plasmid Mega Kit	No.: 12381	Qiagen, Venlo, Netherlands
Ethanol	> 99.8%	Sigma Aldrich GmbH, Steinheim, Germany
Ethyl acetate		Sigma Aldrich GmbH, Steinheim, Germany
Fetal calf serum		Lonza, Basel, Switzerland
FITC-Dextran$_{70}$		TdB Cons., Uppsala, Sweden)
Gelatin A	Bloom 175	Sigma-Aldrich Chemie GmbH, Steinheim, Germany
Gelatin B	Bloom 75	Sigma-Aldrich Chemie GmbH, Steinheim, Germany
Glutamine		Gibco - Thermo Fisher, Carlsbad, US
Glutaraldehyde		Sigma-Aldrich GmbH, Steinheim, Germany
HBSS Buffer		Sigma Aldrich Life Science GmbH, Seelze, Germany
HCl	37%	Bernd Kraft, Duisburg, Germany
HEK293T cells		ATCC, LGC Standards GmbH, Wesel
MTT reagent		Sigma Aldrich Life Science GmbH, Seelze, Germany
N-Hydroxysuccinimid Alexa Flour® 633		Thermo Fisher Scientific Inc., Waltham, MA, USA

Chemical Name	Comment	Supplier
Poloxamer 188		AppliChem, Darmstadt, Germany
Polyethylenimide	~ 25 kDa	Sigma Aldrich GmbH, Steinheim, Germany
Polylactic-co-glycolicacid	Resomer RG 503 H	Evonik Nutrition & Care, Darmstadt, Germany
Polyvinylalcohol		Kururay Europe GmbH, Hattersheim am main, Germany
QuantiPro^{TM} BCA Assay Kit		Sigma Aldrich, Munich, Germany
RPMI-1640 medium		Sigma Aldrich Life Science GmbH, Seelze, Germany
Sodiumhydroxid	> 99% p.a.	Carl Roth GmbH + Co. KG, Karlsruhe, Germany
Tetramethyl-rhodamine isothiocyanate dextran	TRITC-dextran	TdB Cons., Uppsala, Sweden)
Triton X-100		Sigma Aldrich Life Science GmbH, Seelze, Germany

10 List of used Devices

Device	Type	Company
Particle Production		
Autoclave	FVS/2	Fedegari, Integra Biosciences, now ibs Tecnomara, Fernwald, Germany
Centrifuge		Thermo Fisher Scientific, Osterode am harz, Germany
Freeze dryer	Alpha 2-4 LSC	Martin Christ Gefriertrocknungsanlagen GmbH, Osterode am Harz, Germany
Laminar airflow work bench	Technoflow 2F120-II GS	Integra Biosciences AG, now ibs tecnomara GmbH, Fernwald, Germany
Petri dishes		Greiner bio-one GmbH, Frickenhausen, Germany
Plate reader	Infinite®M200	Tecan group Ltd., Männedorf, Switzerland
Ultrasound bath	Elmasonic P	Elma Schmidbauer GmbH, Singen, Germany
UltraTurrax	UltraTurrax T25	IKA®-Werke GmbH & CO. KG, Staufen, Germany
UltraTurrax Disperser	S 25 N – 8 G	IKA®-Werke GmbH & CO. KG, Staufen, Germany
96-well plates		Greiner bio-one GmbH, Frickenhausen, Germany
Size & ζ-Potential		
Zetasizer	Nano ZS	Malvern Instruments Ltd, Malvern, UK
Capillary Cell	DTS 1070	Malvern Instruments Ltd., Malvern, UK
Scanning Electron Microscopy		
Scanning Electron Microscope (HIPS)	EVO HD15	Carl Zeiss Microscopy GmbH, Jena, Germany
Sputter Coater (HIPS)	Quorum Q150R ES	Quorum Technologies Ltd., East Grinstead, UK
Scanning Electron Microscope (WZMW)	JEOL JSM-7500F	JEOL, Tokyo, Japan
Sputter Coater (WZMW)	Edwards S150	Edwards, West Sussex, United Kingdom
Carbon Disk		Plano, Wetzlar, Germany
Pin tube		Plano, Wetzlar, Germany
Silica wafer		Plano, Wetzlar, Germany

Device	Type	Company
Transmission Electron Microscopy		
Transmission Electron Microscope	Joel JEM 2100	JEOL, Tokyo, Japan
TEM Camera	Gatan Orius SC100	Gatan Inc., Pleasanton, CA, United States
Cryoplunger	Gatan CP3	Gatan Inc., Pleasanton, CA, United States
Cryo-TEM holder	Gatan 914	Gatan Inc., Pleasanton, CA, United States
Gatan image filter	GIF 2002	Gatan Inc., Pleasanton, CA, United States
Slow-scan camera	Gatan model 850	Gatan Inc., Pleasanton, CA, United States
Holey Carbon Film	S147-4	Plano, Wetzlar, Germany
Scanning Probe Microscopy		
Scanning Probe Microscope	JPK NanoWizard I	JPK Instruments, Berlin, Germany
SPM Tip Force measurements	MLCT, Cantilever C	Bruker Nano Inc., Camarillo, United States
SPM Tip (in air)	OMCL-AC160TS	Olympus Org, Tokyo, Japan
JPK-SPM Data Progressing Program		JPK Instruments, Berlin, Germany
UV/Ozone cleaner	UV/Ozone ProCleaner™	BioForce Nanosciences Inc., Ames, Iowa, United States
Cellculture & CLSM		
Scanning Confocal Microscope (Particle Interaction)		Carl Zeiss AG, Jena, Germany
Scanning Confocal Microscope (Colocalization)	Axiovert 100M	Carl Zeiss AG, Jena, Germany
Laser Axiovert 100M		Lasos Lasertechnik GmbH, Jena, Germany
Cellculture Microscopy Chambers	ibiTreat®	Ibidi GmbH, Martinsried, Germany

11 Table of Figures

12 Index of Abbreviations

A	Contact area
α	Tip half angle
α^{-1}	Distribution half-life
AFM	Atomic force microscope
API	Active pharmaceutical ingredient
Arg / R	Arginine
Asp / D	Aspartic acid
BCA assay	Bicinchoninic acid assay
BE	Back scattered electrons
BF	Brightfield
CCD	Charge couple device
cGNPs	Crosslinked gelatin nanoparticles
CLSM	Confocal scanning microscope
cpm	Counts per minute
D	Diffusion coefficient
DAPI	4',6-Diamidine-2'-phenylindole dihydrochloride
DDA	Dodecylamine
DDS	Drug delivery system
D_H	Hydrodynamic diameter
DLS	Dynamic light scattering
DMEM	Dulbecco´s Modified Eagle Medi
DMF	Dimethylformamide
DMSO	Dimethyl sulfoxide
DP	Data Progressing Program
E	Young´s modulus
EELS	Electron energy loss spectroscopy
EFTEM	Energy filtered TEM
eGFP	Enhanced green fluorescent protein
EPR	Enhanced permeation and retention
F	Applied force
FA-PLGA	Fluorescein amine labelled PLGA
FCS	Fetal calf serum
FDA	U.S. food and drug administration
FITC	Fluoresceinisothiocyanat
GIT	Gastro intestinal tract
Gly / G	Glycine
GNPs	Gelatin nanoparticles
h_c	Contact depth
HIPS	Helmholtz Institute for Pharmaceutical Research Saarland
HMVEC	Human lung microvascular endothelial cells
HUVEC	Human umbilical vein endothelial cells
IEP	Isoelectric point

k	Spring constant
k_B	Boltzmann constant
l_0	Initial NP height
LaB_6	Lanthanum hexaboride
LDV	Laser Doppler velocimetry
LEI	Lower secondary electron image
LNA	Locked nucleic acid
M3	Mixed mode measurement
MPS	Mononuclear phagocyte system
MTT	3-(4,5-dimethythiazol-2-yl)-2,5-diphenyl tetrazolium bromide
η	Viscosity
NIBS	Non-invasive back-scatter technology
NPs	Nanoparticles
PALS	Phase analysis light scattering
PdI	Polydispersity Index
PEG	Polyethylenglycole
PEGDA	Poly(ethylene glycol) diacrylate
PEI	Polyethylenimine
PLGA	Poly(lactic-co-glycolic acid)
PRINT	Particle replication in nonwetting templates
PSPD	Position-sensitive photodiode
PVA	Polyvinylalcohol
RBCs	Red blood cells
RPMI	Roswell Park Memorial Institute
SEI	Secondary electron image
SEM	Scanning electron microscopy
SPM	Scanning probe microscope
T	Temperatur
TEM	Transmission electron microscopy
T_{max}	Maximum plasma concentration
TRITC	Tetramethyl-rhodamine isothiocyanate
z	Piezo displacement
ZD	Z-average diameter
β^{-1}	Elimination half-life
δ_c	Cantilever deformation
Δl	Indentation depth
ν	Possion´s ratio

13 Scientific Output

ARTICLES

A.-V. Weiss, T. Fischer, J. Iturri, R. Benitez, J. L. Toca-Herrera, M. Schneider

Mechanical Properties of Gelatin Nanoparticles in Dependency of Crosslinking Time and Storage (Submitted)

ORAL PRESENTATIONS

A biocompatible carrier system for hydrophilic macromolecules

A.-V. Weiss, M. Schneider

21st annual meeting, CRS Germany Local Chapter, March 2017, Marburg, Germany (Best Oral Presentation Award)

Mechanical Properties of Gelatin Nanoparticles and their Influence on cellular Interaction

A.-V. Weiss, T. Fischer, M. Schneider

22nd annual meeting, CRS Germany Local Chapter, March 2018, Halle, Germany

POSTER PRESENTATIONS

Hydrophobic-coated non-crosslinked Gelatin Nanoparticles as Carrier System for Hydrophilic Macromolecules

A.-V. Weiss, M. Schneider

11th Conference and Workshop on Biological Barriers, March 2016, Saarbrücken, Germany

Gelatin based nanoscale Drug Delivery System for hydrophilic Macromolecules

A.-V. Weiss, M. Schneider

Doktorandentag Saarland University, November 2016, Saarbrücken, Germany

Gelatin Nanocarriers stabilized by Incorporation in PLGA for the Delivery of Hydrophilic Macromolecules

A.-V. Weiss, M. Schneider

GPEN2016, November 2016, Lawrence, KS, US

Insight in the Viscoelastic Characteristics of Gelatin Nanoparticles as Drug Delivery System

A.-V. Weiss, J. Iturri, J. L. Toca-Herrera and M. Schneider

13th Zsigmondy Colloquium; April 2017, Saarbrücken, Germany

Evaluating the mechanical Properties of Gelatin Nanoparticles and the Influence on cellular Uptake

A.-V. Weiss, T. Fischer, M. Schneider

45th Annual Meeting Exposition of the Controlled Release Society, July 2018, New York, US

(Submitted)

14 Curriculum Vitae

PERSONAL DATA:

Date/ Place of birth: 22.07.1987 in Filderstadt

Citizenship: German

EDUCATION

April 2014 – March 2018:	Doctoral Thesis:
	Saarland University, Biopharmaceutics and Pharmaceutical Technology (4/2015 – 03/2018) and
	Philipps University Marburg; Pharmaceutics and Biopharmacy (04/2014- - 03/2015)
Feb. 2014:	Licensed Pharmacist (Approbation)
2007 to 2012	Pharmacy at the University of Erlangen-Nürnberg
June 2007	High School Diploma

INTERNSHIPS AND WORK EXPERIENCE:

Since May 2016	Emergency Services in a Community Pharmacy, Glückaufapotheke, Saarbrücken-Burbach, Germany
Since April 2015	PhD Student, Saarland University, Biopharmacy und Pharmaceutical Technology, Prof. Dr. Marc Schneider, Saarbrücken, Germany
June 2016 & Aug 2015	Visiting Researcher, University of Natural Resources and Life Science, Center for Nanobiotechnology, Biophysics, Prof. Dr. José Luis Toca-Herrera; Vienna, Austria
April 2014 –March 2015	PhD Student, Philipps-University Marburg, Pharmaceutical Technology und Biopharmacy, Prof. Dr. Marc Schneider, Marburg, Germany
Feb. – April 2014	Pharmacist, Community Pharmacy, Sonnen Apotheke, Roßtal
May – Nov. 2013	Preregistration Internship, Community Pharmacy, Linden Apotheke, Nürnberg, Germany
Nov. 2012 - April 2013	Preregistration Internship, School of Pharmacy and Pharmaceutical Sciences, Trinity College Dublin, Biopharmacy, Assoc. Prof. Carsten Ehrhardt, Dublin, Irland

15 Acknowledgement

I would like to give a grateful acknowledgement to my supervisor Prof. Marc Schneider. Thank you Marc for the opportunity to work and grow, personally and scientifically, in your group. You have always been there for advices but gave me the opportunity to work independently and choose the focus of my thesis. I really enjoy working in the group and the comfortable atmosphere you created. Thank you.

Thank you Prof. Claus-Michael Lehr for the input to my thesis during the PhD seminars and for being my scientific advisor as well as being available to review my thesis. Here I would like to attach acknowledgements for the whole thesis committee.

I thank Arnold Grünweller and Kerstin Lange-Grünweller for the cooperation in the LNA project, for kindly providing the 32P-labelled LNA and the possibility to use the equipment and laboratory for the work with radioactive materials. In this context, I would like to thank Dominik Helmecke for the introduction to work with radioactive substances.

I kindly acknowledge Nadine Wilhelm, Erwin Gorjup and Max Jacobs from the Fraunhofer IBMT for their cooperation and for providing the plasmid DNA as well as for the cell-work performed by Nadine in this project.

Marcus Koch from the Institute of New Materials, thank you for the cryo-TEM and EFTEM analysis and meetings, never tired in explaining the principles behind these fascinating techniques. Even though the results are the opposite of what I aimed for, they give a valuable impact to this thesis.

My special thanks go to all former and current colleagues I want to acknowledge especially Saeed, Chen, Carolin, Julia R., Marcel, Aljoscha, Tamara, Julia M. and Thorben. In addition to the PhD students, I want to thank all diploma students joining our lab. Thanks for the scientific discussions and input, the enjoyable working atmosphere and thanks for all the friendships developing over the time. I thank Thorben for the work he performed during his diploma thesis. It was a very good experience working with you and I am happy we can further work together. Carolin I was not only pleased to share the office with you in good and hard times, going for runs and rollerblading with you, but I am also gratified with your friendship.

Peter and Marijas you are a great constant in our team! Always helpful and creative in trouble shooting, walking memories and last but not least, together with Daniel, a great companion in the office in the new building! Isabelle you indeed are the kindly soul of the

institute, always helpful, not only with all the bureaucracy and always available for a chat. Merci beaucoup!

I thank Prof. Udo Bakowsky and his team for the time we spent in Marburg. Especially Mathias, Shashank und Boris for sharing the office and for all the fruitful discussions going as well beyond scientific content. It was a great time with you. In addition, I would like to highlight the secretary Julia and the technician, Susanne, for their always kind and productive support. As well as Michael Hellwig from the WZMW at Marburg university for the introduction to the SEM and the help with tricky samples.

Prof. José Toca-Herrera thank you for being a great host. I always felt very welcome and supported. I look forward to further cooperations. I was able to get to know and work with people from various scientific backgrounds. This definitely was very inspiring and opened new perspectives. I want to name Jagoba, Alberto, Jacqueline and Dieter but not less appreciate all the others who made me feeling very comfortable at the DNBT. Prof. Rafael Benitez thanks for the patient support regarding all R studio problems.

I thank the entire DDEL group at HIPS for the scientific discussions in the PhD-seminars in SB and in France and the time we spent together outside our institutes. Bedankt voor alles Remi. Special thanks go to Chiara de Rossi for the introduction and help with the SEM.

This thesis was only possible because I had the privilege to grow up in a surrounding supporting education and always respecting the way I choose. Therefore, I want to thank my family. In the first place my parents Renate and Gerhard but as well my brothers Felix and Johannes and my sisters Sarah and Kerstin. Thank you for always being there for me! Kerstin: Ich bewundere dich für deine Lebensfreude, deine Art und deine bedingungslose Freundschaft <3.

I am blessed with amazing friends from all stations I have passed in the last 30 years. Scouts, school, university and in the cities I have lived since. Thank you for always having a sympathetic ear, for everything we went through in our common stations and for the patience especially in the last months. I want to name Keith for his support, not only during my thesis, and for undertaking the final language check. In addition, I want to highlight my flat mates during the final phase of my thesis: Rebecca, Anna and Martin.

Last but not least thank you Torsten for your support, your patients, your consideration and your love!